Unitarity cutting rules for the nucleus excitation and topological cross sections in hard production off nuclei from nonlinear $k_\perp$-factorization

N. N. Nikolaev[1,2,*] and W. Schäfer[3,†]

[1]*Institut für Kernphysik, Forschungszentrum Jülich, D-52425 Jülich, Germany*
[2]*L. D. Landau Institute for Theoretical Physics, 142432 Chernogolovka, Russia*
[3]*Institute of Nuclear Physics PAN, PL-31-342 Cracow, Poland*

(Received 31 July 2006; published 27 October 2006)

At the partonic level, a typical final state in small-x deep inelastic scattering off nuclei and hard proton-nucleus collisions can be characterized by the multiplicity of color-excited nucleons. Within the Reggeon field theory, each color-excited nucleon is associated with the unitarity cut of the Pomeron exchanged between the projectile and nucleus. In this communication we derive the unitarity rules for the multiplicity of excited nucleons, alias cut pomerons, alias topological cross sections, for typical hard dijet production processes. We demonstrate how the coupled-channel non-Abelian intranuclear evolution of color dipoles, inherent to pQCD, gives rise to the Reggeon field theory diagrams for final states in terms of the uncut, and two kinds of cut, Pomerons. Upon the proper identification of the uncut and cut-Pomeron exchanges, the topological cross sections for dijet production follow in a straightforward way from the earlier derived nonlinear $k_\perp$ factorization quadratures for the inclusive dijet cross sections. The concept of a coherent (collective) nuclear glue proves extremely useful for the formulation of the Reggeon field theory vertices of multi-Pomeron—cut and uncut—couplings to particles and between themselves. A departure of our unitarity cutting rules from the ones suggested by the pre-QCD Abramovsky-Kancheli-Gribov rules, stems from the coupled-channel features of non-Abelian intranuclear pQCD. We propose a multiplicity resummation as a tool for the isolation of topological cross sections for single-jet production.

DOI: 10.1103/PhysRevD.74.074021 PACS numbers: 13.87.−a, 11.80.La, 12.38.Bx, 13.85.−t

I. INTRODUCTION

The subject of this communication is a study of the unitarity cutting rules for long-range rapidity correlations between the forward, and midrapidity, jet and dijet production and multiproduction in the target-nucleus fragmentation region—one of the important experimental observables ([1,2] and references therein). In perturbative quantum chromodynamics (pQCD), hard single-jet or dijet production in the beam hemisphere of high-energy deep inelastic scattering (DIS) or a hard nucleon-nucleon collision can be viewed as a hard photon-gluon fusion, $\gamma^* g_t \to q\bar{q}$, or hard scattering of the valence quark of the nucleon, $qg_t \to qg$. At midrapidity, the dominant gluon-gluon dijets come from $gg_t \to gg$, the open-charm production is driven by $gg_t \to c\bar{c}$. Here g_t stands for the target gluon—in the target rest frame it is the gluon exchanged in the t-channel. Hard scattering leaves the target-nucleon debris in the color-octet state. In hard scattering off a heavy nucleus multiple gluon exchanges are enhanced by a large thickness of the target nucleus, and a typical inelastic event leaves behind many bound nucleons in the color-excited state. Their multiplicity defines the hadronic activity in the nucleus hemisphere, i.e., the centrality of collisions—a fundamental concept in the physics of ultrarelativistic nuclear collisions ([3,4], for reviews and further references see [2]).

In the Reggeon field theory (RFT) language [5,6], pQCD offers a perfect definition of cut Pomerons: each and every excited nucleon can be associated with the unitarity cut of a Pomeron exchanged between the beam and target. Then our pQCD unitarity rules for color excitation of the nucleus give a multiplicity of cut Pomerons, alias the topological cross sections—a subject of much discussion ever since the pre-QCD unitarity cutting rules suggested in 1972 by Abramovsky, Gribov, and Kancheli (AGK) [6]. A casual reference to the AGK rules appears in numerous discussions of multiproduction in ultrarelativistic (nuclear) collisions ([7–16], for more references see the recent reviews by Bartels and by Kowalski in Ref. [17]). Here we address the issue of pQCD unitarity rules on an example of interaction of small projectiles with large nuclear targets, where one can take advantage of a new large parameter—the thickness (diameter $2R_A$ of the target nucleus of mass number A) of a heavy nucleus. We discuss observables of different degrees of resummation over this large parameter.

There are two principal novelties in our approach to topological cross sections. The first one is a manifest imposition of the unitarity constraints at each step of the derivation. This is readily achieved within the color-dipole S-matrix approach to high-energy hard processes developed in Refs. [18–23]. We start from the basic pQCD, follow carefully a separation of color-diagonal and color-excitation interactions of color dipoles, diagonalize the

*Electronic address: N.Nikolaev@fz-juelich.de
†Electronic address: Wo.Schaefer@fz-juelich.de

non-Abelian intranuclear evolution, and relate the topological cross sections with a fixed multiplicity of color-excited nucleons—cut Pomerons—to properties of the collective nuclear glue of spatially overlapping nucleons in the Lorentz-contracted ultrarelativistic nucleus. A consistent treatment of the coupled-channel aspects of the non-Abelian intranuclear evolution of color dipoles is behind the universality classes for nonlinear $k_\perp$-factorization for hard processes in a nuclear environment [24–31]. And it is behind the second principal novelty of this paper—the finding that in the description of topological cross sections one needs two kinds of cut Pomerons. One of these two, $\not{P}_r$ (the subscript "r" stands for the rotation), describes color excitations of the nucleus by color rotations of the color dipole within the same color multiplet. The second one, $\not{P}_e$ (the subscript "e" stands for the excitation), is for the transition between color multiplets the dimensions of which differ by the factor $\mathcal{O}(N_c^2)$, where N_c is the number of colors. As a matter of fact, this distinction between $\not{P}_r$ and $\not{P}_e$ had to a large extent been anticipated in the first publication [24] on the nonlinear $k_\perp$-factorization. Finally, uncut Pomerons $\mathbb{P}$ are associated with the color-diagonal (elastic) intranuclear interactions of dipoles.

To the leading order of the large-N_c perturbation theory, we formulate simple RFT diagram rules for the calculation of topological cross sections for the dijet spectra. To this end, upon the proper identification of the uncut, $\mathbb{P}$, and the two cut, $\not{P}_r$ and $\not{P}_e$, Pomerons our task of the derivation of the topological cross sections boils down to a simple—in one stroke—reinterpretation of the nonlinear $k_\perp$-factorization results for the inclusive dijet spectra [24–31]. Here a concept of the collective nuclear glue as a coherent state of the in-vacuum (Reggeized) gluons emerges and proves an extremely useful one. What we report are only prolegomena to a full fledged RFT: we confine ourselves to tree diagrams, the hot issue of an extension to Pomeron loops in the spirit of Ref. [32] needs further scrutiny (also see the reviews [33]). Even at the tree level, and to the leading order of large-N_c perturbation theory, we find a very rich variety of the cut-Pomeron multiplicity distributions which vary substantially from one reaction universality class [27,28,30] to another, and give rise to a whole family of the t-channel multi-Pomeron vertices for t-channel transitions from one cut Pomeron $\not{P}_r$ to $\not{P}_r$'s and $\not{P}_e$'s, and their s-channel unitarity cuts. Arguably, this distinction between universality classes will persist under small-x evolution—the unitarity-cut content of this evolution is one of the obvious future applications of the emerging formalism.

As far as the single-jet and still more integrated observables are concerned, an important, and obvious, feature of topological cross sections is the Cheshire Cat grin (CCG) of the spectator interactions. Specifically, if one starts with the dijet cross section and integrates over the phase space of the spectator jet, then all the spectator interaction effects would cancel in the nonlinear $k_\perp$-factorization quadratures for the single-jet spectrum. The spectator contribution to the nucleus excitation and cut Pomerons—the CCG—stays on. CCG is a physics observable and has important implications for the long-range rapidity correlations between the beam, and midrapidity, and the target-nucleus fragmentation regions. In this respect, our concept of the color-excited nucleons, and the associated cut Pomeron, is close to the concept of wounded (participant) nucleons [34,35]. The wounded nucleon multiplicity distributions are customarily evaluated within a certain interpretation of the Glauber model for the hadron-nucleus interactions ([7–9], for the review see [36], for the relation to the collision centrality see [2–4]). Such a Glauber model interpretation is not borne out by our pQCD coupled-channel approach to topological cross sections, and we discuss the origin of this distinction to a great detail.

On the event-by-event basis, the single midrapidity gluon spectra are infested by the CCG of the spectator, and comover, parton interactions. What is remarkable is that the effect of spectator parton interactions can be eliminated entirely, and meaningful topological cross sections for single-jet spectra can be defined, upon certain multiplicity resummations. Upon these resummations, the single midrapidity gluon spectra serve as a definition of the t-channel transitions of the in-vacuum $\not{P}_r$ to multiple $\not{P}_e$'s and $\not{P}_r$'s. The emerging multi-Pomeron vertices are universal and do not depend on the projectile. We strongly advocate an analysis of the experimental data using this multiplicity resummation technique.

One important application of cutting rules for these long-range rapidity correlations is a nonperturbative quenching (stopping) of leading jets and the dependence of this quenching on the nucleus excitation (for reviews on quenching see [2,37–39]). One customarily associates with cut Pomerons color strings stretched between the color-excited nucleons of the nucleus and the projectile system. Hadronization of the color string into small-$p_\perp$ hadrons—the underlying minimal-bias event for hard dijets—slows down the projectile system. The energy flow from the projectile system to the nucleus, and the accompanying nonperturbative quenching (stopping) of leading jets, depends on the hadronization model. In one extreme scenario, which goes back to the ITEP-Orsay model of the mid-70's [7,9], strings hadronize independently of each other in the whole rapidity span from the nucleus up to the projectile, see Fig. 1(b). In such a scenario the projectile loses a finite fraction of its energy per color string, so that the nonperturbative quenching of forward jets and particles, and the related breaking of the limiting fragmentation, would persist at high energy. In still another extreme scenario, suggested by the formation length considerations, hadronization of color strings attached to a high-$p_\perp$ parton in the final state, is independent only up to rapidities

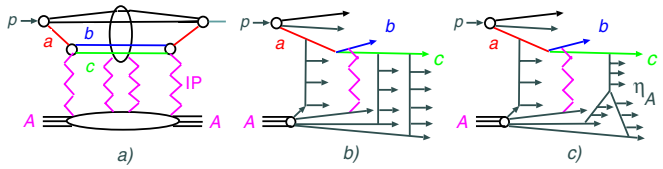

FIG. 1 (color online). (a) A contribution of multi-Pomeron exchanges to the forward elastic proton-nucleus scattering amplitude from final states containing the dijet bc, (b) an example of the unitarity cut with independent hadronization of color strings over all rapidities from the target to a projectile, (c) an example of the unitarity cut with the fan structure of hadronizing strings with string junction at the rapidity η_A.

$$\eta_A \approx \log\frac{1}{2R_A m_p}, \tag{1}$$

from the target-nucleus rapidity [38,40–42] (here m_p is the proton mass). When viewed in the antilaboratory frame with a Lorentz-contracted ultrarelativistic nucleus, at rapidities $\eta > \eta_A$ the strings overlap spatially. One would argue that the overlapping strings fragment as one string, see Fig. 1(c), for the recent string phenomenology see [43]. In such a scenario, the projectile loses a finite energy per color string. In a dilute nucleus, strings of length $\sim R_A$ are stretched also between different color centers in the nucleus, and the energy loss will be larger than the collisional loss for the recoil of struck quarks in the nucleus [44]. In any case, it is imperative to understand the relevant topological cross sections and identify the quenching of the parton parent to the specific observed jet and the much discussed breaking of the limiting fragmentation [45–47]. This is our major task in this study.

Our treatment is applicable when the beam and final-state partons interact coherently over the whole longitudinal extension of the nucleus,

$$x = \frac{(Q^*)^2 + M_\perp^2}{2m_p\nu} \lesssim x_A = \frac{1}{2R_A m_p} \approx 0.1A^{-1/3}, \tag{2}$$

where $M_\perp$ is the transverse mass of the dijet, ν is the energy of the projectile parton in the target rest frame, and $(Q^*)^2$ is its virtuality: $(Q^*)^2 = Q^2$ in DIS and $(Q^*)^2 = \boldsymbol{p}_q^2$ in qA collisions, where $\boldsymbol{p}_q$ is the transverse momentum of the incident valence quark in the beam proton [19,41]. At the Relativistic Heavy Ion Collider (RHIC) this amounts to precisely the leading dijets in the proton fragmentation region (for the discussion of the possible upgrade of detectors at RHIC II for the improved coverage of the proton fragmentation region see [48]).

The presentation of the main material is organized as follows. In Secs. II and III we introduce the basics of the color-dipole approach, formulate the master formula for the dijet spectrum and present the unitarity based derivation of the topological cross sections—alias the multiplicity distribution of cut Pomerons—in terms of the multiplicity of color-excited nucleons. Here the major novelty is an integral representation for the corresponding nuclear S-matrices in terms of elastic and color-excitation free-nucleon interactions, which has a built-in unitarity property. Section IV is an introduction to the correspondence between the color dipole and RFT approaches. We define the collective nuclear glue based on the color-dipole S-matrix, comment on its coherent state property, and establish its connection to quasielastic scattering of quarks. The subject of Sec. V is a nonlinear $k_\perp$-factorization for topological cross sections for the universality classes of coherent diffraction (CD), inelastic and pseudodiffractive DIS off nuclei, and their RFT interpretation in terms of the cut and uncut-Pomeron exchanges. Here we identify two kinds of cut Pomerons, $\not{P}_e$ and $\not{P}_r$, as an indispensable feature of pQCD. Based on this new finding and the identification of the role of $\not{P}_e$ and $\not{P}_r$, we show how the topological cross sections follow in one stroke from the nonlinear $k_\perp$-factorization quadratures for inclusive dijet cross sections. Inspired by this success, in Sec. VI we address an important issue of whether the topological cross sections can be guessed from the Glauber model results for the fully integrated total cross section. We show that within pQCD this is not the case, and derive new results for the multiplicity distribution of cut Pomerons in the fully integrated cross sections. The possible phenomenological applications of our results to the multiplicity distributions in the backward (nucleus) hemisphere and long-range rapidity correlations between leading jets and rapidity spectra of backward particles in DIS off nuclei are commented on in Sec. VII. Here we introduce the multiplicity resummations which enable one to eliminate the spectator quark interaction effects in the nucleus excitation. In Secs. VIII, IX, and X we extend our treatment of DIS to qg final states in qA collisions, gg final states in gA collisions, and open-charm $c\bar{c}$ states in gA collisions, respectively. We formulate the RFT diagram rules for each universality class and offer a fresh look at slight variations from one projectile to another. In Sec. XI we briefly revisit topological cross sections in single midrapidity gluon production. Here the CCG precludes the determination of the relevant multiplicity of cut Pomerons on an event-by-event basis. Still upon certain multiplicity resummations, one can define single-jet topological cross sections which exhibit a remarkable universality for the quark and gluon projectiles modulo to the Casimirs in the Regge-factorizable coupling of the projectile to a Pomeron $\not{P}_r$. We comment on the variety of triple-Pomeron couplings which appear in the RFT description of the resummed topological cross sections. In Sec. XII we summarize our principal conclusions. The technicalities of the diagonalization of the non-Abelian evolution of color dipoles which is a basis for the derivation of topological cross sections are presented in Appendices A, B, and C.

II. THE MASTER FORMULA FOR HARD DIJET PRODUCTION OFF FREE NUCLEONS AND NUCLEI

To the lowest order in pQCD, the underlying hard subprocess is of the general form $ag_t \to bc$. In the photon fragmentation region of DIS the projectile is the virtual photon, $a = \gamma^*$, in the proton fragmentation region of proton-nucleus collisions one would focus on interactions of valence quarks, $a = q$, the production of open charm and of midrapidity jets in proton-nucleus collisions will be dominated by gluons of the projectile hadron, $a = g$. From the laboratory frame standpoint, the dijet production is an excitation of the perturbative $|bc\rangle$ Fock state of the physical projectile $|a\rangle_{\rm phys}$ by a one-gluon t-channel exchange with the target nucleon. In our discussion we follow a general treatment of multiple gluon exchanges in nuclear targets developed in, and use the principal notations from, our earlier publications [22,24,26,29–31].

To the lowest order in the perturbative transition $a \to bc$ the Fock state expansion for the physical state $|a\rangle_{\rm phys}$ reads

$$|a\rangle_{\rm phys} = \sqrt{Z_a}|a\rangle_0 + \Psi(z_b, \boldsymbol{r})|bc\rangle_0, \tag{3}$$

where $\Psi(z_b, \boldsymbol{r})$ is the probability amplitude to find the bc system with the separation (color dipole) $\boldsymbol{r}$ in the two-dimensional impact parameter space, the subscript "0" refers to bare partons. The perturbative coupling of the $a \to bc$ transition is reabsorbed into the light-cone wave function $\Psi(z_b, \boldsymbol{r})$ which depends on the virtuality of the incident parton a, i.e., $Q_a^2 = Q^2$ for the virtual photon in DIS or $Q_a^2 = \boldsymbol{p}_a^2$ in qA collisions, where $\boldsymbol{p}_a$ is the transverse momentum of the parton a in the proton. Explicit expressions for various pQCD subprocess in terms of the familiar parton splitting functions are found in [26]. In this paper we focus on the lowest order (Born) excitation processes $a \to bc$ without production of more secondary partons in the rapidity span between η_a and η_c.

We use the light-cone S-matrix approach. For the sake of simplicity we work in the aA collision frame. If $\boldsymbol{b} \equiv \boldsymbol{b}_a$ is the impact parameter of the projectile a, then

$$\boldsymbol{b}_b = \boldsymbol{b} + z_c\boldsymbol{r}, \qquad \boldsymbol{b}_c = \boldsymbol{b} - z_b\boldsymbol{r}, \tag{4}$$

where $z \equiv z_b$, $z_c = (1 - z_b)$ is the partition of the beam momentum between the final-state partons. Participating partons propagate along a straight path and the interaction is coherent over the whole nucleus in the high-energy limit of $x \lesssim x_A$. The contribution from transitions $a \to bc$ inside the target nucleus vanishes in the high-energy limit.

Evidently, the S-matrix for interaction of the bc state equals $S_{bc}(\boldsymbol{b}_b, \boldsymbol{b}_c) = S_b(\boldsymbol{b}_b)S_c(\boldsymbol{b}_c)$ and the action of the S-matrix on $|a\rangle_{\rm phys}$ takes a simple form

$$\begin{aligned} S|a\rangle_{\rm phys} &= \sqrt{Z_a}S_a(\boldsymbol{b})|a\rangle_0 + S_b(\boldsymbol{b}_b)S_c(\boldsymbol{b}_c)\Psi(z, \boldsymbol{r})|bc\rangle_0 \\ &= S_a(\boldsymbol{b})|a\rangle_{\rm phys} + [S_b(\boldsymbol{b}_b)S_c(\boldsymbol{b}_c) - S_a(\boldsymbol{b})] \\ &\quad \times \Psi(z, \boldsymbol{r})|bc\rangle_0. \end{aligned} \tag{5}$$

Here we explicitly decomposed the final state into the elastically scattered $|a\rangle_{\rm phys}$ and the excited state $|bc\rangle_0$. The wave function renormalization $\sqrt{Z_a}$ in (3) does not enter the excitation amplitude. The two terms in the latter describe a scattering on the target of the bc system formed way in front of the target and the transition $a \to bc$ after the interaction of the state $|a\rangle_0$ with the target, as illustrated in Fig. 2. Whenever it would not cause any confusion, we shall use the shorthand notations, $S(\boldsymbol{b}) \equiv S_a(\boldsymbol{b})$ for the beam-target S-matrix and $S(\boldsymbol{B}) \equiv S_{bc}(\boldsymbol{b}_b, \boldsymbol{b}_c)$ for the bc-target S-matrix where $\boldsymbol{B} = \{\boldsymbol{b}_b, \boldsymbol{b}_c\}$ is a shorthand notation for the impact parameters of the two-parton system.

Usually one discusses fully inclusive nuclear cross sections summed over all nuclear—and nucleon—excitations. The specific problem of interest in this communication—the properties of final states tagged by the degree of excitation of the target nucleus and their RFT interpretation—calls for a somewhat more detailed treatment of color properties of final states. The probability amplitude for the two-jet spectrum is given by the Fourier transform

$$\begin{aligned} &\int d^2\boldsymbol{b}_b d^2\boldsymbol{b}_c \exp[-i(\boldsymbol{p}_b\boldsymbol{b}_b + \boldsymbol{p}_c\boldsymbol{b}_c)] \\ &\quad \times \langle A_f|[S(\boldsymbol{B}) - S(\boldsymbol{b})]|A_{\rm in}\rangle_{c_f c_i}\Psi(z, \boldsymbol{r}), \end{aligned} \tag{6}$$

where we show explicitly the matrix element over the configuration and color space wave functions of the target $|A_{\rm in}\rangle$ and final-state nucleus $\langle A_f|$. We average the cross section over the unobserved color states c_i of the incident parton. We sum over the unobserved color states c_f of the dijet. Then, the differential cross section for a specific final state $\langle A_f|$ of the target is proportional to the modulus squared of (6),

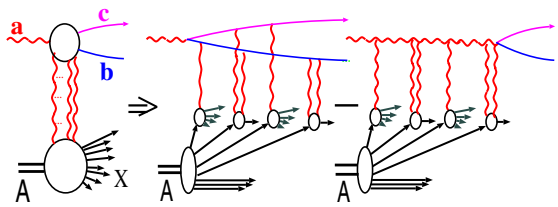

FIG. 2 (color online). Typical contribution to the excitation amplitude for $aA \to bcX$, with multiple color excitations of the nucleus. The amplitude receives contributions from processes that involve interactions with the nucleus after and before the virtual decay which interfere destructively. Notice a distinction between color-excitation (single-gluon, i.e., cut-Pomeron, exchange) and color-diagonal (elastic two-gluon, uncut-Pomeron, exchange) interactions between the target nucleons and the projectile and produced parton systems.

$$\frac{d\sigma(aA\to(bc)A_f)}{dzd^2\boldsymbol{p}_bd^2\boldsymbol{p}_c}=\frac{1}{(2\pi)^4}\int d^2\boldsymbol{b}_b'd^2\boldsymbol{b}_c'\int d^2\boldsymbol{b}_bd^2\boldsymbol{b}_c\exp[-i\boldsymbol{p}_b(\boldsymbol{b}_b-\boldsymbol{b}_b')-i\boldsymbol{p}_c(\boldsymbol{b}_c-\boldsymbol{b}_c')]\Psi^*(z,\boldsymbol{r}')\Psi(z,\boldsymbol{r})$$
$$\times\frac{1}{\dim[\mathrm{in}]}\sum_{c_fc_i}\langle A_{\mathrm{in}}|[S^\dagger(\boldsymbol{B}')-S^\dagger(\boldsymbol{b}')]|A_f\rangle_{c_ic_f}\langle A_f|[S(\boldsymbol{B})-S(\boldsymbol{b})]|A_{\mathrm{in}}\rangle_{c_fc_i},\tag{7}$$

where dim[in] is the number of color states in the $SU(N_c)$ multiplet the incident parton belongs to.

Hereafter we describe the final state in terms of $\boldsymbol{p}\equiv\boldsymbol{p}_b, z\equiv z_b$ and the dijet acoplanarity momentum $\boldsymbol{\Delta}=\boldsymbol{p}_b+\boldsymbol{p}_c$. We also introduce $\boldsymbol{s}=\boldsymbol{b}_b-\boldsymbol{b}_b'$, in terms of which $\boldsymbol{b}_c-\boldsymbol{b}_c'=\boldsymbol{s}-\boldsymbol{r}+\boldsymbol{r}'$. Notice that $\boldsymbol{s}$ is conjugate to the acoplanarity momentum $\boldsymbol{\Delta}$:

$$\exp[-i\boldsymbol{p}_b(\boldsymbol{b}_b-\boldsymbol{b}_b')-i\boldsymbol{p}_c(\boldsymbol{b}_c-\boldsymbol{b}_c')]=\exp[-i\boldsymbol{\Delta}\boldsymbol{s}-i(\boldsymbol{p}-\boldsymbol{\Delta})(\boldsymbol{r}-\boldsymbol{r}')].\tag{8}$$

Our main task will be an evaluation of the color trace which emerged in (7),

$$\begin{aligned}\mathcal{T}(\boldsymbol{B},\boldsymbol{B}',\boldsymbol{b},\boldsymbol{b}')&=\mathrm{Tr}\{\langle A_{\mathrm{in}}|[S^\dagger(\boldsymbol{B}')-S^\dagger(\boldsymbol{b}')]|A_f\rangle\langle A_f|[S(\boldsymbol{B})-S(\boldsymbol{b})]|A_{\mathrm{in}}\rangle\}\\&=\mathrm{Tr}\{\langle A_{\mathrm{in}}|S^\dagger(\boldsymbol{B}')|A_f\rangle\langle A_f|S(\boldsymbol{B})|A_{\mathrm{in}}\rangle\}+\mathrm{Tr}\{\langle A_{\mathrm{in}}|S^\dagger(\boldsymbol{b}')|A_f\rangle\langle A_f|S(\boldsymbol{b})|A_{\mathrm{in}}\rangle\}\\&\quad-\mathrm{Tr}\{\langle A_{\mathrm{in}}|S^\dagger(\boldsymbol{B}')|A_f\rangle\langle A_f|S(\boldsymbol{b})|A_{\mathrm{in}}\rangle\}-\mathrm{Tr}\{\langle A_{\mathrm{in}}|S^\dagger(\boldsymbol{b}')|A_f\rangle\langle A_f|S(\boldsymbol{B})|A_{\mathrm{in}}\rangle\}\\&=\mathcal{S}_A^{(4)}(\boldsymbol{B}',\boldsymbol{B})+\mathcal{S}_A^{(2)}(\boldsymbol{b}',\boldsymbol{b})-\mathcal{S}_A^{(3)}(\boldsymbol{B}',\boldsymbol{b})-\mathcal{S}_A^{(3)}(\boldsymbol{b}',\boldsymbol{B}),\end{aligned}\tag{9}$$

(wherever it would not cause a confusion, we suppress the superscript (n) for the n-parton states). The crucial point is that $S^\dagger$ can be interpreted as an S-matrix for the scattering of antiquarks [18,22,24,26,29]. Then four terms in the last line of (9) are contributions from the intermediate nuclear state with a certain set of color-excited and ground-state nucleons, $|A_f\rangle$, to the S-matrices of the interaction of color-singlet multiparton states with the ground state of the nucleus $|A_{\mathrm{in}}\rangle$. This point will be explained in more detail below in Sec. III.

III. THE MASTER FORMULA FOR TOPOLOGICAL NUCLEAR CROSS SECTIONS

A. Basics of the color-dipole approach

To the lowest order in pQCD, the inelastic color triplet-antitriplet dipole-nucleon interaction is driven by the one-gluon exchange and the total inelastic cross section is described by the two-gluon exchange approximation [19,24]. Correspondingly, the S-matrices of the quark-nucleon and antiquark-nucleon interaction must be evaluated to the second order in pQCD. They equal, respectively,

$$\begin{aligned}S(\boldsymbol{b}_q)&=\mathbb{1}+i\hat{\chi}(\boldsymbol{b}_q)-\tfrac{1}{2}\hat{\chi}^2(\boldsymbol{b}_q)\\&=\mathbb{1}+iT^aV_a\chi(\boldsymbol{b}_q)-\tfrac{1}{2}T^aT^a\chi^2(\boldsymbol{b}_q),\\S^\dagger(\boldsymbol{b}_{\bar{q}})&=\mathbb{1}-i\hat{\chi}(\boldsymbol{b}_{\bar{q}})-\tfrac{1}{2}\hat{\chi}^2(\boldsymbol{b}_{\bar{q}})\\&=\mathbb{1}-iT^aV_a\chi(\boldsymbol{b}_{\bar{q}})-\tfrac{1}{2}T^aT^a\chi^2(\boldsymbol{b}_{\bar{q}}),\end{aligned}\tag{10}$$

where $\hat{\chi}(\boldsymbol{b})=T^aV_a\chi(\boldsymbol{b})$, proportional to the strong coupling α_S, is the eikonal for the quark-nucleon single-gluon exchange, the summation goes over the color-octet indices a. The terms linear in $\chi(\boldsymbol{b})$ describe the scattering with color excitation of the target nucleon. To the desired pQCD accuracy, in the second order terms in (10) we only keep the contribution which is diagonal in the target color state. The distinction between the color-excitation and color-diagonal—elastic—interaction is explicit in Fig. 2. The vertex V_a for excitation of the nucleon $g^aN\to N_a^*$ into color-octet state is so normalized that after application of closure over the final-state excitations N^* the vertex g^ag^bNN equals $\langle N|V_a^\dagger V_b|N\rangle=\delta_{ab}$. The second order terms in (10) already use this normalization. The S-matrix (10) satisfies the unitarity condition $S(\boldsymbol{b}_q)S^\dagger(\boldsymbol{b}_q)=\mathbb{1}$.

The S-matrix of the $(q\bar{q})$-nucleon interaction equals

$$S_{q\bar{q}}(\boldsymbol{b}_q,\boldsymbol{b}_{\bar{q}})=\frac{\langle N|\mathrm{Tr}[S(\boldsymbol{b}_q)S^\dagger(\boldsymbol{b}_{\bar{q}})]|N\rangle}{\langle N|\mathrm{Tr}\mathbb{1}|N\rangle}.\tag{11}$$

The corresponding profile function is $\Gamma_{q\bar{q}}(\boldsymbol{b}_q,\boldsymbol{b}_{\bar{q}})=1-S_{q\bar{q}}(\boldsymbol{b}_q,\boldsymbol{b}_{\bar{q}})$. The dipole cross section for interaction of the color-singlet $q\bar{q}$ dipole, $\boldsymbol{r}=\boldsymbol{b}_q-\boldsymbol{b}_{\bar{q}}$, with the free nucleon is obtained upon the integration over the overall impact parameter,

$$\sigma(x,\boldsymbol{r})=C_F\int d^2\boldsymbol{b}_q[\chi(\boldsymbol{b}_q)-\chi(\boldsymbol{b}_q-\boldsymbol{r})]^2,\tag{12}$$

whereas for a dipole made of a parton R and antiparton $\bar{R}$ in the color representation R

$$\begin{aligned}\sigma_{R\bar{R}}(x,\boldsymbol{r})&=2\int d^2\boldsymbol{b}_q\Gamma_{R\bar{R}}(\boldsymbol{b}_q,\boldsymbol{b}_q-\boldsymbol{r})\\&=\int d^2\boldsymbol{b}_q\frac{\langle N|\mathrm{Tr}[\hat{\chi}(\boldsymbol{b}_q)-\hat{\chi}(\boldsymbol{b}_q-\boldsymbol{r})]^2|N\rangle}{\dim[R]}\\&=\frac{C_R}{C_F}\sigma(x,\boldsymbol{r}).\end{aligned}\tag{13}$$

Here C_R is the quadratic Casimir operator for, and dim$[R]$ is the dimension of, the multiplet R.

The $k_\perp$-factorization formula in terms of the glue in the target reads [21,49]

$$\sigma(x,\boldsymbol{r}) = \int d^2\boldsymbol{\kappa} f(x,\boldsymbol{\kappa})[1-\exp(i\boldsymbol{\kappa}\boldsymbol{r})] = \frac{1}{2}\int d^2\boldsymbol{\kappa} f(x,\boldsymbol{\kappa})[1-\exp(i\boldsymbol{\kappa}\boldsymbol{r})][1-\exp(-i\boldsymbol{\kappa}\boldsymbol{r})], \tag{14}$$

where

$$f(x,\boldsymbol{\kappa}) = \frac{4\pi\alpha_S(r)}{N_c}\cdot\frac{1}{\boldsymbol{\kappa}^4}\cdot\mathcal{F}(x,\kappa^2) \tag{15}$$

and

$$\mathcal{F}(x,\kappa^2) = \frac{\partial G(x,\kappa^2)}{\partial\log\kappa^2} \tag{16}$$

is the unintegrated glue in the target nucleon. The second integral form of the dipole cross section is the preferred one from the viewpoint of the summation of four Feynman diagrams with t-channel two-gluon exchange. We shall also encounter the dipole cross section for large $q\bar{q}$ dipoles,

$$\sigma_0(x) \equiv \sigma(x,\infty) = 2C_F\int d^2\boldsymbol{b}_q\chi^2(\boldsymbol{b}_q) = \int d^2\boldsymbol{\kappa} f(x,\boldsymbol{\kappa}). \tag{17}$$

The leading $\log\frac{1}{x}$ evolution of the dipole cross section is governed by the color-dipole Balitsky-Fadin-Kuraev-Lipatov (BFKL) evolution [20,21], the same evolution for the unintegrated gluon density is governed by the familiar momentum-space BFKL equation [50]. Hereafter, unless it may cause confusion, we suppress the variable x in the gluon densities, dipole cross sections, and S-matrices.

B. Basics of the Glauber-Gribov approach

We follow the standard treatment of a nucleus as *an uncorrelated dilute gas of color-singlet nucleons* with the total wave function

$$|A_{\rm in}\rangle = \Psi_{\rm in}(\boldsymbol{r}_A,\ldots,\boldsymbol{r}_i)\prod_{i=1}^{A}|N_i\rangle, \tag{18}$$

where $|N_i\rangle$ is the intrinsic wave function of the nucleon N_i with the coordinate $\boldsymbol{r}_i = (\boldsymbol{b}_i, z_i)$ and $\Psi_{\rm in}(\boldsymbol{r}_A,\ldots,\boldsymbol{r}_i)$ is the configuration-space wave function. Relativistic partons propagate along straight-path trajectories, see the frozen configuration of the nucleus, and the S-matrix for interaction with the nucleus equals (here $\boldsymbol{B} = \boldsymbol{b}_a, \{\boldsymbol{b}_b, \boldsymbol{b}_c\}$) [51,52]

$$S_A(\boldsymbol{B}-\boldsymbol{b}_{\{A\}}) = \prod_{i=1}^{A} S(\boldsymbol{B}-\boldsymbol{b}_i). \tag{19}$$

The matrix product in the color space and the longitudinal ordering $z_A \geq z_{A-1} \geq \ldots \geq z_2 \geq z_1$ are understood.

For the transition from the ground state of the target nucleus to the final state with the nucleon N_i produced in the state $|N_{if}\rangle$ one needs

$$\langle A_f|S_A(\boldsymbol{B})|A_{\rm in}\rangle = \int d^3\boldsymbol{r}_1\ldots d^3\boldsymbol{r}_A\Psi^*_f(\boldsymbol{r}_A,\ldots,\boldsymbol{r}_1)\Psi_{\rm in}(\boldsymbol{r}_A,\ldots,\boldsymbol{r}_1)(\langle N_{Af}|S(\boldsymbol{B}-\boldsymbol{b}_A)|N_A\rangle\cdot\langle N_{(A-1)f}|S(\boldsymbol{B}-\boldsymbol{b}_{A-1})|N_{(A-1)}\rangle \times\ldots\times\langle N_{2f}|S(\boldsymbol{B}-\boldsymbol{b}_2)|N_2\rangle\cdot\langle N_{1f}|S(\boldsymbol{B}-\boldsymbol{b}_1)|N_1\rangle)_{c_fc_i}. \tag{20}$$

The next step is an evaluation of the multiparton $\mathcal{S}_A(\boldsymbol{B}',\boldsymbol{B})$ in (9):

$$\mathcal{S}_A(\boldsymbol{B}',\boldsymbol{B}) = A!\int d^3\boldsymbol{r}'_1\ldots d^3\boldsymbol{r}'_A d^3\boldsymbol{r}_1\ldots d^3\boldsymbol{r}_A\theta(z'_A-z'_{A-1})\ldots\theta(z'_2-z'_1)\theta(z_A-z_{A-1})\ldots\theta(z_2-z_1)\Psi^*_{\rm in}(\boldsymbol{r}'_A,\ldots,\boldsymbol{r}'_1) \times\Psi_f(\boldsymbol{r}'_A,\ldots,\boldsymbol{r}'_1)\Psi^*_f(\boldsymbol{r}_A,\ldots,\boldsymbol{r}_1)\Psi_{\rm in}(\boldsymbol{r}_A,\ldots,\boldsymbol{r}_1)\,{\rm Tr}\{\langle N_1|S^\dagger(\boldsymbol{B}'-\boldsymbol{b}'_1)|N_{1f}\rangle\cdot\langle N_2|S^\dagger(\boldsymbol{B}'-\boldsymbol{b}'_2)|N_{2f}\rangle \times\ldots\times\langle N_A|S^\dagger(\boldsymbol{B}'-\boldsymbol{b}'_A)|N_{Af}\rangle\cdot\langle N_{Af}|S(\boldsymbol{B}-\boldsymbol{b}_A)|N_A\rangle\times\ldots\times\langle N_{2f}|S(\boldsymbol{B}-\boldsymbol{b}_2)|N_2\rangle \cdot\langle N_{1f}|S(\boldsymbol{B}-\boldsymbol{b}_{A-1})|N_1\rangle\}. \tag{21}$$

The color trace in the integrand of (21) contains the product of the string of S-matrices and the string of $S^\dagger$-matrices and graphically can be represented by the color loop diagram in the top part of Fig. 3. Notice the inverted z-ordering in the string for $S^\dagger_A$, by which, after the Fierz transformation, the color loop diagram reduces to the product of matrix elements

$$\langle N_i|S^\dagger(\boldsymbol{B}'-\boldsymbol{b}'_i)|N_{if}\rangle\cdot\langle N_{if}|S(\boldsymbol{B}-\boldsymbol{b}_i)|N_i\rangle \tag{22}$$

for transitions $R_{i-1}\bar{R}_{i-1}\to R_i\bar{R}_i$ with the intermediate state nucleon in the color state $|N_{if}\rangle$, see below Sec. III C. One sums over all allowed multiparton color-singlet states $R_i\bar{R}_i = a\bar{a}$, $a\{\bar{b}\,\bar{c}\}$, $\bar{a}\{bc\}$, $\{bc\}\{\bar{b}\,\bar{c}\}$, where $R_i = \bar{R}_i$ are color representations of the parton and anti-parton systems. This is shown schematically in the bottom part of Fig. 3.

C. Fully inclusive nuclear cross section

First we recall the relevant Glauber-Gribov formalism for the fully inclusive case, when one sums over nuclear

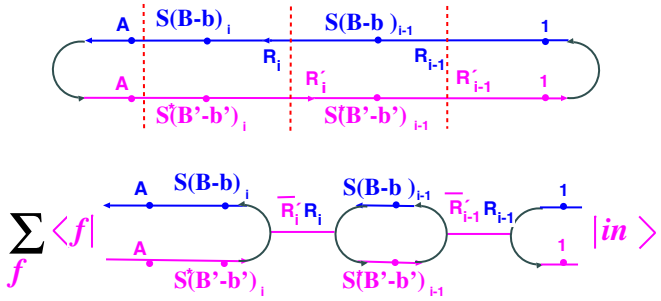

FIG. 3 (color online). The top diagram shows a trace $\mathcal{S}_A(\boldsymbol{B}', \boldsymbol{B})$ of the product of strings of nucleonic matrix elements of S-matrices and $S^\dagger$-matrices which enters the calculation of the dijet spectrum. The bottom diagram shows the result for $\mathcal{S}_A(\boldsymbol{B}', \boldsymbol{B})$ after the Fierz transformation to the basis of multiparton Fock states $R_i\bar{R}_i'$. The color-representation structure of the sum over final states is specified in Appendices A, B, and C.

final states and all color excitations of nucleons. The application of the configuration-space closure relation over nuclear final states gives

$$\sum_f \Psi_f(\boldsymbol{r}_A', \ldots, \boldsymbol{r}_1')\Psi_f^*(\boldsymbol{r}_A, \ldots, \boldsymbol{r}_1) = \prod_{i=1}^A \delta(\boldsymbol{r}_i' - \boldsymbol{r}_i)$$
$$= \prod_{i=1}^A \delta(z_i' - z_i)\delta(\boldsymbol{b}_i' - \boldsymbol{b}_i). \quad (23)$$

Then, upon the application of the closure relation, $\sum_f |N_{if}\rangle\langle N_{if}| = 1$, Eq. (22) reduces to the single-nucleon matrix element

$$\sum_f \langle N|S^\dagger(\boldsymbol{B}' - \boldsymbol{b}_i')|N_{if}\rangle \cdot \langle N_{if}|S(\boldsymbol{B} - \boldsymbol{b}_i)|N\rangle$$
$$= \langle N|S^\dagger(\boldsymbol{B}' - \boldsymbol{b}_i')S(\boldsymbol{B} - \boldsymbol{b}_i)|N\rangle = \mathcal{S}(\boldsymbol{C} - \boldsymbol{b}_i), \quad (24)$$

where $\mathcal{S}(\boldsymbol{C} - \boldsymbol{b}_i)$ is the S-matrix in the basis of multiparton states $R_i\bar{R}_i$ and $\boldsymbol{C}$ is a shorthand notation for sets of impact parameters $\boldsymbol{C} = \{\boldsymbol{B}', \boldsymbol{B}\}, \{\boldsymbol{B}', \boldsymbol{b}\}, \{\boldsymbol{b}', \boldsymbol{B}\}, \{\boldsymbol{b}', \boldsymbol{b}\}$. The coupled-channel multiparton $\mathcal{S}(\boldsymbol{C})$ defines the coupled-channel profile function, $\hat{\Gamma}(\boldsymbol{C}) = \mathbb{1} - \mathcal{S}(\boldsymbol{C})$, and the coupled-channel operator of dipole cross sections, which is obtained upon the integration over the overall impact parameter $\boldsymbol{c}$:

$$\hat{\Sigma}(\boldsymbol{C}) = 2\int d^2\boldsymbol{c}\hat{\Gamma}(\boldsymbol{C}). \quad (25)$$

Equation (21) becomes a target-nucleus expectation value

$$\mathcal{S}_A(\boldsymbol{C}) = A!\int d^3\boldsymbol{r}_1 \ldots d^3\boldsymbol{r}_A\theta(z_A - z_{A-1})\ldots\theta(z_2 - z_1)$$
$$\times \Psi_{\rm in}^*(\boldsymbol{r}_A', \ldots, \boldsymbol{r}_1')\Psi_{\rm in}(\boldsymbol{r}_A, \ldots, \boldsymbol{r}_1)$$
$$\times \prod_{i=1}^A [1 - \hat{\Gamma}(\boldsymbol{C} - \boldsymbol{b}_i)]. \quad (26)$$

In the dilute nucleonic gas approximation

$$|\Psi_{\rm in}(\boldsymbol{r}_A, \ldots, \boldsymbol{r}_1)|^2 = \left(\frac{1}{A}\right)^A \prod_{i=1}^A n_A(\boldsymbol{r}_i), \quad (27)$$

and

$$\mathcal{S}_A(\boldsymbol{C}) = A!\int dz_1 \ldots dz_A\theta(z_A - z_{A-1})\ldots\theta(z_2 - z_1)$$
$$\times \prod_{i=1}^A \left\{\frac{1}{A}\int d^2\boldsymbol{b}_i n_A(z_i, \boldsymbol{b}_i)[1 - \hat{\Gamma}(\boldsymbol{C} - \boldsymbol{b}_i)]\right\}, \quad (28)$$

where the nuclear matter density is normalized according to $\int d^3\vec{r}n_A(\boldsymbol{r}) = A$. The size of the multiparton system is much smaller than the radius of the nucleus and

$$\int d^2\boldsymbol{b}_i n_A(z_i, \boldsymbol{b}_i)\hat{\Gamma}(\boldsymbol{C} - \boldsymbol{b}_i) = n_A(z_i, \boldsymbol{b})\int d^2\boldsymbol{c}\hat{\Gamma}(\boldsymbol{C})$$
$$= \frac{1}{2}\hat{\Sigma}(\boldsymbol{C})n_A(z_i, \boldsymbol{b}), \quad (29)$$

where $\boldsymbol{b}$ is the impact parameter of the multiparton system with respect to the center of mass of the target nucleus. The z-integrations introduce the optical thickness of the nucleus

$$T(\boldsymbol{b}) = \int_{-\infty}^{\infty} dz n_A(\boldsymbol{b}, z). \quad (30)$$

Then the coupled-channel Glauber-Gribov formula [51,52] for the n-parton states is

$$\mathcal{S}_A^{(n)}(\boldsymbol{C}) = \left[1 - \frac{1}{2A}\hat{\Sigma}^{(n)}(\boldsymbol{C})T(\boldsymbol{b})\right]^A$$
$$= \exp\left[-\frac{1}{2}\hat{\Sigma}^{(n)}(\boldsymbol{C})T(\boldsymbol{b})\right] = S[\boldsymbol{b}, \Sigma^{(n)}(\boldsymbol{C})]. \quad (31)$$

The exponentiation holds for medium to heavy nuclei.

D. Separation of elastic and color-excitation scattering

The generalization of the Glauber-Gribov representation to final states with a fixed number of color-excited nucleons proceeds as follows. Let the propagating system—

either incident parton a or the produced state bc undergo color-excitation interactions with nucleons $k_1, \ldots, k_\nu$ at impact parameters $\boldsymbol{c}_1, \ldots, \boldsymbol{c}_\nu$, and color-diagonal, elastic interactions with all other nucleons $\{1, \ldots, k_1 - 1\}, \{k_1 + 1, \ldots, k_2 - 1\}, \ldots, \{k_\nu + 1, \ldots, A\}$ at corresponding sets of impact parameters $\{\boldsymbol{b}_i\}$. A configuration-space closure over nuclear final states is understood; we are only after the color algebra. The case of $\nu = 0$, i.e., diffractive interaction without color excitations, must be included too. The operator of interest, summed over fixed configurations of scatterers, is

$$\begin{aligned}\mathcal{G}_\nu(\boldsymbol{C}, \{\boldsymbol{b}_j\}, \{\boldsymbol{c}_i\}) = \sum_{k_\nu > k_\nu - 1 > \ldots > k_1}^{A} \mathrm{Tr}\Big\{\Big[\prod_{i=1}^{k_1-1}\langle N_i|S^\dagger(\boldsymbol{B}' - \boldsymbol{b}_i)|N_i\rangle\Big]\langle N_1|S^\dagger(\boldsymbol{B}' - \boldsymbol{c}_1)|N_1^*\rangle\Big[\prod_{i=k_1+1}^{k_2-1}\langle N_i|S^\dagger(\boldsymbol{B}' - \boldsymbol{b}_i)|N_i\rangle\Big] \times \ldots \\ \times \langle N_\nu|S^\dagger(\boldsymbol{B}' - \boldsymbol{c}_\nu)|N_\nu^*\rangle \times \Big[\prod_{i=k_\nu+1}^{A}\langle N_i|S^\dagger(\boldsymbol{B}' - \boldsymbol{b}_i)|N_i\rangle\Big]\Big[\prod_{i=k_\nu+1}^{A}\langle N_i|S(\boldsymbol{B} - \boldsymbol{b}_i)|N_i\rangle\Big]\langle N_\nu^*|S(\boldsymbol{B} - \boldsymbol{c}_\nu)|N_\nu\rangle \\ \times \ldots \times \Big[\prod_{i=k_1+1}^{k_2-1}\langle N_i|S(\boldsymbol{B} - \boldsymbol{b}_i)|N_i\rangle\Big]\langle N_1^*|S(\boldsymbol{B} - \boldsymbol{c}_1)|N_1\rangle\prod_{i=1}^{k_1-1}\Big[\langle N_i|S(\boldsymbol{B} - \boldsymbol{b}_i)|N_i\rangle\Big]\Big\} \\ + \delta_{\nu 0}\,\mathrm{Tr}\Big\{\Big[\prod_{i=A}^{1}\langle N_i|S^\dagger(\boldsymbol{B}' - \boldsymbol{b}_i)|N_i\rangle\Big]\prod_{i=1}^{A}[\langle N|S(\boldsymbol{B} - \boldsymbol{b}_i)|N\rangle]\Big\}. \qquad (32)\end{aligned}$$

Here $|N_i^*\rangle$ denotes the color-excited nucleon. Based on the above described Fierz transformation technique, we reduce (32) to the product of multiparton operators.

Let $\hat{\chi}(\boldsymbol{B})$ and $\hat{\chi}(\boldsymbol{B}')$ be the eikonals for the interaction with the nucleon of the partonic and antipartonic system, respectively. The terms linear in $\hat{\chi}(\boldsymbol{B})$ and $\hat{\chi}(\boldsymbol{B}')$ in the expansion (10) do not contribute to color-diagonal interactions, where one encounters

$$\begin{aligned}\mathbb{1} - \hat{\Gamma}_{\mathrm{el}}(\boldsymbol{C} - \boldsymbol{b}) &= \langle N|S^\dagger(\boldsymbol{B}' - \boldsymbol{b})|N\rangle\langle N|S(\boldsymbol{B} - \boldsymbol{b})|N\rangle = \langle N|S^\dagger(\boldsymbol{B}' - \boldsymbol{b})|N\rangle\langle N|\mathbb{1}|N\rangle + \langle N|\mathbb{1}|N\rangle\langle N|S(\boldsymbol{B} - \boldsymbol{b})|N\rangle - \mathbb{1} \\ &= \mathbb{1} - \frac{1}{2}[\langle N|\hat{\chi}^2(\boldsymbol{B} - \boldsymbol{b})|N\rangle + \langle N|\hat{\chi}^2(\boldsymbol{B}' - \boldsymbol{b})|N\rangle]. \qquad (33)\end{aligned}$$

It sums the Feynman diagrams of Fig. 4(a) and 4(b) when both gluons are exchanged with either a partonic or antipartonic subsystem. The profile function $\hat{\Gamma}_{\mathrm{el}}(\boldsymbol{C})$ is still an operator in the space of multiparton color-singlet states. The color-excitation scattering is described by diagrams of Fig. 4(c) and 4(d) in which one of the t-channel gluons is exchanged with the partonic subsystem while the second is exchanged with the antipartonic subsystem. Only the terms linear in $\hat{\chi}(\boldsymbol{B})$ and $\hat{\chi}(\boldsymbol{B}')$ in the expansion (10) contribute. The diagonal matrix elements vanish, $\langle N|\hat{\chi}(\boldsymbol{B}' - \boldsymbol{c})|N\rangle = 0$, and one can sum over unobservable color states of excited nucleons N^* making use of the closure:

$$\begin{aligned}\hat{\Gamma}_{\mathrm{ex}}(\boldsymbol{C}) &= -\sum_{N^*}\langle N|S^\dagger(\boldsymbol{B}' - \boldsymbol{c})|N^*\rangle\langle N^*|S(\boldsymbol{B} - \boldsymbol{c})|N\rangle \\ &= -\sum_{N^*}\langle N|\hat{\chi}(\boldsymbol{B}' - \boldsymbol{c})|N^*\rangle\langle N^*|\hat{\chi}(\boldsymbol{B} - \boldsymbol{c})|N\rangle \\ &= -\langle N|\hat{\chi}(\boldsymbol{B}' - \boldsymbol{c})\hat{\chi}(\boldsymbol{B} - \boldsymbol{c})|N\rangle. \qquad (34)\end{aligned}$$

Now we notice that $\hat{\Gamma}(\boldsymbol{C}) = \hat{\Gamma}_{\mathrm{ex}}(\boldsymbol{C}) + \hat{\Gamma}_{\mathrm{el}}(\boldsymbol{C})$ and

$$\hat{\Sigma}_{\mathrm{ex}}(\boldsymbol{C}) + \hat{\Sigma}_{\mathrm{el}}(\boldsymbol{C}) = \hat{\Sigma}(\boldsymbol{C}) \qquad (35)$$

holds for the corresponding cross section operators, $\hat{\Sigma}_{\mathrm{el,ex}}(\boldsymbol{C}) = 2\int d^2\boldsymbol{c}\,\Gamma_{\mathrm{el,ex}}(\boldsymbol{C})$.

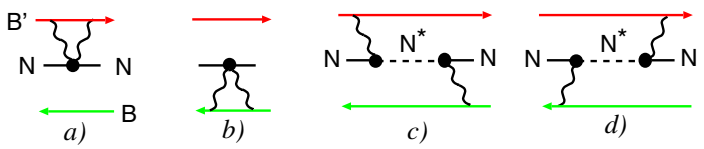

FIG. 4 (color online). Color-diagonal elastic (a, b) and color-excitation (c, d) scattering of multiparton states. In elastic scattering both gluons couple to either the partonic subsystem at impact parameters $\{\boldsymbol{B}\}$ or the antipartonic subsystem at impact parameters $\{\boldsymbol{B}'\}$. In color-excitation scattering one gluon couples to the partonic subsystem and the other to the antipartonic subsystem.

E. The unitarity relation for color excitation of the nucleus

In terms of $\Gamma_{\rm ex}(\boldsymbol{C})$ and $\Gamma_{\rm el}(\boldsymbol{C})$ we obtain

$$\mathcal{G}_\nu(\boldsymbol{C},\{\boldsymbol{b}_j\},\{\boldsymbol{c}_i\}) = \sum_{k_\nu>k_\nu-1>\ldots>k_1}^{A}\Big\{\prod_{i=k_\nu+1}^{A}[1-\hat\Gamma_{\rm el}(\boldsymbol{C}-\boldsymbol{b}_i)]\Big\}\cdot\{-\hat\Gamma_{\rm ex}(\boldsymbol{C}-\boldsymbol{c}_\nu)\}\Big\{\prod_{i=k_{\nu-1}+1}^{k_\nu-1}[1-\hat\Gamma_{\rm el}(\boldsymbol{C}-\boldsymbol{b}_i)]\Big\}\ldots$$
$$\times\Big\{\prod_{i=k_1+1}^{k_2-1}[1-\hat\Gamma_{\rm el}(\boldsymbol{C}-\boldsymbol{b}_i)]\Big\}\{-\hat\Gamma_{\rm ex}(\boldsymbol{C}-\boldsymbol{c}_1)\}\Big\{\prod_{i=1}^{k_1-1}[1-\hat\Gamma_{\rm el}(\boldsymbol{C}-\boldsymbol{b}_i)]\Big\}+\delta_{\nu 0}\Big\{\prod_{i=1}^{A}[1-\hat\Gamma_{\rm el}(\boldsymbol{C}-\boldsymbol{b}_i)]\Big\}, \tag{36}$$

where the last term, $\propto\delta_{\nu 0}$, describes CD. Now, consider an expansion of

$$\prod_{i=1}^{A}[1-\hat\Gamma(\boldsymbol{C}-\boldsymbol{b}_i)]=\prod_{i=1}^{A}[1-\hat\Gamma_{\rm el}(\boldsymbol{C}-\boldsymbol{b}_i)-\hat\Gamma_{\rm ex}(\boldsymbol{C}-\boldsymbol{b}_i)] \tag{37}$$

in powers of $\hat\Gamma_{\rm ex}$. One must be careful about the ordering of the not-commuting $\hat\Gamma_{\rm ex}(\boldsymbol{C})$ and $\hat\Gamma_{\rm el}(\boldsymbol{C})$:

$$\prod_{i=1}^{A}[1-\hat\Gamma_{\rm el}(\boldsymbol{C}-\boldsymbol{b}_i)-\hat\Gamma_{\rm ex}(\boldsymbol{C}-\boldsymbol{b}_i)]=\prod_{i=1}^{A}[1-\hat\Gamma_{\rm el}(\boldsymbol{C}-\boldsymbol{b}_i)]+\sum_{k_1=1}^{A}\Big\{\prod_{i=k+1}^{A}[1-\hat\Gamma_{\rm el}(\boldsymbol{C}-\boldsymbol{b}_i)]\Big\}\{-\hat\Gamma_{\rm ex}(\boldsymbol{C}-\boldsymbol{b}_{k_1})\}$$
$$\times\Big\{\prod_{i=1}^{k-1}[1-\hat\Gamma_{\rm el}(\boldsymbol{C}-\boldsymbol{b}_i)]\Big\}+\sum_{k_2>k_1=1}^{A}\Big\{\prod_{i=k_2+1}^{A}[1-\hat\Gamma_{\rm el}(\boldsymbol{C}-\boldsymbol{b}_i)]\Big\}\{-\hat\Gamma_{\rm ex}(\boldsymbol{C}-\boldsymbol{b}_{k_2})\}$$
$$\times\Big\{\prod_{i=1}^{k_2-1}[1-\hat\Gamma_{\rm el}(\boldsymbol{C}-\boldsymbol{b}_i)]\Big\}\{-\hat\Gamma_{\rm ex}(\boldsymbol{C}-\boldsymbol{b}_{k_1})\}\Big\{\prod_{i=1}^{k_1-1}[1-\hat\Gamma_{\rm el}(\boldsymbol{C}-\boldsymbol{b}_i)]\Big\}+\ldots$$
$$=\sum_{\nu=0}^{A}\mathcal{G}_\nu(\boldsymbol{C},\{\boldsymbol{b}_j\},\{\boldsymbol{c}_i\}), \tag{38}$$

where $\{\boldsymbol{c}_i\}\equiv\{\boldsymbol{b}_{k_i}\}$. This identification of $\mathcal{G}_\nu(\boldsymbol{C},\{\boldsymbol{b}_j\},\{\boldsymbol{c}_i\})$ furnishes a proof of the unitarity relation: the reaction operators for topological cross sections with color excitation of ν nucleons sum up to exactly the reaction operator for the total cross section.

The operators $\hat\Gamma_{\rm ex}(\boldsymbol{C})$ and $\hat\Gamma_{\rm el}(\boldsymbol{C})$ separate specific color transitions and, in the general case, will have certain infrared sensitivity. The above proof of the unitarity shows that this infrared sensitivity exactly cancels out in the total cross section described by the infrared-safe $\hat\Gamma(\boldsymbol{C})$.

F. Color excitation of a nucleus: cut and uncut Pomerons

The above proof of the unitarity relation spares the rederivation of the nuclear matrix element

$$\mathcal{S}_{A,\nu}(\boldsymbol{C})=\langle A_{\rm in}|\mathcal{G}_\nu(\boldsymbol{C},\{\boldsymbol{b}_j\},\{\boldsymbol{c}_i\})|A_{\rm in}\rangle. \tag{39}$$

It is obtained by a direct expansion of the Glauber-Gribov result (31) in powers of $\hat\Sigma_{\rm ex}$. Going from z_i to a depth in the nucleus in units of $T(\boldsymbol{b})$,

$$\beta_i T(\boldsymbol{b})=\int_{-\infty}^{z_i}dz n_A(\boldsymbol{b},z), \tag{40}$$

we find

$$\mathcal{S}_{A,\nu}(\boldsymbol{C})=\int_0^1 d\beta_\nu\ldots d\beta_1\theta(1-\beta_\nu)\theta(\beta_\nu-\beta_{\nu-1})\ldots\theta(\beta_2-\beta_1)\theta(\beta_1)\exp[-\tfrac{1}{2}(1-\beta_\nu)\hat\Sigma_{\rm el}(\boldsymbol{C})T(\boldsymbol{b})]\{-\tfrac{1}{2}\hat\Sigma_{\rm ex}(\boldsymbol{C})T(\boldsymbol{b})\}$$
$$\times\exp[-\tfrac{1}{2}(\beta_\nu-\beta_{\nu-1})\hat\Sigma_{\rm el}(\boldsymbol{C})T(\boldsymbol{b})]\ldots\{-\tfrac{1}{2}\hat\Sigma_{\rm ex}(\boldsymbol{C})T(\boldsymbol{b})\}\exp[-\tfrac{1}{2}\beta_1\hat\Sigma_{\rm el}(\boldsymbol{C})T(\boldsymbol{b})]+\delta_{\nu 0}\exp[-\tfrac{1}{2}\hat\Sigma_{\rm el}(\boldsymbol{C})T(\boldsymbol{b})]. \tag{41}$$

An alternative derivation of (41) is useful. The heavy-nucleus Glauber-Gribov result (31) can be viewed as a solution of the differential equation

$$\frac{d}{dz}\mathcal{S}_A(\boldsymbol{C},z)=-\frac{1}{2}n_A(\boldsymbol{b},z)\hat{\Sigma}(\boldsymbol{C})\mathcal{S}_A(\boldsymbol{C},z) \tag{42}$$

i.e.,

$$\begin{aligned}\frac{d}{d\beta}\mathcal{S}_A(\boldsymbol{C},\beta)&=-\frac{1}{2}T(\boldsymbol{b})\hat{\Sigma}(\boldsymbol{C})\mathcal{S}_A(\boldsymbol{C},\beta)\\&=-\frac{1}{2}T(\boldsymbol{b})[\hat{\Sigma}_{\rm el}(\boldsymbol{C})+\hat{\Sigma}_{\rm ex}(\boldsymbol{C})]\mathcal{S}_A(\boldsymbol{C},\beta)\end{aligned} \tag{43}$$

subject to the boundary condition $\mathcal{S}_A(\boldsymbol{C},0)=\mathbb{1}$. A full thickness of the nucleus corresponds to $\beta=1$. Solve this equation treating $\hat{\Sigma}_{\rm ex}$ as a perturbation. The νth iteration will give precisely (41).

Finally, the counterpart of $\mathcal{T}(\boldsymbol{B},\boldsymbol{B}',\boldsymbol{b},\boldsymbol{b}')$ of Eq. (9) takes the form

$$\begin{aligned}\mathcal{T}_\nu(\boldsymbol{B},\boldsymbol{B}',\boldsymbol{b},\boldsymbol{b}')&=\mathcal{S}^{(4)}_{A,\nu}(\boldsymbol{B}',\boldsymbol{B})+\mathcal{S}^{(2)}_{A,\nu}(\boldsymbol{b}',\boldsymbol{b})\\&\quad-\mathcal{S}^{(3)}_{A,\nu}(\boldsymbol{B}',\boldsymbol{b})-\mathcal{S}^{(3)}_{A,\nu}(\boldsymbol{b}',\boldsymbol{B}).\end{aligned} \tag{44}$$

Equations (41) and (44) are our manifestly unitary master formulas for the hard scattering accompanied by color excitation of ν-nucleons. They allow us to classify the color-excitation final states according to the universality classes for nonlinear $k_\perp$-factorization introduced in [27,29]. A contact with the Reggeon field theory is obvious: *each and every* $\hat{\Sigma}_{\rm ex}$ *will be associated with a cut Pomeron, while the exponentials of* $\hat{\Sigma}_{\rm el}$ *resum absorption corrections for multiple exchanges by the uncut Pomerons.*

IV. COLLECTIVE NUCLEAR GLUE: CUT AND UNCUT NUCLEAR POMERONS AND SEQUENTIAL QUASIELASTIC RESCATTERING OF QUARKS

A. Collective glue from the color-dipole S-matrix

In the master formula (7) for the dijet cross section one encounters the Fourier transform of the nuclear S-matrix $S[\boldsymbol{b},\hat{\Sigma}(\boldsymbol{C})]$. The matrix elements of $\hat{\Sigma}(\boldsymbol{C})$ are superpositions of the elementary dipole cross sections and, consequently, $S[\boldsymbol{b},\Sigma(\boldsymbol{C})]$ will be a product of S matrices for elementary dipoles. The Fourier transform of $S[\boldsymbol{b},\sigma(x,\boldsymbol{r})]$ for the elementary $q\bar{q}$ dipole gives the amplitude for coherent excitation of hard dijets in πA collisions—the reference process for the definition of the collective nuclear unintegrated glue [23,24,31].

Specifically, for the color triplet-antitriplet dipoles we define

$$\begin{aligned}\Phi(\boldsymbol{b},x,\boldsymbol{\kappa})&=\frac{1}{(2\pi)^2}\int d^2\boldsymbol{r}S[\boldsymbol{b},\sigma(x,\boldsymbol{r})]\exp[-i\boldsymbol{\kappa}\boldsymbol{r}]\\&=S[\boldsymbol{b},\sigma_0(x)]\delta^{(2)}(\boldsymbol{\kappa})+\phi(\boldsymbol{b},x,\boldsymbol{\kappa}),\end{aligned} \tag{45}$$

$$\begin{aligned}1-S[\boldsymbol{b},\sigma(x,\boldsymbol{r})]&=\int d^2\boldsymbol{\kappa}\phi(\boldsymbol{b},x,\boldsymbol{\kappa})[1-\exp(i\boldsymbol{\kappa}\boldsymbol{r})]\\&=\tfrac{1}{2}\int d^2\boldsymbol{\kappa}\phi(\boldsymbol{b},x,\boldsymbol{\kappa})[1-\exp(i\boldsymbol{\kappa}\boldsymbol{r})]\\&\quad\times[1-\exp(-i\boldsymbol{\kappa}\boldsymbol{r})],\end{aligned} \tag{46}$$

where $\phi(\boldsymbol{b},x,\boldsymbol{\kappa})$ is a collective unintegrated glue per unit area in the impact parameter plane. The second form of (46) is the preferred one from the Feynman diagram viewpoint. The collective nuclear glue admits a simple expansion in terms of the collective glue, $f^{(j)}(x,\boldsymbol{\kappa})$, for j spatially overlapping nucleons of the Lorentz-contracted ultrarelativistic nucleus:

$$\phi(\boldsymbol{b},x,\boldsymbol{\kappa})=\frac{1}{\sigma_0(x)}\sum_{j=1}w_j(\nu_A(\boldsymbol{b}))f^{(j)}(x,\boldsymbol{\kappa}). \tag{47}$$

Here

$$f^{(j)}(x,\boldsymbol{\kappa})=\frac{1}{\sigma_0(x)}\int d^2\boldsymbol{\kappa}_1\cdot f(x,\boldsymbol{\kappa}_1)f^{(j-1)}(x,\boldsymbol{\kappa}-\boldsymbol{\kappa}_1), \tag{48}$$

where $f^{(1)}(x,\boldsymbol{\kappa})=f(x,\boldsymbol{\kappa})$, an extension to $j=0$ is $f^{(0)}(x,\boldsymbol{\kappa})=\sigma_0(x)\delta^{(2)}(\boldsymbol{\kappa})$,

$$w_j(\nu_A(\boldsymbol{b}))=\frac{1}{j!}\nu_A^j(\boldsymbol{b})S[\boldsymbol{b},\sigma_0(x)] \tag{49}$$

is a probability to find j spatially overlapping nucleons in the tube of cross section $\frac{1}{2}\sigma_0(x)$ in the Lorentz-contracted ultrarelativistic nucleus and

$$\nu_A(\boldsymbol{b})=\tfrac{1}{2}\sigma_0(x)T(\boldsymbol{b}) \tag{50}$$

is the thickness of the nucleus in units of the interaction length for large dipoles. All $f^{(j)}(x,\boldsymbol{\kappa})$ have the same normalization $\int d^2\boldsymbol{\kappa}f^{(j)}(x,\boldsymbol{\kappa})=\sigma_0(x)$.

B. Collective glue: from the optical theorem perspective to a coherent state of the in-vacuum gluons

The expansion (47) admits two interpretations. On the one hand, from the optical theorem perspective, $f(x,\boldsymbol{\kappa})$ describes the unitarity cut $\not{P}$ of the t-channel Pomeron $\mathbb{P}$—a color-singlet composite state of two (reggeized) in-vacuum gluons g_R in the t-channel, Figs. 5(a) and 5(b). Likewise, the $q\bar{q}$ dipole-nucleus total cross section equals [19]

$$\frac{d\sigma_A(x,\boldsymbol{r})}{d^2\boldsymbol{b}}=2\int d^2\boldsymbol{\kappa}\phi(\boldsymbol{b},x,\boldsymbol{\kappa})[1-\exp(i\boldsymbol{\kappa}\boldsymbol{r})]. \tag{51}$$

For very large dipoles we tentatively identify the (inelastic) quark-nucleus cross section

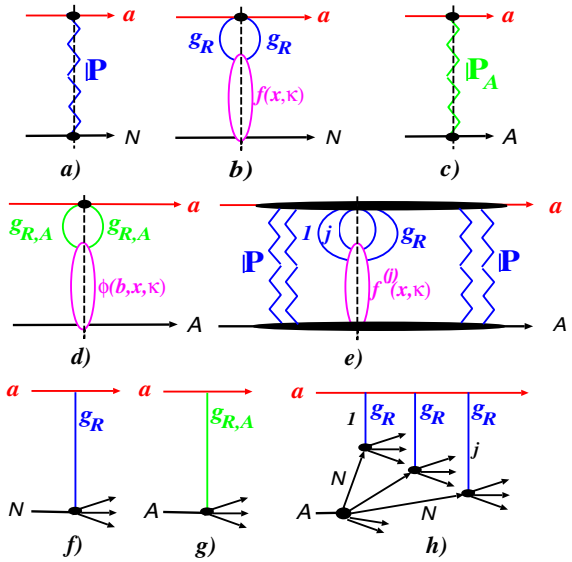

FIG. 5 (color online). The cut-Pomeron interpretation of the unintegrated glue: (a) the optical theorem unitarity cut for aN scattering; (b) the unitarity cut in terms of the exchange by two in-vacuum Reggeized gluons in the t-channel and the free-nucleon glue $f(x, \boldsymbol{\kappa})$; (c) the optical theorem for a nuclear target, and (d) its tentative interpretation in terms of the unitarity cut of the exchange by two coherent nuclear gluons $g_{R,A}$ in the t-channel, and the collective nuclear gluon density $\phi(\boldsymbol{b}, x, \boldsymbol{\kappa})$; (e) the contribution to the cut nuclear Pomeron from the j in-vacuum gluon component of the coherent nuclear gluon $g_{R,A}$ and the related collective gluon density $f^{(j)}(x, \boldsymbol{\kappa})$, the absorption corrections for the exchange by uncut Pomerons on either side of the unitarity cut are indicated; (f) the final state in the unitarity diagram (b) in terms of the quasielastic scattering of the quark a by the t-channel exchange by the in-vacuum gluon g_R, (g) quasielastic scattering of a quark a off a nucleus by exchange by the coherent nuclear gluon $g_{R,A}$; (h) t-channel exchange by a jg_R component of the coherent nuclear glue in terms of the sequential j-fold quasielastic aN scattering in the aA interaction, the absorption by uncut Pomerons explicit in diagram (e) is suppressed here.

$$\frac{d\sigma_{qA}(x)}{d^2\boldsymbol{b}} = \int d^2\boldsymbol{\kappa}\phi(\boldsymbol{b}, x, \boldsymbol{\kappa}) \tag{52}$$

and, in the optical theorem perspective, view it as a unitarity cut of the exchange by a nuclear Pomeron $\mathbb{P}_A$, Fig. 5(c). In the analogy to the in-vacuum Pomeron, we view $\mathbb{P}_A$ as a composite state of two nuclear (Reggeized) gluons $g_{R,A}$. The cut Pomeron $\mathbb{P}_A$ in terms of $g_{R,A}$ on two sides of the unitarity cut, and the role of the collective $\phi(\boldsymbol{b}, x, \boldsymbol{\kappa})$, are shown in Fig. 5(d).

Furthermore, the Poisson distribution (49) suggests that such an operationally defined $g_{R,A}$ can be viewed as a coherent state [53] of the in-vacuum gluons g_R with the average multiplicity $\langle j\rangle = \nu_A(\boldsymbol{b})$. The j-gluon composite component of $g_{R,A}$ describes the j-gluon unitarity cut, Fig. 5(e), of the $2jg_R$ component of the Pomeron $\mathbb{P}_A$. This composite state $\mathbb{P}_A^{(2j)}$ will be associated with the collective glue $f^{(j)}(x, \boldsymbol{\kappa})$ and is universal for all targets. What changes from one nuclear target to another is the probability $w_j(\nu_A(\boldsymbol{b}))$ in the expansion (47). Finally, the kth order term in

$$S[\boldsymbol{b}, \sigma_0(x)] = \sum_{j=0}\frac{1}{k!}(-1)^k\left[\frac{1}{2}T(\boldsymbol{b})\right]^k\left[\int d^2\boldsymbol{\kappa}f(x, \boldsymbol{\kappa})\right]^k \tag{53}$$

can be viewed as an absorption correction for k uncut-Pomeron exchanges as indicated in Fig. 5(e). These highly tentative operational definitions for uncut and cut-Pomeron exchanges need a qualification which can only be achieved by consideration of specific final states.

C. Collective glue and quasielastic quark-nucleus scattering

On the other hand, according to Ref. [31], the differential cross section of inclusive quasielastic quark-nucleon scattering, $qN \to q'N^*$, summed over all excitations of the target nucleon, is linear $k_\perp$-factorizable,

$$\frac{d\sigma_{\rm Qel}}{d^2\boldsymbol{q}} = \frac{1}{2}f(x, \boldsymbol{q}), \tag{54}$$

where $\boldsymbol{q}$ is the transverse momentum of the scattered quark. One would identify the unintegrated glue with the cut-Pomeron contribution to the leading-quark spectrum, cf. diagrams 5(b) and 5(f). This $k_\perp$-factorization is exact to the Born approximation, to higher orders it holds to the leading $\log\frac{1}{x}$ ($\mathrm{LL}\frac{1}{x}$) approximation, when the radiation energy loss is neglected.

The total cross section of the quasielastic scattering integrates to

$$\sigma_{\rm Qel} = \tfrac{1}{2}\sigma_0(x) \tag{55}$$

and the differential cross section of the ν-fold quasielastic scattering equals

$$\frac{d\sigma^{(\nu)}_{\rm Qel}(\boldsymbol{q})}{d^2\boldsymbol{q}} = \frac{1}{\sigma_{\rm Qel}}\int d^2\boldsymbol{\kappa}\frac{d\sigma^{(\nu)}_{\rm Qel}(\boldsymbol{\kappa})}{d^2\boldsymbol{\kappa}}\frac{d\sigma^{(\nu-1)}_{\rm Qel}(\boldsymbol{q}-\boldsymbol{\kappa})}{d^2\boldsymbol{q}} = \frac{1}{2}f^{(\nu)}(x, \boldsymbol{q}). \tag{56}$$

To the Born approximation, quasielastic scattering exhausts the inelastic quark-nucleus interaction. According to Ref. [31], the linear $k_\perp$-factorization (54) extends to nuclear targets too,

$$\frac{d\sigma_{{\rm Qel},A}}{d^2\boldsymbol{b}d^2\boldsymbol{q}} = \phi(\boldsymbol{b}, x, \boldsymbol{q}), \tag{57}$$

and here we invoke a similarity between the sets of diagrams 5(b), 5(d), 5(f), and 5(g). Making use of (47) and (56), it can be cast in the form of the Glauber multiple-scattering expansion for quasielastic scattering [51]:

$$\frac{d\sigma_{\mathrm{Qel},A}}{d^2\boldsymbol{b}d^2\boldsymbol{q}} = \sum_{j=1} w_j(\nu_A(\boldsymbol{b}))\frac{d\sigma^{(j)}_{\mathrm{Qel}}(\boldsymbol{q})}{\sigma_{\mathrm{Qel}}d^2\boldsymbol{q}}. \tag{58}$$

Correspondingly, the probability $w_\nu(\nu_A(\boldsymbol{b}))$ to find ν spatially overlapping nucleons in the Lorentz-contracted nucleus amounts, in the target-nucleus frame, to the probability of the ν-fold quasielastic scattering of the quark. In the AGK language, $d\sigma^{(\nu)}_{\mathrm{Qel}}(\boldsymbol{q})/d^2\boldsymbol{q}$ describes the contribution from ν cut Pomerons to the leading-quark spectrum. Here we emphasize that the final state in Fig. 5(h) corresponds to precisely the Mandelstam cut structure [54] of Fig. 5(e). Screening by uncut Pomerons is encoded in $S[\boldsymbol{b}, \sigma_0(x)]$—it gives the alternating sign series in terms of the uncut multi-Pomeron exchanges, familiar from models for absorption corrections.

D. Intranuclear distortion of color dipoles and multi-Pomeron exchanges

In the calculation of topological cross sections we shall often encounter the Glauber-Gribov S-matrix $S[\boldsymbol{b}, \frac{1}{2}\beta\sigma(x,\boldsymbol{r})]$ for a finite slice $[0,\beta]$ of a nucleus. It defines the corresponding collective glue for a slice of a nucleus

$$S[\boldsymbol{b}, \beta\sigma(x,\boldsymbol{r})] = \int d^2\boldsymbol{\kappa}\Phi(\beta;\boldsymbol{b},x,\boldsymbol{\kappa})\exp[i\boldsymbol{\kappa}\boldsymbol{r}]. \tag{59}$$

Evidently, $\Phi(\beta;\boldsymbol{b},x,\boldsymbol{\kappa})$ will expand in terms of the same $f^{(j)}(x,\boldsymbol{\kappa})$, only the expansion coefficients would change:

$$w_j(\beta\nu_A(\boldsymbol{b})) = \frac{1}{j!}\beta^j\nu_A^j(\boldsymbol{b})S[\boldsymbol{b}, \beta\sigma_0(x)]. \tag{60}$$

A pertinent quantity in our derivations will be the coherently distorted wave functions of color dipoles

$$\Psi(\beta;z,\boldsymbol{r}) \equiv S[\boldsymbol{b}, \beta\sigma(x,\boldsymbol{r})]\Psi(z,\boldsymbol{r}). \tag{61}$$

In the practical evaluations in the momentum space it is convenient to use

$$\begin{aligned}\Psi(\beta;z,\boldsymbol{p}) &= \int d^2\boldsymbol{r}\exp[-i\boldsymbol{p}\boldsymbol{r}]\Psi(\beta;z,\boldsymbol{r})\\ &= \int d^2\boldsymbol{\kappa}\Phi(\beta,\boldsymbol{b},x,\boldsymbol{\kappa})\Psi(z,\boldsymbol{p}-\boldsymbol{\kappa})\\ &= S[\boldsymbol{b},\beta\sigma_0(x)]\Psi(z,\boldsymbol{p})\\ &\quad + \int d^2\boldsymbol{\kappa}\phi(\beta;\boldsymbol{b},x,\boldsymbol{\kappa})\Psi(z,\boldsymbol{p}-\boldsymbol{\kappa}),\end{aligned} \tag{62}$$

where $\phi(\beta,\boldsymbol{b},x,\boldsymbol{\kappa})$ is positive defined one. The wave function distortions shall always be described by the uncut multi-Pomeron exchanges. In terms of an exchange by the uncut collective nuclear Pomeron $\mathbb{P}_A(\beta)$

$$\begin{aligned}\Psi(\beta;z,\boldsymbol{p}) &= \Psi(z,\boldsymbol{p}) - \tfrac{1}{2}\int d^2\boldsymbol{p}_1 d^2\boldsymbol{\kappa}[2\delta(\boldsymbol{p}-\boldsymbol{p}_1)\\ &\quad - \delta(\boldsymbol{p}-\boldsymbol{\kappa}-\boldsymbol{p}_1) - \delta(\boldsymbol{p}+\boldsymbol{\kappa}-\boldsymbol{p}_1)]\\ &\quad \times \phi(\beta;\boldsymbol{b},x,\boldsymbol{\kappa})\Psi(z,\boldsymbol{p}_1)\\ &\equiv \Psi(z,\boldsymbol{p}) - (\mathbb{P}_A(\beta)\otimes\Psi)(z,\boldsymbol{p}).\end{aligned} \tag{63}$$

The Feynman diagram interpretation of the four terms in the convolution in (63) is the same as for the amplitude of diffractive DIS [19,23]. The kernel $\mathbb{P}_A(\beta)$ can further be expanded in terms of the in-vacuum Pomeron exchanges. If we define

$$\begin{aligned}(\mathbb{P}\otimes\Psi)(z,\boldsymbol{p}) &\equiv \tfrac{1}{2}\int d^2\boldsymbol{p}_1 d^2\boldsymbol{\kappa}[2\delta(\boldsymbol{p}-\boldsymbol{p}_1)\\ &\quad - \delta(\boldsymbol{p}-\boldsymbol{\kappa}-\boldsymbol{p}_1) - \delta(\boldsymbol{p}+\boldsymbol{\kappa}-\boldsymbol{p}_1)]\\ &\quad \times f(x,\boldsymbol{\kappa})\Psi(z,\boldsymbol{p}_1),\end{aligned} \tag{64}$$

then the multi-Pomeron exchange expansion for (63) would read

$$\begin{aligned}\Psi(\beta;z,\boldsymbol{p}) &= \Psi(z,\boldsymbol{p}) - \sum_{\nu=1}\frac{1}{\nu!}(-1)^{\nu-1}\left[\frac{\beta}{2}T(\boldsymbol{b})\right]^\nu(\underbrace{\mathbb{P}\otimes\ldots\otimes\mathbb{P}}_{\nu}\otimes\Psi)(z,\boldsymbol{p})\\ &= \Psi(z,\boldsymbol{p}) - \sum_{\nu=1}\frac{1}{\nu!}(-1)^{\nu-1}\left[\frac{\beta}{2}T(\boldsymbol{b})\right]^\nu\left(\frac{1}{2}\right)^\nu\int d^2\boldsymbol{p}_1 d^2\boldsymbol{\kappa}_1\ldots d^2\boldsymbol{\kappa}_\nu f(x,\boldsymbol{\kappa}_1)\ldots f(x,\boldsymbol{\kappa}_\nu)\Psi(\beta;z,\boldsymbol{p}_1)\\ &\quad\times\sum_{i,j,k,l=0}\frac{\nu!}{i!j!k!l!}(-1)^{k+l}\delta(\nu-i-j-k-l)\delta\left(\boldsymbol{p}-\sum_1^k\boldsymbol{\kappa}_m+\sum_{k+1}^{k+l}\boldsymbol{\kappa}_n-\boldsymbol{p}_1\right).\end{aligned} \tag{65}$$

Although only a special subset of the momenta $\boldsymbol{\kappa}_{m,n}$ appears in the last delta-function, the combinatorial structure of Eq. (65) corresponds to summing over all the relevant permutations of $\boldsymbol{\kappa}_1,\ldots,\boldsymbol{\kappa}_\nu$.

Now we proceed to applications to DIS and other hard processes. The derivation of non-Abelian coupled-channel evolution for multiparton states is found in [24,26,29–31]. The relevant results for the elastic and color-excitation operators are reported in Appendices A, B, and C.

V. NONLINEAR $k_\perp$-FACTORIZATION FOR TOPOLOGICAL CROSS SECTIONS IN DIS OFF NUCLEI

The incident photon γ^* is a color-singlet parton. In the pQCD expansion, DIS starts with the excitation of the $q\bar{q}$ pair which can be in either a color-singlet or color-octet state. Speaking of the octet at arbitrary N_c should not cause any confusion.

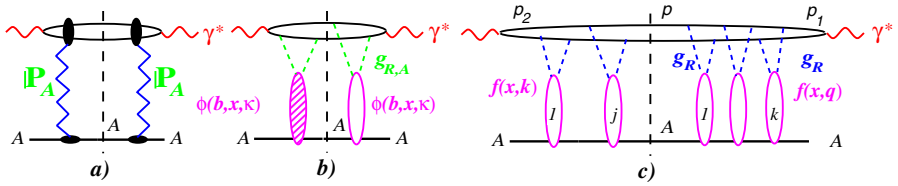

FIG. 6 (color online). (a) The diffractive unitarity cut with the ground state of the target nucleus in the intermediate state, (b) one of the 16 diagrams for diffractive unitarity cut in terms of couplings of coherent nuclear gluons $g_{R,A}$ to quarks and antiquarks, (c) the total coherent diffractive cross section in terms of the $\gamma^*(j\mathbb{P})(k\mathbb{P})\gamma^*$ impact factor.

A. DIS: RFT for the universality class of coherent diffraction

In CD excitation of the color-singlet $\{q\bar{q}\}_0$ the target nucleus is retained in the ground state and $\nu = 0$. Combining

$$\mathcal{S}^{(4)}_{A,0}(\boldsymbol{B}, \boldsymbol{B}) = S[\boldsymbol{b}, \Sigma^{\rm el}_{11}(\boldsymbol{C})T(\boldsymbol{b})] \tag{66}$$

with the results for the two and three-body states, Eq. (A4) from Appendix A, we obtain

$$\mathcal{T}_0(\boldsymbol{B}, \boldsymbol{B}', \boldsymbol{b}, \boldsymbol{b}) = \{1 - \exp[-\tfrac{1}{2}\sigma(x, \boldsymbol{r})T(\boldsymbol{b})]\} \times \{1 - \exp[-\tfrac{1}{2}\sigma(x, \boldsymbol{r}')T(\boldsymbol{b})]\}. \tag{67}$$

The CD quark-antiquark dijet spectrum equals [23,24,29]

$$\frac{d\sigma_\nu(\gamma^* A \to \{q\bar{q}\}_0 A)}{dz d^2\boldsymbol{p} d^2\boldsymbol{\Delta}} = \frac{1}{(2\pi)^2}\delta_{\nu 0}\delta(\boldsymbol{\Delta}) \times |\Psi(1; z, \boldsymbol{p}) - \Psi(z, \boldsymbol{p})|^2, \tag{68}$$

where $\delta(\boldsymbol{\Delta})$ approximates a sharp diffractive peak of width $\boldsymbol{\Delta}^2 \lesssim 1/R_A^2$.

Now we proceed to the RFT reinterpretation of this simple result. Making use of Eq. (63), we first represent (68) in terms of the collective nuclear gluon diagrams, Fig. 6,

$$\begin{aligned}\frac{d\sigma_\nu(\gamma^* A \to \{q\bar{q}\}_0 A)}{d^2\boldsymbol{b} dz d^2\boldsymbol{p} d^2\boldsymbol{\Delta}} &= \frac{1}{4(2\pi)^2}\delta_{\nu 0}\delta(\boldsymbol{\Delta}) \int d^2\boldsymbol{p}_1 d^2\boldsymbol{p}_2 d^2\boldsymbol{\kappa}_1 d^2\boldsymbol{\kappa}_2 [2\delta(\boldsymbol{p} - \boldsymbol{p}_1) - \delta(\boldsymbol{p} - \boldsymbol{\kappa}_1 - \boldsymbol{p}_1) - \delta(\boldsymbol{p} + \boldsymbol{\kappa}_1 - \boldsymbol{p}_1)] \\ &\times [2\delta(\boldsymbol{p} - \boldsymbol{p}_2) - \delta(\boldsymbol{p} - \boldsymbol{\kappa}_2 - \boldsymbol{p}_2) - \delta(\boldsymbol{p} + \boldsymbol{\kappa}_2 - \boldsymbol{p}_2)]\phi(\boldsymbol{b}, x, \boldsymbol{\kappa}_1)\phi(\boldsymbol{b}, x, \boldsymbol{\kappa}_2)\Psi^*(z, \boldsymbol{p}_2)\Psi(z, \boldsymbol{p}_1) \\ &= \frac{1}{(2\pi)^2}\delta_{\nu 0}\int d^2\boldsymbol{p}_1 d^2\boldsymbol{p}_2 d^2\boldsymbol{\kappa}_1 d^2\boldsymbol{\kappa}_2 \phi(\boldsymbol{b}, x, \boldsymbol{\kappa}_2)\phi(\boldsymbol{b}, x, \boldsymbol{\kappa}_1) \\ &\times \not{\Phi}_{CD}(\gamma^* \to \{q\bar{q}\}_0; \mathbb{P}_A, \mathbb{P}_A; \boldsymbol{p}, \boldsymbol{p}_1, \boldsymbol{\kappa}_1, \boldsymbol{p}_2, \boldsymbol{\kappa}_2),\end{aligned} \tag{69}$$

which suggests the following diagram rules in the two-dimensional transverse momentum space: For a heavy nucleus the Pomerons carry a vanishing transverse momentum. To each collective gluon loop there corresponds $\int d^2\boldsymbol{\kappa}\phi(\boldsymbol{b}, x, \boldsymbol{\kappa})$ where the propagators of $g_{R,A}$, their coupling to quarks and the uncut nuclear Pomeron and coupling of the nuclear Pomeron to a nucleus are absorbed in $\phi(\boldsymbol{b}, x, \boldsymbol{\kappa})$. Following Sec. VI D, we find it convenient to introduce integrals over the transverse momenta $\boldsymbol{p}_{1,2}$ of quarks at the $\gamma^* q\bar{q}$ vertices, and the integral over the transverse momenta of the quark and antiquark at the unitarity cut which we have taken in the differential form: $d^2\boldsymbol{p}_+ d^2\boldsymbol{p}_- = d^2\boldsymbol{p} d^2\boldsymbol{\Delta}$.

The contribution from the CD quark loop to the unitary cut $\gamma^* g_{R,A} g_{R,A} g_{R,A} g_{R,A} \gamma^*$ vertex $\not{\Phi}_{CD}(\mathbb{P}_A, \mathbb{P}_A)$ can be read from (69):

$$\begin{aligned}\not{\Phi}_{CD}(\gamma^* \to \{q\bar{q}\}_0; \mathbb{P}_A, \mathbb{P}_A; \boldsymbol{p}, \boldsymbol{p}_1, \boldsymbol{\kappa}_1, \boldsymbol{p}_2, \boldsymbol{\kappa}_2) &= \delta(\boldsymbol{\Delta})\tfrac{1}{4}\Psi^*(z, \boldsymbol{p}_2)[2\delta(\boldsymbol{p} - \boldsymbol{p}_1) - \delta(\boldsymbol{p} - \boldsymbol{\kappa}_1 - \boldsymbol{p}_1) - \delta(\boldsymbol{p} + \boldsymbol{\kappa}_1 - \boldsymbol{p}_1)] \\ &\times [2\delta(\boldsymbol{p} - \boldsymbol{p}_2) - \delta(\boldsymbol{p} - \boldsymbol{\kappa}_2 - \boldsymbol{p}_2) - \delta(\boldsymbol{p} + \boldsymbol{\kappa}_2 - \boldsymbol{p}_2)]\Psi(z, \boldsymbol{p}_1).\end{aligned} \tag{70}$$

Here $\Psi(z, \boldsymbol{p}_1)$ plays the role of the photon-quark vertex. On each side of the unitarity cut there are four possible couplings of collective gluons $g_{R,A}$ to the quark and antiquark: the terms $\propto \delta(\boldsymbol{p} - \boldsymbol{p}_i)$ describe a coupling of both gluons from $\mathbb{P}_A$ to either quark, or antiquark, as shown by a hatched Pomeron blob in Fig. 6(b), two other terms describe two possible couplings of one gluon from $\mathbb{P}_A$ to the quark, and the second gluon to the antiquark, as shown by on open blob in Fig. 6(b).

Making use of (65) we can expand (69) in contributions from the in-vacuum $j\mathbb{P}$ and $k\mathbb{P}$ exchanges on the two sides of the unitarity cut:

$$\left.\frac{d\sigma_\nu(\gamma^* A\to(q\bar q)A)}{d^2\boldsymbol{b}dzd^2\boldsymbol{p}d^2\boldsymbol{\Delta}}\right|_{CD}=\frac{1}{(2\pi)^2}\delta_{\nu 0}\sum_{j,k=1}\frac{1}{j!k!}(-1)^{j+k}\left[\frac{1}{2}T(\boldsymbol{b})\right]^{j+k}\int d^2\boldsymbol{p}_1d^2\boldsymbol{p}_2d^2\boldsymbol{k}_1\dots d^2\boldsymbol{k}_jd^2\boldsymbol{q}_1\dots d^2\boldsymbol{q}_kf(x,\boldsymbol{k}_1)\dots$$
$$\times f(x,\boldsymbol{k}_j)f(x,\boldsymbol{q}_1)\dots f(x,\boldsymbol{q}_k)D_{CD}(j\mathbb{P},k\mathbb{P};\boldsymbol{p},\boldsymbol{p}_2,\boldsymbol{p}_1,\{\boldsymbol{k}_i\},\{\boldsymbol{q}_m\}). \tag{71}$$

Here the quark loop contribution to the $\gamma^*(j\mathbb{P})(k\mathbb{P})\gamma^*$ vertex equals

$$D_{CD}(\gamma^*\to\{q\bar q\}_0;j\mathbb{P},k\mathbb{P};\boldsymbol{p},\boldsymbol{p}_2,\boldsymbol{p}_1,\{\boldsymbol{k}_i\},\{\boldsymbol{q}_m\})=\delta(\boldsymbol{\Delta})\sum_{j_1,j_2,j_3,j_4=0}^{j}\sum_{k_1,k_2,k_3,k_4=0}^{k}\delta(j-j_1-j_2-j_3-j_4)$$
$$\times\delta(k-k_1-k_2-k_3-k_4)\frac{j!}{j_1!j_2!j_3!j_4!}\cdot\frac{k!}{k_1!k_2!k_3!k_4!}$$
$$\times(-1)^{j_1+j_2+k_1+k_2}\left(\frac{1}{2}\right)^{j+k}\Psi^*(z,\boldsymbol{p}_2)\delta\left(\boldsymbol{p}-\sum_1^{j_1}\boldsymbol{k}_i+\sum_{j_1+1}^{j_1+j_2}\boldsymbol{k}_i-\boldsymbol{p}_2\right)$$
$$\times\delta\left(\boldsymbol{p}-\sum_1^{k_1}\boldsymbol{q}_m+\sum_{k_1+1}^{k_1+k_2}\boldsymbol{q}_m-\boldsymbol{p}_1\right)\Psi(z,\boldsymbol{p}_1), \tag{72}$$

to each gluon loop there corresponds $\int d^2\boldsymbol{\kappa}f(x,\boldsymbol{\kappa})$ and the coupling of the Pomeron $\mathbb{P}$ to a nucleus equals $\frac{1}{2}T(\boldsymbol{b})$.

B. The universality class of dijets in higher color multiplet

In the classification of Refs. [27,29], production of color-octet dijets belongs to the universality class of excitation of dijets in higher representations—here the octet and its large-N_c generalizations—from initial partons in lower color multiplets, which in DIS is the color-singlet photon. Here one needs to solve the non-Abelian evolution for the four-parton problem, the cross section operators in the basis of singlet-singlet $|e_1\rangle$, and octet-octet $|e_2\rangle$, four-partons states are found in Appendix A. The large-N_c expansion parameter is the singlet-to-octet hard transition $\Sigma_{21}\propto 1/N_c$. To the leading order in $1/N_c$ perturbation theory, the singlet-to-octet hard transition must be in the first color-excitation vertex, counting from the front face of the nucleus (Fig. 7). The further non-Abelian intranuclear evolution consists of the color excitation of the nucleus by color rotations within the octet state [24]. The relevant matrix element of $\mathcal{T}_\nu(\boldsymbol{B}',\boldsymbol{B})=\mathcal{S}^{(4)}_{A,\nu}(\boldsymbol{B}',\boldsymbol{B})$ would equal

$$\mathcal{T}_\nu(\boldsymbol{B}',\boldsymbol{B})=\int_0^1 d\beta_\nu\dots d\beta_1\theta(1-\beta_\nu)\theta(\beta_\nu-\beta_{\nu-1})\dots\theta(\beta_2-\beta_1)\theta(\beta_1)S[\boldsymbol{b},(1-\beta_\nu)\hat\Sigma_{\rm el}(\boldsymbol{C})]\left\{-\frac{1}{2}\Sigma^{\rm ex}_{22}P_2T(\boldsymbol{b})\right\}$$
$$\times S[\boldsymbol{b},(\beta_\nu-\beta_{\nu-1})\hat\Sigma_{\rm el}(\boldsymbol{C})]\left\{-\frac{1}{2}\Sigma^{\rm ex}_{22}P_2T(\boldsymbol{b})\right\}\times\dots\times\left\{-\frac{1}{2}\Sigma^{\rm ex}_{21}P_{\rm ex}T(\boldsymbol{b})\right\}S[\boldsymbol{b},\beta_1\hat\Sigma_{\rm el}(\boldsymbol{C})]$$
$$=\int_0^1 d\beta_\nu\dots d\beta_1\theta(1-\beta_\nu)\theta(\beta_\nu-\beta_{\nu-1})\dots\theta(\beta_1)S[\boldsymbol{b},(1-\beta_1)\hat\Sigma^{\rm el}_{22}]\cdot\left\{-\frac{1}{2}\Sigma^{\rm ex}_{22}T(\boldsymbol{b})\right\}^{\nu-1}$$
$$\times\frac{1}{2\sqrt{N_c^2-1}}\Omega T(\boldsymbol{b})\cdot S[\boldsymbol{b},\beta_1\Sigma^{\rm el}_{11}]. \tag{73}$$

The explicit integration over $\beta_2,\dots,\beta_\nu$ gives the factor $(1-\beta_1)^{\nu-1}/(\nu-1)!$. To the leading order of the large-N_c perturbation theory $\Sigma^{\rm el}_{22}=2\sigma_0(x)$ and

$$S[\boldsymbol{b},(1-\beta_1)\hat\Sigma^{\rm el}_{22}]=S[\boldsymbol{b},(1-\beta_1)\sigma_0(x)]\cdot S[\boldsymbol{b},(1-\beta_1)\sigma_0(x)]. \tag{74}$$

In conjunction with the expansion (A11) for $\{\Sigma^{\rm ex}_{22}\}^{\nu-1}$, this gives rise to

$$\frac{1}{(\nu-1)!}\left[\frac{1}{2}(1-\beta_1)\sigma_0T(\boldsymbol{b})\right]^{\nu-1}S[\boldsymbol{b},(1-\beta_1)\sigma_0(x)]\cdot S[\boldsymbol{b},(1-\beta_1)\sigma_0(x)](-\Sigma^{\rm ex}_{22})^{\nu-1}$$
$$=\sum_{j,k=0}^{\nu-1}\delta(\nu-1-j-k)\int d^2\boldsymbol{\kappa}_1d^2\boldsymbol{\kappa}_2\exp[i\boldsymbol{\kappa}_1\boldsymbol{s}+i\boldsymbol{\kappa}_2(\boldsymbol{s}-\boldsymbol{r}+\boldsymbol{r}')]w_j((1-\beta_1)\nu_A(\boldsymbol{b}))w_k((1-\beta_1)\nu_A(\boldsymbol{b}))$$
$$\times\frac{d\sigma^{(k)}_{\rm Qel}(\boldsymbol{\kappa}_1)}{\sigma_{\rm Qel}d^2\boldsymbol{\kappa}_1}\cdot\frac{d\sigma^{(j)}_{\rm Qel}(\boldsymbol{\kappa}_2)}{\sigma_{\rm Qel}d^2\boldsymbol{\kappa}_2}. \tag{75}$$

The nuclear attenuation factor $S[\boldsymbol{b},\beta_1\Sigma^{\rm el}_{11}]=S[\boldsymbol{b},\beta_1\sigma(x,\boldsymbol{r})]\cdot S[\boldsymbol{b},\beta_1\sigma(x,\boldsymbol{r}')]$ describes the coherent distortion of the color-singlet dipole in the slice $[0,\beta_1]$. Upon the summation over color states of dijets, see Eq. (A5), we obtain the

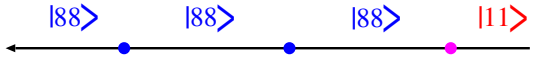

FIG. 7 (color online). The sequence of color excitations for production of color-octet dijets to the leading order in large-N_c perturbation theory.

nonlinear $k_\perp$-factorization for topological cross sections of DIS followed by color excitation of ν nucleons (ν cut Pomerons):

$$\frac{d\sigma_\nu(\gamma^* A \to \{q\bar{q}\}_8 X)}{d^2\boldsymbol{b}dzd^2\boldsymbol{p}d^2\boldsymbol{\Delta}} = \frac{1}{(2\pi)^2} T(\boldsymbol{b}) \int_0^1 d\beta \int d^2\boldsymbol{\kappa}_1 d^2\boldsymbol{\kappa}_2 d^2\boldsymbol{\kappa} \delta(\boldsymbol{\Delta} - \boldsymbol{\kappa}_1 - \boldsymbol{\kappa}_2 - \boldsymbol{\kappa}) \frac{d\sigma_{\rm Qel}(\boldsymbol{\kappa})}{d^2\boldsymbol{\kappa}}$$
$$\times |\Psi(\beta; z, \boldsymbol{p} - \boldsymbol{\kappa}_1) - \Psi(\beta; z, \boldsymbol{p} - \boldsymbol{\kappa}_1 - \boldsymbol{\kappa})|^2 \sum_{j,k=0} \delta(\nu - 1 - j - k) w_j((1-\beta)\nu_A(\boldsymbol{b}))$$
$$\times w_k((1-\beta)\nu_A(\boldsymbol{b})) \frac{d\sigma^{(k)}_{\rm Qel}(\boldsymbol{\kappa}_1)}{\sigma_{\rm Qel} d^2\boldsymbol{\kappa}_1} \cdot \frac{d\sigma^{(j)}_{\rm Qel}(\boldsymbol{\kappa}_2)}{\sigma_{\rm Qel} d^2\boldsymbol{\kappa}_2}. \tag{76}$$

C. From total to topological: the unitarity connection between partial and inclusive cross sections

With the perfect hindsight, the topological cross section (76) could have been guessed from the inclusive cross section for the color-octet dijets derived in [24]:

$$\frac{d\sigma(\gamma^* A \to \{q\bar{q}\}_8 X)}{d^2\boldsymbol{b}dzd^2\boldsymbol{p}d^2\boldsymbol{\Delta}} = \frac{1}{2(2\pi)^2} T(\boldsymbol{b}) \int_0^1 d\beta \int d^2\boldsymbol{\kappa} d^2\boldsymbol{\kappa}_1 d^2\boldsymbol{\kappa}_2 \delta(\boldsymbol{\Delta} - \boldsymbol{\kappa} - \boldsymbol{\kappa}_1 - \boldsymbol{\kappa}_2) f(x, \boldsymbol{\kappa}) \Phi(1-\beta; \boldsymbol{b}, x, \boldsymbol{\kappa}_1)$$
$$\times \Phi(1-\beta; \boldsymbol{b}, x, \boldsymbol{\kappa}_2) |\Psi(\beta; z, \boldsymbol{p} - \boldsymbol{\kappa}_1) - \Psi(\beta; z, \boldsymbol{p} - \boldsymbol{\kappa}_1 - \boldsymbol{\kappa})|^2. \tag{77}$$

Namely, making use of Eqs. (54), (57), and (58), this inclusive cross section can be cast in the form

$$\frac{d\sigma(\gamma^* A \to \{q\bar{q}\}_8 X)}{d^2\boldsymbol{b}dzd^2\boldsymbol{p}d^2\boldsymbol{\Delta}} = \frac{1}{(2\pi)^2} T(\boldsymbol{b}) \int_0^1 d\beta \int d^2\boldsymbol{\kappa} d^2\boldsymbol{\kappa}_1 d^2\boldsymbol{\kappa}_2 \delta(\boldsymbol{\Delta} - \boldsymbol{\kappa} - \boldsymbol{\kappa}_1 - \boldsymbol{\kappa}_2) \frac{d\sigma_{\rm Qel}(\boldsymbol{\kappa})}{d^2\boldsymbol{\kappa}}$$
$$\times |\Psi(\beta; z, \boldsymbol{p} - \boldsymbol{\kappa}_1) - \Psi(\beta; z, \boldsymbol{p} - \boldsymbol{\kappa}_1 - \boldsymbol{\kappa})|^2 \sum_{k=0} w_k((1-\beta)\nu_A(\boldsymbol{b})) \frac{d\sigma^{(k)}_{\rm Qel}(\boldsymbol{\kappa}_1)}{\sigma_{\rm Qel} d^2\boldsymbol{\kappa}_1}$$
$$\times \sum_{n=0} w_n((1-\beta)\nu_A(\boldsymbol{b})) \frac{d\sigma^{(n)}_{\rm Qel}(\boldsymbol{\kappa}_1)}{\sigma_{\rm Qel} d^2\boldsymbol{\kappa}_1}. \tag{78}$$

An obvious rearrangement of the summation

$$\sum_{k,n=0} = \sum_{\nu=1} \sum_{k,n=0} \delta(\nu - 1 - k - n) \tag{79}$$

gives

$$\frac{d\sigma(\gamma^* A \to \{q\bar{q}\}_8 X)}{d^2\boldsymbol{b}dzd^2\boldsymbol{p}d^2\boldsymbol{\Delta}} = \sum_{\nu=1} \frac{d\sigma_\nu(\gamma^* A \to \{q\bar{q}\}_8 X)}{d^2\boldsymbol{b}dzd^2\boldsymbol{p}d^2\boldsymbol{\Delta}}, \tag{80}$$

where $d\sigma_\nu$ is precisely the cross section (76). In conformity to the discussion of the unitarity in Sec. IV C, the topological cross sections sum up to exactly the inclusive cross section (77).

What is not obvious from such a guesswork is that the unitarity cuts are only allowed for Pomerons entering the factor $f(x, \boldsymbol{\kappa})\Phi(1-\beta; \boldsymbol{b}, x, \boldsymbol{\kappa}_1)\Phi(1-\beta; \boldsymbol{b}, x, \boldsymbol{\kappa}_2)$ in the inclusive cross section, while the initial-state coherent distortions (62) of wave functions depend neither on ν nor k and are always described by uncut-Pomeron exchanges which simply do not affect the unitarity cuts.

D. Reggeon field theory interpretation of topological cross sections

It is instructive to start with the Impulse Approximation (IA)

$$\frac{d\sigma_{\rm IA}(\gamma^* A \to \{q\bar{q}\}_8 X)}{d^2\boldsymbol{b}dzd^2\boldsymbol{p}d^2\boldsymbol{\Delta}} = \delta_{\nu 1} T(\boldsymbol{b}) \frac{1}{(2\pi)^2} \cdot \frac{d\sigma_{\rm Qel}(\boldsymbol{\Delta})}{d^2\boldsymbol{\Delta}} |\Psi(z, \boldsymbol{p}) - \Psi(z, \boldsymbol{p} - \boldsymbol{\Delta})|^2$$
$$= \delta_{\nu 1} \cdot \frac{1}{(2\pi)^2} \cdot \frac{1}{2} T(\boldsymbol{b}) \int d^2\boldsymbol{\kappa} d^2\boldsymbol{p}_1 d^2\boldsymbol{p}_2 \delta(\boldsymbol{\Delta} - \boldsymbol{\kappa}) \Psi^*(z, \boldsymbol{p}_2)[\delta(\boldsymbol{p} - \boldsymbol{p}_2) - \delta(\boldsymbol{p} - \boldsymbol{p}_2 - \boldsymbol{\kappa})]$$
$$\times [\delta(\boldsymbol{p} - \boldsymbol{p}_1) - \delta(\boldsymbol{p} - \boldsymbol{p}_1 - \boldsymbol{\kappa})] \Psi^*(z, \boldsymbol{p}_1) f(x, \boldsymbol{\kappa}). \tag{81}$$

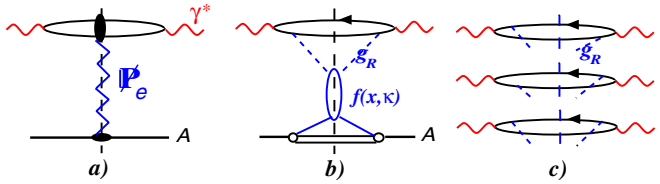

FIG. 8 (color online). (a) The impulse approximation contribution to inelastic DIS, (b) the Reggeon field theory diagrams for the cut Pomeron with one of the possible coupling of gluons to the quark loop, (c) three other possible couplings of gluons to the quark loop.

Here the cut Pomeron $\not{P}_e$ (e = excitation) corresponds to *the excitation from the color-singlet to color-octet dipole* which is driven by the free-nucleon quasielastic scattering $d\sigma_{\rm Qel}(\boldsymbol{\kappa})/d^2\boldsymbol{\kappa}$. The RFT structure of (81) is shown in Fig. 8.

One would identify $|\Psi(z,\boldsymbol{p})-\Psi(z,\boldsymbol{p}-\boldsymbol{\Delta})|^2$ with the unitarity-cut impact factor of the projectile photon, the last form in (81) gives the impulse approximation (free-nucleon) $\gamma^*\not{P}_e\gamma^*$ vertex $\not{\Phi}(\{q\bar{q}\}_8;\not{P}_e)$:

$$\begin{aligned}\not{\Phi}(\gamma^*\to\{q\bar{q}\}_8;\not{P}_e;\boldsymbol{p},\boldsymbol{\Delta},\boldsymbol{p}_1,\boldsymbol{p}_2,\boldsymbol{\kappa})&\\ =\delta(\boldsymbol{\Delta}-\boldsymbol{\kappa})\Psi^*(z,\boldsymbol{p}_2)[\delta(\boldsymbol{p}-\boldsymbol{p}_2)-\delta(\boldsymbol{p}-\boldsymbol{p}_2&\\ -\boldsymbol{\kappa})][\delta(\boldsymbol{p}-\boldsymbol{p}_1)-\delta(\boldsymbol{p}-\boldsymbol{p}_1-\boldsymbol{\kappa})]\Psi(z,\boldsymbol{p}_1).&\end{aligned}\tag{82}$$

Now notice that the color-dipole properties of $\Sigma_{22}^{\rm ex}$ are different from those of $\Sigma_{12}^{\rm ex}$, see Appendix A. This invites the introduction of still another cut Pomeron $\not{P}_r$ (r = rotation) which describes excitation of the nucleus by *color rotations within the octet dipoles*. Specifically, regarding its quasielastic scattering content, see Sec. IV C, the collective nuclear Pomeron belongs to the last category. The RFT diagram for the total inclusive inelastic dijet cross section of Ref. [24] is shown in Fig. 9. It is obtained from the diagram of Fig. 8(b) by the insertion of couplings of the quark and antiquark to collective nuclear gluons $g_{R,A}$. Similar insertions must be made in three other diagrams of Fig. 8(c). There are two nucleus-slice-dependent cut Pomerons $\not{P}_{A,r}(1-\beta)$ accompanying the in-vacuum $\not{P}_e$ (and uncut Pomerons $\mathbb{P}_A(\beta)$ which describe the nuclear

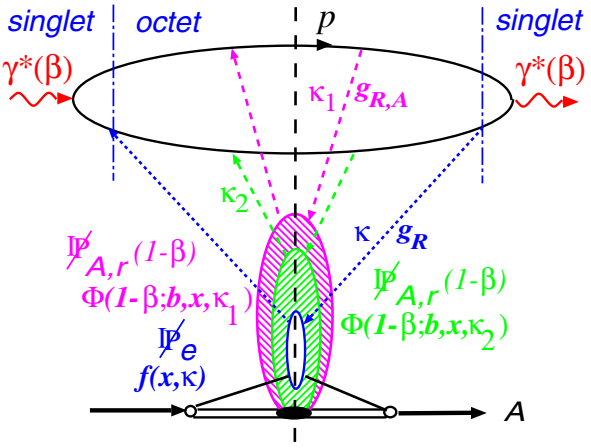

FIG. 9 (color online). One of four Reggeon field theory diagrams for the unitarity cut for inelastic DIS in terms of the cut in-vacuum Pomeron $\not{P}_e$ (color-singlet to color-octet excitation) and two cut nuclear Pomerons $\not{P}_{A,r}$ (color rotations within color-octet dipole). Three more diagrams are obtained recoupling in-vacuum gluons g_R to the quark loop as shown in Fig. 8(c). The uncut Pomeron $\mathbb{P}_A(\beta)$ exchange content of $|\gamma^*(\beta)\rangle$ is read from Eq. (63).

distortions in $\Psi(\beta,z,\boldsymbol{p})$). Gluons from the free-nucleon $\not{P}_e$ have all four possible couplings to both the quark and antiquarks. In striking contrast to that, to the leading order of large-N_c perturbation theory one of the two nuclear cut Pomerons $\not{P}_{A,r}(1-\beta)$ couples exclusively to the quark, while the second one couples exclusively to the antiquark, the diagrams with two gluons of the same nuclear Pomeron coupling to the quark and antiquark are suppressed $\propto 1/N_c^2$. Such an emergence of two distinct cut Pomerons is a deep consequence of the non-Abelian coupled-channel intranuclear evolution of color dipoles in QCD. In Fig. 9 we suppressed uncut coherent $\mathbb{P}_A(\beta)$ exchanges between the dipole and nucleus on both sides of the unitarity cut; they are encoded in the distorted $\Psi(\beta;z,\boldsymbol{p})$ the uncut multi-Pomeron exchange interpretation of which is given in Sec. IV, Eq. (63).

Following (81), we define the quark loop contribution to the $\gamma^*\not{P}_{A,r}\not{P}_e\not{P}_{A,r}\gamma^*$ vertex in terms of $\Psi(\beta;z,\boldsymbol{p})$,

$$\begin{aligned}\frac{d\sigma(\gamma^*A\to\{q\bar{q}\}_8X)}{d^2\boldsymbol{b}dzd^2\boldsymbol{p}d^2\boldsymbol{\Delta}}=\frac{1}{(2\pi)^2}\cdot\frac{1}{2}T(\boldsymbol{b})\int_0^1 d\beta\int d^2\boldsymbol{p}_1d^2\boldsymbol{p}_2d^2\boldsymbol{\kappa}d^2\boldsymbol{\kappa}_1d^2\boldsymbol{\kappa}_2\delta(\boldsymbol{\Delta}-\boldsymbol{\kappa}_1-\boldsymbol{\kappa}_2-\boldsymbol{\kappa})\Psi^*(\beta;z,\boldsymbol{p}_2)&\\ \times[\delta(\boldsymbol{p}-\boldsymbol{\kappa}_1-\boldsymbol{p}_2)-\delta(\boldsymbol{p}-\boldsymbol{\kappa}_1-\boldsymbol{\kappa}-\boldsymbol{p}_2)][\delta(\boldsymbol{p}-\boldsymbol{\kappa}_1-\boldsymbol{p}_1)-\delta(\boldsymbol{p}-\boldsymbol{\kappa}_1-\boldsymbol{\kappa})-\boldsymbol{p}_1)]&\\ \times\Psi^*(\beta;z,\boldsymbol{p}_1)\Phi(1-\beta;\boldsymbol{b},x,\boldsymbol{\kappa}_1)\Phi(1-\beta;\boldsymbol{b},x,\boldsymbol{\kappa}_2)f(x,\boldsymbol{\kappa}),&\end{aligned}\tag{83}$$

which entails

$$\begin{aligned}\not{\Phi}(\gamma^*\to\{q\bar{q}\}_8;\not{P}_{A,r}(1-\beta),\not{P}_e,\not{P}_{A,r}(1-\beta);\beta;\boldsymbol{p},\boldsymbol{\Delta},\boldsymbol{p}_1,\boldsymbol{p}_2,\boldsymbol{\kappa},\boldsymbol{\kappa}_1,\boldsymbol{\kappa}_2)&\\ =\delta(\boldsymbol{\Delta}-\boldsymbol{\kappa}_1-\boldsymbol{\kappa}_2-\boldsymbol{\kappa})\Psi^*(\beta;z,\boldsymbol{p}_2)[\delta(\boldsymbol{p}-\boldsymbol{\kappa}_1-\boldsymbol{p}_2)-\delta(\boldsymbol{p}-\boldsymbol{\kappa}_1-\boldsymbol{\kappa}-\boldsymbol{p}_2)][\delta(\boldsymbol{p}-\boldsymbol{\kappa}_1-\boldsymbol{p}_1)-\delta(\boldsymbol{p}-\boldsymbol{\kappa}_1-\boldsymbol{\kappa}-\boldsymbol{p}_1)]&\\ \times\Psi(\beta;z,\boldsymbol{p}_1).&\end{aligned}\tag{84}$$

The transition to topological cross sections with $j + k$ cut in-vacuum Pomerons $\not{\mathbb{P}}_r$ and one cut $\mathbb{P}_e$ is straightforward ($\nu = j + k + 1$):

$$\frac{d\sigma_{j+k+1}(\gamma^* A \to \{q\bar{q}\}_8 X)}{d^2\boldsymbol{b}dzd^2\boldsymbol{p}d^2\boldsymbol{\Delta}} = \frac{1}{(2\pi)^2}\cdot\left[\frac{1}{2}T(\boldsymbol{b})\right]^{j+k+1}\frac{1}{j!k!}\int_0^1 d\beta(1-\beta)^{j+k}S[\boldsymbol{b},(1-\beta)\sigma_0(x)]S[\boldsymbol{b},(1-\beta)\sigma_0(x)]$$
$$\times\int d^2\boldsymbol{p}_1 d^2\boldsymbol{p}_2 d^2\boldsymbol{\kappa} d^2\boldsymbol{k}_1\ldots d^2\boldsymbol{k}_j d^2\boldsymbol{q}_1\ldots d^2\boldsymbol{q}_k\,\delta\Big(\boldsymbol{\Delta}-\sum_{i=1}^{j}\boldsymbol{k}_i-\sum_{m=1}^{k}\boldsymbol{q}_m-\boldsymbol{\kappa}\Big)\Psi^*(\beta;z,\boldsymbol{p}_2)$$
$$\times\left[\delta\Big(\boldsymbol{p}-\sum_{i=1}^{j}\boldsymbol{k}_i-\boldsymbol{p}_2\Big)-\delta\Big(\boldsymbol{p}-\sum_{i=1}^{j}\boldsymbol{k}_i-\boldsymbol{\kappa}-\boldsymbol{p}_2\Big)\right]$$
$$\times\left[\delta\Big(\boldsymbol{p}-\sum_{i=1}^{j}\boldsymbol{k}_i-\boldsymbol{p}_1\Big)-\delta\Big(\boldsymbol{p}-\sum_{i=1}^{j}\boldsymbol{k}_i-\boldsymbol{\kappa}-\boldsymbol{p}_1\Big)\right]\Psi(\beta;z,\boldsymbol{p}_1)\prod^{j}f(x,\boldsymbol{k}_i)\prod^{k}f(x,\boldsymbol{q}_m). \quad (85)$$

Here the transverse momenta $\boldsymbol{k}_i$ belong to j gluons g_R from j cut Pomerons $\not{\mathbb{P}}_r$ entering $\Phi(1-\beta;\boldsymbol{b},x,\boldsymbol{\kappa}_1)$, and $\boldsymbol{\kappa}_1 = \sum_i \boldsymbol{k}_i$. Both gluons from each such Pomeron couple to a quark. Similarly, $\boldsymbol{q}_m$ are the transverse momenta of k-gluons from k-cut Pomerons $\not{\mathbb{P}}_r$ entering $\Phi(1-\beta;\boldsymbol{b},x,\boldsymbol{\kappa}_2)$, here $\boldsymbol{\kappa}_2 = \sum_m \boldsymbol{q}_m$, and both gluons from each such Pomeron couple to an antiquark. Likewise, it is expedient to suppress the familiar multiple uncut-Pomeron exchanges which enter $\Psi(\beta;z,\boldsymbol{p}_i)$. We identify

$$\not{\mathbb{O}}(\gamma^*\to\{q\bar{q}\}_8; j\not{\mathbb{P}}_r, \not{\mathbb{P}}_e, k\not{\mathbb{P}}_r;\beta;\boldsymbol{p},\boldsymbol{\Delta},\boldsymbol{p}_1,\boldsymbol{p}_2,\boldsymbol{\kappa},\{\boldsymbol{k}_i\},\{\boldsymbol{q}_m\})$$
$$=\delta\Big(\boldsymbol{\Delta}-\sum_{i=1}^{j}\boldsymbol{\kappa}_{1i}-\sum_{m=1}^{k}\boldsymbol{\kappa}_{2i}-\boldsymbol{\kappa}\Big)S[\boldsymbol{b},(1-\beta)\sigma_0(x)]S[\boldsymbol{b},(1-\beta)\sigma_0(x)](1-\beta)^{j+k}\Psi^*(\beta;z,\boldsymbol{p}_2)$$
$$\times\left[\delta\Big(\boldsymbol{p}-\sum_{i=1}^{j}\boldsymbol{k}_i-\boldsymbol{p}_2\Big)-\delta\Big(\boldsymbol{p}-\sum_{i=1}^{j}\boldsymbol{k}_i-\boldsymbol{\kappa}-\boldsymbol{p}_2\Big)\right]\left[\delta\Big(\boldsymbol{p}-\sum_{i=1}^{j}\boldsymbol{k}_i-\boldsymbol{p}_1\Big)-\delta\Big(\boldsymbol{p}-\sum_{i=1}^{j}\boldsymbol{k}_i-\boldsymbol{\kappa}-\boldsymbol{p}_1\Big)\right]\Psi(\beta;z,\boldsymbol{p}_1). \quad (86)$$

Here our RFT diagrams rules must be complemented by the β-integration $\int_0^1 d\beta$. For the sake of brevity we suppressed the representation of the distorted wave functions and the two absorption factors $S[\boldsymbol{b},(1-\beta)\sigma_0(x)]$ in terms of multiple uncut-Pomeron exchanges on the two sides of the unitarity cut. The RFT diagram of Fig. 9 has a manifestly Mandelstam cut structure, the same is true of its expansion in $\not{\mathbb{P}}_e$ and $\not{\mathbb{P}}_r$'s.

The special case $j = k = 0$ corresponds to the absorbed impulse approximation. The two special cases $(j,k) = (1,0)$ and $(j,k) = (0,1)$ give rise to final states with two cut Pomerons. From the viewpoint of gluon couplings, the function of two cut pomerons in such a vertex

$$\not{\mathbb{O}}_2 = (1-\beta)\not{\mathbb{O}}(\gamma^*\to\{q\bar{q}\}_8;\not{\mathbb{P}}_r,\not{\mathbb{P}}_e,0;\beta;\boldsymbol{p},\boldsymbol{\Delta},\boldsymbol{p}_1,\boldsymbol{p}_2,\boldsymbol{\kappa},\boldsymbol{\kappa}_1,0)$$
$$+(1-\beta)\not{\mathbb{O}}(\gamma^*\to\{q\bar{q}\}_8;0,\not{\mathbb{P}}_e,\not{\mathbb{P}}_r;\beta;\boldsymbol{p},\boldsymbol{\Delta},\boldsymbol{p}_1,\boldsymbol{p}_2,\boldsymbol{\kappa},0,\boldsymbol{\kappa}_2) \quad (87)$$

is very different—singlet-to-octet excitation $\not{\mathbb{P}}_e$ vs octet-to-octet color rotations $\not{\mathbb{P}}_r$—and they enter such a cut vertex in a very asymmetric fashion. All vertices $\not{\mathbb{O}}$ vanish, and $\not{\mathbb{P}}_e$ decouples, at $\boldsymbol{\kappa}\to 0$—large wavelength gluons cannot resolve the intrinsic structure of, and cannot excite to the color octet, the initial color-single $\{q\bar{q}\}_0$. In contrast to that, upon this excitation, gluons of all wavelengths contribute to color rotations of $\{q\bar{q}\}_8$ which carries a net color charge and, consequently, the $\not{\mathbb{O}}$'s are not constrained to vanish at $\boldsymbol{\kappa}_i\to 0$. Consequently, for hard dijets $\not{\mathbb{P}}_e$ is always in the hard regime, while $\not{\mathbb{P}}_r$'s are not necessarily hard. This distinction has been noted already in Ref. [24], it is a deep feature of the non-Abelian intranuclear evolution of color dipoles. Our unitarity rules with two kinds of cut Pomerons is a new result, such a two-cut-Pomeron picture did not appear in the extensive earlier literature on the AGK rules.

E. Pseudodiffractive color-singlet dijets

In the conventional diffractive production the target nucleus either stays in the ground state (coherent diffraction) or breaks up with emission of nucleons (incoherent diffraction). Each exchanged Pomeron couples to a color-singlet nucleon of the nucleus. In DIS, as well as in scattering of other color-singlet projectiles, there exists a very interesting pseudodiffractive channel when after several intranuclear color-excitations the dijet ends up in the

color-singlet state [24] accompanied by the nucleus debris also in the overall color-singlet state. There is a possibility of a survival of a large rapidity gap between the dijet and the nucleus debris, and this process would mimic the conventional incoherent diffractive dijet production. The color excitation stretches over the whole thickness of the nucleus and a signature of such a pseudodiffractive scattering would be a multiparticle production in the nucleus fragmentation region.

The pseudodiffractive channel starts with $\nu = 2$—the singlet-to-octet excitation on one nucleon is compensated for by an octet-to-singlet deexcitation on another nucleon.

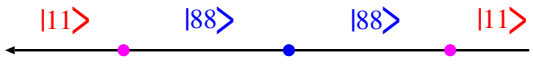

FIG. 10 (color online). The sequence of large-N_c perturbation theory color excitations for production of the pseudodiffractive color-singlet dijets.

To higher orders, it is complemented by color-excitation transitions between the color-octet states as shown in Fig. 10. We readily find

$$\begin{aligned}\mathcal{T}_\nu(\boldsymbol{B}',\boldsymbol{B}) &= \int_0^1 d\beta_\nu \dots d\beta_1 \theta(1-\beta_\nu)\theta(\beta_\nu-\beta_{\nu-1})\dots\theta(\beta_2-\beta_1)\theta(\beta_1) S[\boldsymbol{b},(1-\beta_\nu)\hat{\Sigma}_{\rm el}(\boldsymbol{C})]\left\{-\frac{1}{2}\Sigma^{\rm ex}_{12}P_{\rm ex}T(\boldsymbol{b})\right\} \\ &\times S[\boldsymbol{b},(\beta_\nu-\beta_{\nu-1})\hat{\Sigma}_{\rm el}(\boldsymbol{C})]\left\{-\frac{1}{2}\Sigma^{\rm ex}_{22}P_2T(\boldsymbol{b})\right\}\times\dots\times\left\{-\frac{1}{2}\Sigma^{\rm ex}_{21}P_{\rm ex}T(\boldsymbol{b})\right\}S[\boldsymbol{b},\beta_1\hat{\Sigma}_{\rm el}(\boldsymbol{C})] \\ &= \int_0^1 d\beta_\nu \dots d\beta_1 \theta(1-\beta_\nu)\theta(\beta_\nu-\beta_{\nu-1})\dots\theta(\beta_1) S[\boldsymbol{b},(\beta_\nu-\beta_1)\hat{\Sigma}^{\rm el}_{22}]\cdot\left\{-\frac{1}{2}\Sigma^{\rm ex}_{22}T(\boldsymbol{b})\right\}^{\nu-2} \\ &\times\frac{1}{4(N_c^2-1)}\Omega^2T^2(\boldsymbol{b})\cdot S[\boldsymbol{b},(\beta_1+1-\beta_\nu)\Sigma^{\rm el}_{11}] \\ &= \int_0^1 d\beta\beta(1-\beta)^{\nu-2}\frac{1}{(\nu-2)!}\frac{1}{4(N_c^2-1)}\Omega^2T^2(\boldsymbol{b})\left\{-\frac{1}{2}\Sigma^{\rm ex}_{22}T(\boldsymbol{b})\right\}^{\nu-2} S[\boldsymbol{b},(1-\beta)\hat{\Sigma}^{\rm el}_{22}]\cdot S[\boldsymbol{b},\beta\Sigma^{\rm el}_{11}]. \end{aligned} \tag{88}$$

Here we lumped together the coherent distortions of the color-singlet dipole in the entrance, $[0,\beta_1]$, and exit, $[1-\beta_\nu,1]$, slices of the nucleus: $\beta=\beta_1+(1-\beta_\nu)$. Proceeding as in the previous section, we obtain the pseudodiffractive topological cross sections

$$\begin{aligned}\frac{d\sigma_\nu(\gamma^*A\to\{q\bar{q}\}_0X)}{d^2\boldsymbol{b}dzd^2\boldsymbol{p}d^2\boldsymbol{\Delta}} &= \frac{1}{(N_c^2-1)}\frac{1}{(2\pi)^2}T^2(\boldsymbol{b})\int_0^1 d\beta\beta\int d^2\boldsymbol{\kappa}_1d^2\boldsymbol{\kappa}_2d^2\boldsymbol{\kappa}_3d^2\boldsymbol{\kappa}_4\delta(\boldsymbol{\Delta}-\boldsymbol{\kappa}_1-\boldsymbol{\kappa}_2-\boldsymbol{\kappa})\frac{d\sigma_{\rm Qel}(\boldsymbol{\kappa}_3)}{d^2\boldsymbol{\kappa}_3} \\ &\cdot\frac{d\sigma_{\rm Qel}(\boldsymbol{\kappa}_4)}{d^2\boldsymbol{\kappa}_4}|\Psi(\beta;z,\boldsymbol{p}-\boldsymbol{\kappa}_2)+\Psi(\beta;z,\boldsymbol{p}-\boldsymbol{\kappa}_2-\boldsymbol{\kappa}_3-\boldsymbol{\kappa}_4)-\Psi(\beta;z,\boldsymbol{p}-\boldsymbol{\kappa}_2-\boldsymbol{\kappa}_3) \\ &-\Psi(\beta;z,\boldsymbol{p}-\boldsymbol{\kappa}_2-\boldsymbol{\kappa}_4)|^2\sum_{k=0}^{\nu-2}w_k((1-\beta)\nu_A(\boldsymbol{b}))w_{\nu-2-k}((1-\beta)\nu_A(\boldsymbol{b}))\frac{d\sigma^{(k)}_{\rm Qel}(\boldsymbol{\kappa}_1)}{\sigma_{\rm Qel}d^2\boldsymbol{\kappa}_1} \\ &\cdot\frac{d\sigma^{(\nu-2-k)}_{\rm Qel}(\boldsymbol{\kappa}_2)}{\sigma_{\rm Qel}d^2\boldsymbol{\kappa}_2}. \end{aligned} \tag{89}$$

For the RFT interpretation of this result take the diagram of Fig. 9 and add one more exchange by the in-vacuum $\not{P}_e$ which describes deexcitation from the color-octet to color-singlet dipole. The two new gluons g_R would couple all four possible ways to the quarks loop. This explains the structure of the generalized cut impact factor which is proportional to

$$\begin{aligned}&|\Psi(\beta;z,\boldsymbol{p}-\boldsymbol{\kappa}_2)+\Psi(\beta;z,\boldsymbol{p}-\boldsymbol{\kappa}_2-\boldsymbol{\kappa}_3-\boldsymbol{\kappa}_4) \\ &-\Psi(\beta;z,\boldsymbol{p}-\boldsymbol{\kappa}_2-\boldsymbol{\kappa}_3)-\Psi(\beta;z,\boldsymbol{p}-\boldsymbol{\kappa}_2-\boldsymbol{\kappa}_4)|^2\end{aligned} \tag{90}$$

and now contains 16 terms. Incidentally, a very similar generalized impact factor made an appearance in CD off nuclei [55], see also the excitation of gluon-gluon dijets in [30]. The contribution from exchanges by cut Pomerons $\not{P}_{A,r}$, $\not{P}_r$ has exactly the same structure as in Fig. 9. The same is true of absorption of color-octet dipole by multiple exchanges by uncut Pomerons $\mathbb{P}$. Finally, the coherent multiple Pomeron exchange in $\Psi(\beta;z,\boldsymbol{p})$ look the same as in Fig. 9, the extra factor β in the integrand is a manifestation of lumping together the coherent distortions of color-singlet dipoles in the entrance and exit states.

A generalization of (78) to the sequential singlet-to-octet to singlet-to-octet, and still higher order contributions in $1/N_c$-perturbation theory, is straightforward, we shall not dwell into that in this communication.

VI. UNITARITY RULES FOR THE SINGLE-JET SPECTRA AND CHESHIRE CAT GRIN

Our findings on deducing the topological dijet cross sections in DIS from the inclusive ones prompt an important question: is it always possible to go from the total cross sections to topological ones or to the single-parton spectra? The literature abounds with such reinterpretations and it is important to assess their credibility. Specifically, the often discussed pre-QCD AGK approach does not contain salient features of our pQCD cutting rules—coupled-channel non-Abelian evolution of dipoles and two kinds of cut Pomerons—which lead to important new properties. In this section we comment on these distinctions. Of particular importance is the issue of cancellations of spectator interactions when going from the dijet to single-jet cross sections: spectators do not affect the single-jet spectrum but the CCG —the spectator contribution to the nucleus excitation—persists all the way through and is a physics observable.

A. Topological vs total cross section in DIS

We start with two examples when going from the total to topological and/or differential cross section works.

1. From total to topological and differential: qA scattering

In Sec. IV B we correctly guessed the unitarity content of $\phi(\boldsymbol{b}, x, \boldsymbol{\kappa})$, although the true distinction between two kinds of cut Pomerons $I\!P_{r,e}$ was as yet elusive. We notice that by the very definition

$$\int d^2\boldsymbol{\kappa}\phi(\boldsymbol{b}, x, \boldsymbol{\kappa}) = 1 - \exp[-\tfrac{1}{2}\sigma_0 T(\boldsymbol{b})] = 1 - \exp[-\sigma_{qN} T(\boldsymbol{b})] \tag{91}$$

is an integrand of the quark-nucleus inelastic cross section. Now we will try to revert the considerations of Sec. IV B. A series of transformations gives

$$\begin{aligned} 1 - \exp[-\sigma_{qN}T(\boldsymbol{b})] &= \exp[-\sigma_{qN}T(\boldsymbol{b})]\{\exp[\sigma_{qN}T(\boldsymbol{b})] - 1\} = \exp[-\sigma_{qN}T(\boldsymbol{b})]\sum_{j=1}\frac{1}{j!}[\sigma_{qN}T(\boldsymbol{b})]^j \\ &= \exp[-\sigma_{qN}T(\boldsymbol{b})]\frac{1}{j!}\left[\frac{1}{2}T(\boldsymbol{b})\right]^j\left[\int d^2\boldsymbol{\kappa} f(x,\boldsymbol{\kappa})\right]^j \\ &= \exp\left[-\frac{1}{2}\sigma_0 T(\boldsymbol{b})\right]\frac{1}{j!}\left[\frac{1}{2}T(\boldsymbol{b})\right]^j\int d^2\boldsymbol{\kappa}d^2\boldsymbol{\kappa}_1\ldots d^2\boldsymbol{\kappa}_j\delta\left(\boldsymbol{\kappa} - \sum^j\boldsymbol{\kappa}_i\right)f(x,\boldsymbol{\kappa}_1)\ldots f(x,\boldsymbol{\kappa}_j). \end{aligned} \tag{92}$$

Unfold the $d^2\boldsymbol{\kappa}$ integration and associate the j-fold convolution with the j-cut-Pomeron exchange. By a miracle—evidently, such a differential form of the left-hand side (l.h.s.) of (91) is by no means unique—the correct form of $\phi(\boldsymbol{b}, x, \boldsymbol{\kappa})$ is recovered.

2. From total to differential: leading quarks in DIS

We recall the cancellation of spectator interaction effects in the quadrature for the fully inclusive single-particle spectra of partons b from the pQCD subprocess $a \to bc$ upon the integration over the transverse momentum $\boldsymbol{p}_c$ [22,26]. Indeed, such an integration amounts to putting $\boldsymbol{b}'_c = \boldsymbol{b}_c$ in Eq. (7), and in the fully inclusive case

$$\begin{aligned} \mathcal{T}(\boldsymbol{B}, \boldsymbol{B}', \boldsymbol{b}, \boldsymbol{b}') &= S^{(4)}_{\bar{b}\,\bar{c}\,cb}(\boldsymbol{b}'_b, \boldsymbol{b}'_c, \boldsymbol{b}_b, \boldsymbol{b}_c) + S^{(2)}_{\bar{a}a}(\boldsymbol{b}', \boldsymbol{b}) - S^{(3)}_{\bar{b}\,\bar{c}\,a}(\boldsymbol{b}, \boldsymbol{b}'_b, \boldsymbol{b}'_c) - S^{(3)}_{\bar{a}bc}(\boldsymbol{b}', \boldsymbol{b}_b, \boldsymbol{b}_c) \\ &= S^\dagger_b(\boldsymbol{b}'_b)S^\dagger_c(\boldsymbol{b}_c)S_c(\boldsymbol{b}_c)S_b(\boldsymbol{b}_b) + S^\dagger_a(\boldsymbol{b}')S_a(\boldsymbol{b}) - S^\dagger_a(\boldsymbol{b}')S_b(\boldsymbol{b}_b)S_c(\boldsymbol{b}_c) - S^\dagger_b(\boldsymbol{b}'_b)S^\dagger_c(\boldsymbol{b}_c)S_a(\boldsymbol{b}) \\ &= S[\boldsymbol{b}, \sigma(x, \boldsymbol{r} - \boldsymbol{r}')] + \mathbb{1} - S[\boldsymbol{b}, \sigma(x, \boldsymbol{r})] - S[\boldsymbol{b}, \sigma(x, \boldsymbol{r}')]. \end{aligned} \tag{93}$$

Here we made use of $S_a(\boldsymbol{b}) = \mathbb{1}$ for the color-singlet projectile, $a = \gamma^*$, and the unitarity relation $S^\dagger_c(\boldsymbol{b}_c)S_c(\boldsymbol{b}_c) = \mathbb{1}$. The resulting leading-quark spectrum is a single-channel problem. The result is a linear $k_\perp$-factorization quadrature for the single leading-quark spectrum when both the coherent diffractive and truly inelastic DIS are lumped together,

$$\frac{d\sigma(\gamma^* A \to qX)}{d^2\boldsymbol{b}dzd^2\boldsymbol{p}} = \frac{1}{(2\pi)^2}\int d^2\boldsymbol{\kappa}\phi(\boldsymbol{b}, x, \boldsymbol{\kappa})|\Psi(z, \boldsymbol{p}) - \Psi(z, \boldsymbol{p} - \boldsymbol{\kappa})|^2, \tag{94}$$

which is exact for all N_c [24,56].

The same result can be obtained in a risky way of undoing the integrations in the formal Fourier representation for the total DIS cross section:

$$\frac{d\sigma}{d^2\boldsymbol{b}} = 2\int_0^1 dz \int d^2\boldsymbol{r}\Psi^*(z,\boldsymbol{r})\Psi(z,\boldsymbol{r})\left\{1-\exp\left[-\frac{1}{2}\sigma(x,\boldsymbol{r})T(\boldsymbol{b})\right]\right\}$$
$$= \frac{1}{(2\pi)^4}\int_0^1 dz \int d^2\boldsymbol{\kappa}\phi(\boldsymbol{b},x,\boldsymbol{\kappa})[1-\exp(i\boldsymbol{\kappa}\boldsymbol{r})][1-\exp(-i\boldsymbol{\kappa}\boldsymbol{r})]\iint d^2\boldsymbol{p}_1 d^2\boldsymbol{p}_2\Psi^*(z,\boldsymbol{p}_2)\Psi(z,\boldsymbol{p}_1)\exp(i\boldsymbol{p}_2\boldsymbol{r}-i\boldsymbol{p}_1\boldsymbol{r})$$
$$= \frac{1}{(2\pi)^2}\int_0^1 dz \int d^2\boldsymbol{\kappa} d^2\boldsymbol{p}_1 d^2\boldsymbol{p}_2\phi(\boldsymbol{b},x,\boldsymbol{\kappa})\Psi^*(z,\boldsymbol{p}_2)\Psi(z,\boldsymbol{p}_1)$$
$$\times[\delta(\boldsymbol{p}_1-\boldsymbol{p}_2)-\delta(\boldsymbol{p}_1-\boldsymbol{p}_2+\boldsymbol{\kappa})-\delta(\boldsymbol{p}_1-\boldsymbol{p}_2-\boldsymbol{\kappa})+\delta((\boldsymbol{p}_1+\boldsymbol{\kappa})-(\boldsymbol{p}_2+\boldsymbol{\kappa}))]. \quad (95)$$

At this point one needs a judicious identification of the Fourier parameters $\boldsymbol{p}_{1,2}$, or $\boldsymbol{p}_{1,2}+\boldsymbol{\kappa}$, with the momentum of the observed leading quark. Taking literally a concept of a collective nuclear gluon $g_{R,A}$, and drawing the relevant four Feynman diagrams, see Fig. 8, makes such an identification unique and (95) boils down to (94). Such a mock derivation does not tell, though, why one must not take for the final-state momentum $\boldsymbol{p}$ the momentum of the quark somewhere in between the in-vacuum gluons of the multigluon components of $g_{R,A}$.

B. From total inclusive to topological: Cheshire Cat grin stays on

Inspired by the successful, though marred by question marks, guesswork in Secs. VI A 1 and VI A 2, one can substitute for $\phi(\boldsymbol{b},x,\boldsymbol{\kappa})$ the expansion (58) and define the ''topological cross sections'' for the single leading-quark spectrum in DIS:

$$\frac{d\sigma^*_\nu(\gamma^*A\to qX)}{d^2\boldsymbol{b}dzd^2\boldsymbol{p}} = \frac{1}{(2\pi)^2}w_\nu(\nu_A(\boldsymbol{b}))\int d^2\boldsymbol{\kappa}\frac{d\sigma^{(\nu)}_{\rm Qel}(\boldsymbol{\kappa})}{d^2\boldsymbol{\kappa}}$$
$$\times|\Psi(z,\boldsymbol{p})-\Psi(z,\boldsymbol{p}-\boldsymbol{\kappa})|^2. \quad (96)$$

This reinterpretation of the so-guessed $d\sigma^*_\nu$ as topological single-jet cross sections for DIS with color excitation of ν nucleons (ν cut Pomerons) would be erroneous, though. The trouble is that, although our guesswork (95) proved a success, an important distinction between the two kinds of cut Pomerons $\not{\mathbb{P}}_{r,e}$ has been lost in the final form of (96).

The correct result for the single-jet spectrum derives from the dijet spectrum integrating in (76) over the transverse momentum of the unobserved antiquark. This lifts $\delta(\boldsymbol{\Delta}-\boldsymbol{\kappa}-\boldsymbol{\kappa}_1-\boldsymbol{\kappa}_2)$ and the $\boldsymbol{\kappa}_2$ integration can be carried out explicitly,

$$\int d^2\boldsymbol{\kappa}_2\frac{d\sigma^{(\nu-1-k)}_{\rm Qel}(\boldsymbol{\kappa}_2)}{\sigma_{\rm Qel}d^2\boldsymbol{\kappa}_2} = 1, \quad (97)$$

the result is

$$\frac{d\sigma_\nu(\gamma^*A\to qX)}{d^2\boldsymbol{b}dzd^2\boldsymbol{p}} = \frac{1}{2(2\pi)^2}T(\boldsymbol{b})\int_0^1 d\beta\sum_{j,k=0}\delta(\nu-1-j-k)w_k((1-\beta)\nu_A(\boldsymbol{b}))w_j((1-\beta)\nu_A(\boldsymbol{b}))\int d^2\boldsymbol{\kappa}_1 d^2\boldsymbol{\kappa}\frac{d\sigma_{\rm Qel}(\boldsymbol{\kappa})}{d^2\boldsymbol{\kappa}}$$
$$\times\frac{d\sigma^{(k)}_{\rm Qel}(\boldsymbol{\kappa}_1)}{\sigma_{\rm Qel}d^2\boldsymbol{\kappa}_1}|\Psi(\beta;z,\boldsymbol{p}-\boldsymbol{\kappa}_1)-\Psi(\beta;z,\boldsymbol{p}-\boldsymbol{\kappa}_1-\boldsymbol{\kappa})|^2+\frac{1}{(2\pi)^2}\delta_{\nu 0}|\Psi(1;z,\boldsymbol{p})-\Psi(z,\boldsymbol{p})|^2. \quad (98)$$

The RFT diagram for (98) is obtained from Fig. 9 striking out the second nuclear cut Pomeron $\not{\mathbb{P}}_{A,r}$, which is a graphic counterpart of cancellations of the spectator antiquark interactions in (93). This makes clear the role of the CCG and its meaning as a physics observable: by the unitarity the second nuclear Pomeron is gone, but it still contributes to the ν and the target-nucleus excitation: the Chesire Cat grin stays on.

Needless to say the correct topological cross sections $d\sigma_\nu$ are unequal to the ill-guessed $d\sigma^*_\nu$. For instance, the β-dependence of exchanges by uncut Pomerons $\mathbb{P}$ and cut Pomerons $\not{\mathbb{P}}_r$ is entirely missed in $d\sigma^*_\nu$. The case of $\nu=0$ is the most striking one: at Q^2 below the saturation scale, the coherent diffractive component of (98) makes $\approx$ 50 percent of the total DIS cross section [57], while the contribution with $\nu=0$ is entirely missed in the ill-guessed $d\sigma^*_\nu$ of Eq. (96).

C. Isolate coherent diffraction: still more guesswork for inelastic σ_ν

Try correcting (95) for the CD,

$$\underbrace{2\{1-\exp[-\tfrac{1}{2}\sigma(x,\boldsymbol{r})T(\boldsymbol{b})]\}}_{\rm tot} = \underbrace{\{1-\exp[-\tfrac{1}{2}\sigma(x,\boldsymbol{r})T(\boldsymbol{b})]\}^2}_{\rm coherent\ diffraction}$$
$$+\underbrace{\{1-\exp[-\sigma(x,\boldsymbol{r})T(\boldsymbol{b})]\}}_{\rm inelastic}, \quad (99)$$

and focus on the inelastic cross section

$$\frac{d\sigma^{\rm in}}{d^2\boldsymbol{b}} = \int_0^1 dz\int d^2\boldsymbol{r}\Psi^*(z,\boldsymbol{r})\Psi(z,\boldsymbol{r})$$
$$\times\{1-\exp[-\sigma(x,\boldsymbol{r})T(\boldsymbol{b})]\}. \quad (100)$$

The substitution

$$1-\exp[-\sigma(x,\boldsymbol{r})T(\boldsymbol{b})]=\frac{1}{2}\int d^2\boldsymbol{\kappa}[1-\exp(i\boldsymbol{\kappa r})]\times[1-\exp(-i\boldsymbol{\kappa r})]\times\sum_{j=1}w_j(2\nu_A(\boldsymbol{b}))\frac{d\sigma_{\rm Qel}^{(\nu)}(\boldsymbol{\kappa})}{\sigma_{\rm Qel}d^2\boldsymbol{\kappa}} \tag{101}$$

in (100) would suggest

$$\frac{d\sigma_\nu^*}{d^2\boldsymbol{b}dzd^2\boldsymbol{p}}=\frac{1}{2(2\pi)^2}w_\nu(2\nu_A(\boldsymbol{b}))\int_0^1dz\int d^2\boldsymbol{\kappa}\frac{d\sigma_{\rm Qel}^{(\nu)}(\boldsymbol{\kappa})}{d^2\boldsymbol{\kappa}}\times|\Psi(z,\boldsymbol{p})-\Psi(z,\boldsymbol{p}-\boldsymbol{\kappa})|^2. \tag{102}$$

Once again $d\sigma_\nu^*\neq d\sigma_\nu$ and (102) must be rejected for the same reason as (96).

Still another possibility is a representation

$$1-\exp[-\sigma(x,\boldsymbol{r})T(\boldsymbol{b})]=\int_0^1d\beta\sigma(x,\boldsymbol{r})T(\boldsymbol{b})\exp[-\beta\sigma(x,\boldsymbol{r})T(\boldsymbol{b})]=2T(\boldsymbol{b})\int_0^1d\beta\exp[-\beta\sigma(x,\boldsymbol{r})T(\boldsymbol{b})]\int d^2\boldsymbol{\kappa}[1-\exp(i\boldsymbol{\kappa r})]\frac{d\sigma_{\rm Qel}(\boldsymbol{\kappa})}{d^2\boldsymbol{\kappa}}. \tag{103}$$

Upon the reabsorption of $\exp[-\beta\sigma(x,\boldsymbol{r})T(\boldsymbol{b})]=S[\boldsymbol{b},\beta\sigma(x,\boldsymbol{r})]\cdot S[\boldsymbol{b},\beta\sigma(x,\boldsymbol{r})]$ into the coherent distortions of the dipole wave functions in (100), one would find

$$\frac{d\sigma^{\rm in}}{d^2\boldsymbol{b}}=\frac{1}{(2\pi)^2}T(\boldsymbol{b})\int_0^1d\beta\int_0^1dz\int d^2\boldsymbol{p}d^2\boldsymbol{\kappa}\frac{d\sigma_{\rm Qel}(\boldsymbol{\kappa})}{d^2\boldsymbol{\kappa}}|\Psi(\beta;z,\boldsymbol{p})-\Psi(\beta;z,\boldsymbol{p}-\boldsymbol{\kappa})|^2. \tag{104}$$

As far as coherent distortions of dipoles are concerned, it is reminiscent of (98), but suggests an absurd result that there is only one cut Pomeron, $d\sigma_\nu^*=\delta_{\nu1}d\sigma^{\rm in}$.

The reason for all those failures is simple. Isolate CD in (93):

$$\mathcal{T}(\boldsymbol{B},\boldsymbol{B}',\boldsymbol{b},\boldsymbol{b}')=\underbrace{1-S[\boldsymbol{b},\sigma(x,\boldsymbol{r})]-S[\boldsymbol{b},\sigma(x,\boldsymbol{r}')]+S[\boldsymbol{b},\sigma(x,\boldsymbol{r})]S[\boldsymbol{b},\sigma(x,\boldsymbol{r}')]}_{\text{coherent diffraction}}+\underbrace{S[\boldsymbol{b},\sigma(x,\boldsymbol{r}-\boldsymbol{r}')]-S[\boldsymbol{b},\sigma(x,\boldsymbol{r})]S[\boldsymbol{b},\sigma(x,\boldsymbol{r}')]}_{\text{inelastic}}. \tag{105}$$

The single-quark spectrum from inelastic DIS would equal [24]

$$\frac{d\sigma^{\rm in}(\gamma^*A\to qX)}{d^2\boldsymbol{b}dzd^2\boldsymbol{p}}=\frac{1}{(2\pi)^2}\int d^2\boldsymbol{r}d^2\boldsymbol{r}'\exp[i\boldsymbol{p}(\boldsymbol{r}'-\boldsymbol{r})]\Psi^*(z,\boldsymbol{r}')\Psi(z,\boldsymbol{r})\{S[\boldsymbol{b},\sigma(x,\boldsymbol{r}-\boldsymbol{r}')]-S[\boldsymbol{b},\sigma(x,\boldsymbol{r})]S[\boldsymbol{b},\sigma(x,\boldsymbol{r}')]\}. \tag{106}$$

The integration over the momentum of the leading quark gives $\delta(\boldsymbol{r}-\boldsymbol{r}')$ and (100) is recovered

$$\frac{d\sigma^{\rm in}}{d^2\boldsymbol{b}}=\int_0^1dz\int d^2\boldsymbol{r}\Psi^*(z,\boldsymbol{r})\Psi(z,\boldsymbol{r})\{1-S^2[\boldsymbol{b},\sigma(x,\boldsymbol{r})]\}=\int d^2\boldsymbol{r}|\Psi(z,\boldsymbol{r})|^2\{1-\exp[-\sigma(x,\boldsymbol{r})T(\boldsymbol{b})]\}. \tag{107}$$

Mimicking (95) did a bad service in (102) and (104): there is no way to guess the crucial $S[\boldsymbol{b},\sigma(x,\boldsymbol{r}-\boldsymbol{r}')]$ from 1 in the integrand of (107).

D. The color dipole form of σ_ν in DIS

In the fully integrated inelastic cross sections $\boldsymbol{s}=0$ and $\boldsymbol{r}=\boldsymbol{r}'$, which entails $\Sigma_{11}^{\rm el}=\Omega=2\sigma(x,\boldsymbol{r})$, $\Sigma_{22}^{\rm el}=-\Sigma_{22}^{\rm ex}=2\sigma_0$ and

$$\frac{d\sigma_\nu^{\rm in}}{d^2\boldsymbol{b}}=\int_0^1dz\int d^2\boldsymbol{r}|\Psi(z,\boldsymbol{r})|^2\int_0^1d\beta\frac{1}{(\nu-1)!}[(1-\beta)\sigma_0T(\boldsymbol{b})]^{\nu-1}\exp[-(1-\beta)\sigma_0T(\boldsymbol{b})]\sigma(x,\boldsymbol{r})T(\boldsymbol{b})\times\exp[-\beta\sigma(x,\boldsymbol{r})T(\boldsymbol{b})]$$
$$=\int_0^1dz\int d^2\boldsymbol{r}|\Psi(z,\boldsymbol{r})|^2\int_0^1d\beta w_{\nu-1}(2(1-\beta)\nu_A(\boldsymbol{b}))\sigma(x,\boldsymbol{r})T(\boldsymbol{b})\exp[-\beta\sigma(x,\boldsymbol{r})T(\boldsymbol{b})]. \tag{108}$$

This is a new result. Of course, upon summing over all $\nu \geq 1$ we recover (100):

$$\sum_{\nu\geq 1}\int_0^1 d\beta w_{\nu-1}(2(1-\beta)\nu_A(\boldsymbol{b}))\sigma(x,\boldsymbol{r})T(\boldsymbol{b})\exp[-\beta\sigma(x,\boldsymbol{r})T(\boldsymbol{b})] = \int_0^1 d\beta\sigma(x,\boldsymbol{r})T(\boldsymbol{b})\exp[-\beta\sigma(x,\boldsymbol{r})T(\boldsymbol{b})]$$
$$= 1-\exp[-\sigma(x,\boldsymbol{r})T(\boldsymbol{b})]. \tag{109}$$

Following the 1976 version of AGK rules for hadron-nucleus collisions [7–9], one often defines $d\sigma_\nu^*$ via the expansion (for the recent review see [17])

$$1-\exp[-\sigma(x,\boldsymbol{r})T(\boldsymbol{b})] = \exp[-\sigma(x,\boldsymbol{r})T(\boldsymbol{b})]\sum_{\nu=1}\frac{1}{\nu!}[\sigma(x,\boldsymbol{r})T(\boldsymbol{b})]^\nu,$$
$$\frac{d\sigma_\nu^*}{d^2\boldsymbol{b}} = \int_0^1 dz\int d^2\boldsymbol{r}|\Psi(z,\boldsymbol{r})|^2\frac{1}{\nu!}[\sigma(x,\boldsymbol{r})T(\boldsymbol{b})]^\nu\exp[-\sigma(x,\boldsymbol{r})T(\boldsymbol{b})]. \tag{110}$$

Such a $d\sigma_\nu^*$ would coincide with the correct result (108) only if $\sigma_0 = \sigma(x,\boldsymbol{r})$, which is nonsensical in pQCD. We conclude that the version (110) is an unwarranted one. This discussion casts shadow on the routinely used Glauber model statistics for wounded nucleon distributions which is based on [7,9], we shall revisit this issue elsewhere.

To summarize this discussion, it is crystal clear that the unitarity definition of topological cross sections must be applied before integrating out the spectator-jet variables—the two procedures do not commute because the spectator-jet integrations (i) involve shifts of the Fourier parameter $\boldsymbol{p}$ which then can no longer be correctly related to the observed momentum of the jet, (ii) the distinction between two kinds of cut Pomerons—the crucial feature of pQCD unitarity—is missed upon the spectator integrations, (iii) the Chesire cat grin is a physics observable—spectator interaction cancellations make, by virtue of the completeness of states and unitarity relations, some important operators equal to unity and the contribution of those states to topological cross sections is missed. The whole variety of plausible "unitarity" reinterpretations (95), (100), (104), and (110) is simply unwarranted. For a similar failure of naive unitarity reinterpretations of diffractive cross sections see Ref. [55].

E. pQCD version of the AGK ratios

We close this dispute by the comparison of different two-Pomeron exchange cross sections, i.e., terms $\propto T^2(\boldsymbol{b})$ in the total cross section, coherent diffractive cross section, the two-cut Pomeron exchange cross section $\sigma_2^{\rm in}$ and the first absorption correction to $\sigma_1^{\rm in}$. Such a comparison can be carried out at the level of color-dipole profile functions. The expansion of

$$\Gamma_{\rm tot}(\boldsymbol{b},\boldsymbol{r}) = 2\{1-\exp[-\tfrac{1}{2}\sigma(x,\boldsymbol{r})T(\boldsymbol{b})]\}$$

gives

$$\Delta_2\Gamma_{\rm tot}(\mathbb{P}\mathbb{P};\boldsymbol{b},\boldsymbol{r}) = -\tfrac{1}{4}[\sigma(x,\boldsymbol{r})T(\boldsymbol{b})]^2, \tag{111}$$

while for the CD

$$\Gamma_D(\boldsymbol{b},\boldsymbol{r}) = \{1-\exp[-\tfrac{1}{2}\sigma(x,\boldsymbol{r})T(\boldsymbol{b})]\}^2$$

and

$$\Delta_2\Gamma_D(\mathbb{P}\mathbb{P};\boldsymbol{b},\boldsymbol{r}) = \tfrac{1}{4}[\sigma(x,\boldsymbol{r})T(\boldsymbol{b})]^2. \tag{112}$$

The generic formula (108) for the profile function of $\sigma_2^{\rm in}$ reads

$$\Gamma_2^{\rm in}(\not{p}_r\not{p}_e,\mathbb{P},\ldots,\mathbb{P};\boldsymbol{b},\boldsymbol{r}) = [\sigma_0(x)T(\boldsymbol{b})]\cdot[\sigma(x,\boldsymbol{r})T(\boldsymbol{b})]$$
$$\times\int_0^1 d\beta(1-\beta)$$
$$\times\exp[-\beta\sigma(x,\boldsymbol{r})T(\boldsymbol{b})]$$
$$\times\exp[-(1-\beta)\sigma_0(x)T(\boldsymbol{b})]. \tag{113}$$

To the second order in $T(\boldsymbol{b})$ the β-dependent attenuation must be neglected and

$$\Delta_2\Gamma_2^{\rm in}(\not{p}_r\not{p}_e;\boldsymbol{b},\boldsymbol{r}) = \tfrac{1}{2}\cdot[\sigma_0(x)T(\boldsymbol{b})][\sigma(x,\boldsymbol{r})T(\boldsymbol{b})], \tag{114}$$

where $\sigma(x,\boldsymbol{r})$ and σ_0 come from $\not{p}_e$ and $\not{p}_r$, respectively. Finally, the generic formula (108) for the profile function of $\sigma_1^{\rm in}$ reads

$$\Gamma_1^{\rm in}(\not{p}_e,\mathbb{P},\ldots,\mathbb{P};\boldsymbol{b},\boldsymbol{r}) = \sigma(x,\boldsymbol{r})T(\boldsymbol{b})$$
$$\times\int_0^1 d\beta\exp[-\beta\sigma(x,\boldsymbol{r})T(\boldsymbol{b})]$$
$$\times\exp[-(1-\beta)\sigma_0 T(\boldsymbol{b})]. \tag{115}$$

In order to isolate the first absorption correction, we expand the two attenuation factors to the terms linear in $T(\boldsymbol{b})$ and obtain

$$\Delta_2\Gamma_1^{\rm in}(\not{P}_e\mathbb{P};\boldsymbol{b},\boldsymbol{r}) = -\sigma(x,\boldsymbol{r})T(\boldsymbol{b})\int_0^1 d\beta[(1-\beta)\sigma_0(x)T(\boldsymbol{b}) + \beta\sigma(x,\boldsymbol{r})T(\boldsymbol{b})] = -\tfrac{1}{2}\cdot[\sigma_0(x)T(\boldsymbol{b})]\cdot[\sigma(x,\boldsymbol{r})T(\boldsymbol{b})] - \tfrac{1}{2}[\sigma(x,\boldsymbol{r})T(\boldsymbol{b})]^2. \quad (116)$$

The results for the total and CD cross sections are model independent ones, but the two kinds of cut Pomerons inherent to pQCD make (114) and (116) distinct from the pre-QCD version of the AGK rules. In the pre-QCD AGK rules there is only one kind of cut Pomerons and, based (110), one would have found ([7–9], for the more recent discussion see [17])

$$\Delta_2\Gamma_1^{\rm in}(\not{P}\mathbb{P};\boldsymbol{b},\boldsymbol{r}) = -2\Delta_2\Gamma_2^{\rm in}(\not{P}\not{P};\boldsymbol{b},\boldsymbol{r}) = -[\sigma(x,\boldsymbol{r})T(\boldsymbol{b})]^2, \quad (117)$$

and

$$\Delta_2\Gamma_D(\mathbb{P}\mathbb{P};\boldsymbol{b},\boldsymbol{r}):\Delta_2\Gamma_1^{\rm in}(\not{P}\mathbb{P};\boldsymbol{b},\boldsymbol{r}):\Delta_2\Gamma_2^{\rm in}(\not{P}\not{P};\boldsymbol{b},\boldsymbol{r}) = 1:-4:2. \quad (118)$$

The latter relationship, as well as the cancellation

$$\Delta_2\Gamma_1^{\rm in}(\not{P}\mathbb{P};\boldsymbol{b},\boldsymbol{r}) + 2\Delta_2\Gamma_2^{\rm in}(\not{P}\not{P};\boldsymbol{b},\boldsymbol{r}) = 0, \quad (119)$$

break down in the pQCD world, although the sum rule

$$\Delta_2\Gamma_{\rm tot}(\mathbb{P}\mathbb{P};\boldsymbol{b},\boldsymbol{r}) = \Delta_2\Gamma_D(\not{P}\mathbb{P};\boldsymbol{b},\boldsymbol{r}) + \Delta_2\Gamma_1^{\rm in}(\not{P}\mathbb{P};\boldsymbol{b},\boldsymbol{r}) + \Delta_2\Gamma_2^{\rm in}(\not{P}\not{P};\boldsymbol{b},\boldsymbol{r}) \quad (120)$$

is still retained. In the pre-QCD version of Eq. (120) there is only one kind of cut Pomerons, while the two kinds of cut Pomerons in our pQCD cutting rules can be read from Eqs. (114) and (116).

VII. PHENOMENOLOGICAL APPLICATIONS OF TOPOLOGICAL CROSS SECTIONS

We only briefly sketch possible phenomenological applications of the derived topological cross sections for inelastic DIS. Much guidance comes from the earlier literature on hadron-nucleus interactions [7,9]. We list several observables of increasing complexity.

A. Multiproduction in the backward (nucleus) hemisphere

Consider first the minimal-bias events. We refer to rapidities $\eta < \eta_A$ as the nucleus or backward (B) hemisphere. Arguably, the multiplicity of hadrons in the backward hemisphere, n_B, will be proportional to ν:

$$n_B \approx \nu\langle n_B\rangle_{pN}, \quad (121)$$

which allows to evaluate ν on the event-by-event basis. (Strictly speaking, the backward hemisphere is infested by intranuclear cascading of secondary hadrons formed inside the nucleus [42,58] and Eq. (121) needs further qualification within the nonperturbative hadronization models, we do not dwell into that.)

Then our result (108) for the topological cross sections can readily be applied for a modeling of n_B distributions for inelastic DIS off nuclei. If $P_n(\langle n_B\rangle_{pN})$ is the multiplicity distribution for a free-nucleon target, then the corresponding n_B distribution for ν-cut Pomerons will be a ν-fold convolution of $P_n(\langle n_B\rangle_{pN})$. For instance, the moments $p_k = \langle(\nu-1)\ldots(\nu-k)\rangle$ can readily be evaluated:

$$\sum_{\nu>k}\frac{d\sigma_\nu}{d^2\boldsymbol{b}}(\nu-1)\ldots(\nu-k) = \int_0^1 dz\int d^2\boldsymbol{r}|\Psi(z,\boldsymbol{r})|^2 \times\int_0^1 d\beta[2(1-\beta)\nu_A(\boldsymbol{b})]^k \times\sigma(x,\boldsymbol{r})T(\boldsymbol{b}) \times\exp[-\beta\sigma(x,\boldsymbol{r})T(\boldsymbol{b})]. \quad (122)$$

A manifest dependence of the moments p_k on the infrared-sensitive σ_0 is not disturbing as it comes along with the related infrared-sensitive conversion of the multiplicity of partons to the observed multiplicity of hadrons.

B. Long-range rapidity correlations between leading and backward particles: breaking of limiting fragmentation

1. Radiationless breaking of limiting fragmentation

Consider now the $\boldsymbol{p}$ integrated leading jet spectra. For leading jets z coincides with the Feynman variable x_F. The familiar concept of limiting fragmentation amounts to a target independence of the x_F spectra. There are two sources of the breaking of limiting fragmentation in DIS off nuclei. As we have seen above, the partition of the energy momentum between k-cut Pomerons $\not{P}_r$ which couple to the observed quark contributes to its quenching. We shall discuss it in the next section, here we comment on the radiationless quenching of leading jets—a mechanism inherent to the pQCD color-dipole approach to DIS.

The x_F spectrum of leading-quark jets is obtained from (108) undoing the z integration:

$$\frac{d\sigma_\nu}{d^2\boldsymbol{b}dx_F} = \int d^2\boldsymbol{r}|\Psi(x_F,\boldsymbol{r})|^2\int_0^1 d\beta w_{\nu-1}(2(1-\beta)\nu_A(\boldsymbol{b})) \times\sigma(x,\boldsymbol{r})T(\boldsymbol{b})\exp[-\beta\sigma(x,\boldsymbol{r})T(\boldsymbol{b})]. \quad (123)$$

Here we recall that for transverse and longitudinal photons and the flavor f [19]

$$|\Psi_T(x_F,\boldsymbol{r})|^2 = \frac{6\alpha_{\rm em}}{(2\pi)^2}e_f^2\{[(1-x_F)^2+x_F^2]\varepsilon^2K_1^2(\varepsilon r) + m_f^2K_0^2(\varepsilon r)\},$$
$$|\Psi_L(x_F,\boldsymbol{r})|^2 = \frac{6\alpha_{\rm em}}{(2\pi)^2}e_f^2 4Q^2x_F^2(1-x_F)^2K_0^2(\varepsilon r), \quad (124)$$

where Q^2 is the virtuality of the photon, $\alpha_{\rm em}$ is the QED

fine structure constant, m_f and e_f are the quark mass and electric charge, $K_{0,1}(x)$ are the Bessel functions, and

$$\varepsilon^2 = x_F(1-x_F)Q^2 + m_f^2. \tag{125}$$

By virtue of (125) the resulting x_F distribution depends on the $\boldsymbol{r}$ dependence of the nuclear factor. The latter is controlled by the nuclear impact parameter distribution which depends on ν. It can easily be shown, that the larger ν is the stronger the suppression of the contribution from large dipoles and from x_F close to 1 is. Consequently, even without any nonperturbative energy loss, the x_F spectrum of leading quarks would depend on ν, which we dub the radiationless breaking of limiting fragmentation.

2. Nonperturbative quenching of forward jets in DIS off nuclei

As discussed in the introduction each excited nucleon adds more secondary particles and more energy in the nucleus fragmentation region. This flow of energy into the nucleus hemisphere is a nonperturbative contribution to the quenching of forward jets. It is complementary to radiationless quenching in the Born approximation, Sec. VII B 1, and quenching by the QCD Landau-Pomeranchuk-Migdal (LPM) effect to higher orders discussed in [31,59,60].

The universality class of CD DIS is unique for the lack of the energy loss. Fragmentation of coherent diffractive dijets produced off nuclei will be exactly the same as of dijets from free-nucleon interactions.

In inelastic DIS the color-excitation centers will be scattered along the whole thickness of the nucleus at a given impact parameter $\boldsymbol{b}$. Besides these color centers and projectile partons, color strings will be stretched between the color centers themselves. In a dilute nucleonic gas, the energy stored in the latter string will be of the order of the nuclear radius times the string tension and will be substantially, $\sim A^{1/3}$ times, larger than the elastic recoil energy of nuclear quarks discussed in [44]. The two extreme scenarios for the energy flow from the projectile system to a color-excited nucleus have already been described in the introduction. In the scenario of Fig. 1(b), color strings stretched between color-excited nucleons and the projectile system hadronize independently into small-$p_\perp$ hadrons, i.e., the underlying minimal-bias event. Different versions of this scenario [7,9] are widely used in the Monte Carlo hadronization codes for nuclear interactions [61]. We have shown that in large-N_c DIS quasielastic rescatterings of the quark and antiquark are independent of each other. If $\langle x_{F,1}\rangle$ is the average fraction of the initial energy carried by the quasielastically scattered parton, then after k-sequential scatterings of the observed quark

$$\langle x_{F,k}\rangle \sim \langle x_{F,1}\rangle^k, \tag{126}$$

for instance, see [62]. The equipartition of energy between ν strings,

$$\langle x_{F,\nu}\rangle \sim \frac{1}{\nu}\langle x_F\rangle, \tag{127}$$

is less likely.

The formation length arguments suggest a different pattern of quenching. In the fragmentation of the color string between the propagating quark which changed its color and the color-excited nucleon, the secondary hadron of momentum $x_F E_q$ is formed from the quark-antiquark pair produced in the chromoelectric field of the string. In the comoving frame the hadron formation time $\tau \sim 1/m_\perp$, where $m_\perp$ is the transverse mass of the prompt hadron, in the laboratory frame it is stretched by the γ-factor of the parton ([40,41] for the review see [58]),

$$l_f \approx \frac{x_F E_q}{m_\perp^2}. \tag{128}$$

The second quasielastic scattering would take place at a distance

$$l_{\rm abs} \approx \frac{1}{n_A \sigma_0}. \tag{129}$$

The energy flow $E_{\rm ex}$ into the hadronization between two consecutive interactions can be estimated as

$$E_{\rm ex} \approx l_{\rm abs} m_\perp^2. \tag{130}$$

The energy flow $\Delta_k E$ after k-quasielastic rescatterings can be estimated as

$$\Delta_k E \sim k E_{\rm ex}. \tag{131}$$

It does not increase with the energy of the beam. In this scenario

$$\langle x_{F,k}\rangle \approx \langle x_{F,1}\rangle\left(1 - k\frac{E_{\rm ex}}{E_q}\right) \tag{132}$$

and the impact of nonperturbative nuclear quenching would diminish with the beam energy. Such a scenario is a part of the so-called yo-yo, or the inside-outside cascade, models [38,63,64].

In still another version of the formation length model, the hadronization in the nucleus region does not affect the leading jet production at all. The hadronization of the color string degrees of freedom with the formation length $l_f \gtrsim R_A$, i.e., with the momenta larger than $k_A \approx R_A m_\perp^2$, proceeds way beyond the target nucleus. Then the yield of such hadrons will be independent of the target-nucleus fragmentation. The energy which flows into the excitation of the nucleus will cause a depletion of the density of secondary hadrons with the momenta $p \sim R_A m_\perp^2$, while the spectra of faster secondary hadrons will not be affected by excitation of the nucleus. Such a scenario with $\langle x_{F,k}\rangle = \langle x_F\rangle$ was suggested a long time ago within the pre-QCD parton and multiperipheral models [41,42,58].

The separation between different scenarios can only be done experimentally. First, one must evaluate a quenching

of the leading parton spectrum for the perturbative LPM effect [31]. The nonperturbative quenching will be an extra to the LPM effect, it is characterized by $z_k = \langle x_{F,k}\rangle/\langle x_{F,1}\rangle$. If $D(x_F)$ is the fragmentation function for jets produced off free nucleons, then after k-quasielastic rescatterings of the leading parton

$$D_k(x_F) \approx \frac{1}{z_k} D\left(\frac{x_F}{z_k}\right). \tag{133}$$

The manifest dependence of the fragmentation function $D_k(x_F)$ on k breaks the limiting fragmentation. At a fixed ν, the recoiling jet will be described by the fragmentation function $D_{\nu-1-k}(x_F)$.

3. Going more differential: backward production in semiinclusive DIS

If the nonperturbative quenching is under quantitative control one would be able to reconstruct the parton level jet cross sections. Then, by virtue of (121), and its extension to the rapidity and transverse momentum spectra in backward multiproduction,

$$\frac{dn_B}{d\eta} \approx \nu \frac{dn}{d\eta}\bigg|_{pN}, \tag{134}$$

our topological cross sections (98) and (123) describe a correlation between the leading (antiquark) quark jet and multiproduction in the backward hemisphere. Generalizing the arguments of Sec. VII A, we can predict from (123) the backward multiplicity distributions as a function of x_F of the leading jet. Similarly, (98) can be used to predict the $(x_F, \boldsymbol{p})$ dependence of n_B distributions.

The other way around, (98) predicts the ν, i.e., n_B, dependence of the leading particle spectrum. Here the crucial ingredient is $d\sigma^{(k)}_{\rm Qel}(\boldsymbol{\kappa})/d^2\boldsymbol{\kappa}$. The detailed studies of the collective glue $f^{(k)}(x, \boldsymbol{\kappa})$ are found in Refs. [23,24]. The onset of the unitarity constraints in fully inclusive DIS is controlled by the so-called saturation scale

$$Q_A^2(\boldsymbol{b}, x) \approx \frac{4\pi^2}{N_c}\alpha_S(Q_A^2)G(x, Q_A^2)T(\boldsymbol{b}). \tag{135}$$

In semiinclusive case the relevant k-dependent scale is [24]

$$Q_{A,k}^2(\boldsymbol{b}, x) \approx \frac{k}{\nu_A(\boldsymbol{b})} Q_A^2(\boldsymbol{b}, x). \tag{136}$$

For small momenta, $\boldsymbol{\kappa}^2 \lesssim Q_{A,k}^2(\boldsymbol{b}, x)$, the nuclear attenuation effects take over and

$$\frac{d\sigma^{(k)}_{\rm Qel}(\boldsymbol{\kappa})}{d^2\boldsymbol{\kappa}} \approx \frac{\sigma_{\rm Qel}}{\pi}\cdot\frac{Q_{A,k}^2(\boldsymbol{b}, x)}{[\boldsymbol{\kappa} + Q_{A,k}^2(\boldsymbol{b}, x)]^2 2} \approx \frac{\sigma_{\rm Qel}}{\pi Q_{A,k}^2(\boldsymbol{b}, x)} \propto \frac{1}{k}. \tag{137}$$

Consequently, for semihard $\boldsymbol{p}^2 \lesssim Q_A^2(\boldsymbol{b}, x)$ the contribution from large-k is suppressed.

For large momenta, $\boldsymbol{\kappa}^2 \gtrsim Q_{A,k}^2(\boldsymbol{b}, x)$, the k-dependence of the multiple quasielastic scattering cross section is given by [23]

$$\frac{d\sigma^{(k)}_{\rm Qel}(\boldsymbol{\kappa})}{d^2\boldsymbol{\kappa}} = k\frac{d\sigma_{\rm Qel}(\boldsymbol{\kappa})}{d^2\boldsymbol{\kappa}}\bigg[1 + \frac{k-1}{\nu_A(\boldsymbol{b})}\cdot\frac{\gamma^2}{2} \cdot\frac{\alpha_S(\boldsymbol{\kappa}^2)G(x_A, \boldsymbol{\kappa}^2)}{\alpha_S(Q_A^2)G(x_A, Q_A^2)}\cdot\frac{Q_A^2(\boldsymbol{b}, x_A)}{\boldsymbol{\kappa}^2}\bigg], \tag{138}$$

where $\gamma \approx 2$ is the exponent of the large-$\boldsymbol{\kappa}$ behavior $d\sigma_{\rm Qel}(\boldsymbol{\kappa})/d^2\boldsymbol{\kappa} \sim (\boldsymbol{\kappa}^2)^{-\gamma}$. To the leading twist, the k-fold hard quasielastic scattering is dominated by the single-hard scattering on any of the k-nucleons, on the background of soft scatterings on remaining $(k-1)$ nucleons. This hierarchy goes on: one of those $(k-1)$ rescatterings is again hard and gives rise to the antishadowing nuclear higher twist correction. The latter is behind the nuclear Cronin effect (see [26] and references therein) and our Eq. (98) enables us to predict the ν-dependent Cronin effect for leading jets, the numerical studies will be reported elsewhere.

4. Still more differential: decorrelation of quark-antiquark dijets in DIS

Finally, in the fully differential form, Eq. (76) describes the ν, i.e., centrality, dependence of the out-of-plane (azimuthal, acoplanarity) and in-plane decorrelation of quark-antiquark dijets produced in the current fragmentation region of DIS off nuclei. The relevant discussion for the inclusive case is found in [24].

C. Eliminating the Cheshire Cat grin: isolation of cut Pomerons in single-jet spectrum by multiplicity resummations

The resummation over the spectator antiquark interactions, i.e., over j, in Eq. (98) gives a particularly simple result for the single-quark spectrum (now k is a total number of the nonspectator $\not{p}_e$ and $\not{p}_r$'s):

$$\begin{aligned}\frac{d\sigma^{(k)}(\gamma^* A \to qX)}{d^2\boldsymbol{b}dzd^2\boldsymbol{p}} &= \sum_{\nu>k}\frac{d\sigma_\nu(\gamma^* A \to qX)}{d^2\boldsymbol{b}dzd^2\boldsymbol{p}} \\ &= \frac{1}{2(2\pi)^2}T(\boldsymbol{b})\int_0^1 d\beta w_{k-1}((1-\beta)\nu_A(\boldsymbol{b}))\int d^2\boldsymbol{\kappa}_1 d^2\boldsymbol{\kappa}\frac{d\sigma_{\rm Qel}(\boldsymbol{\kappa})}{d^2\boldsymbol{\kappa}}\cdot\frac{d\sigma^{(k-1)}_{\rm Qel}(\boldsymbol{\kappa}_1)}{\sigma_{\rm Qel}d^2\boldsymbol{\kappa}_1} \\ &\quad\times|\Psi(\beta; z, \boldsymbol{p}-\boldsymbol{\kappa}_1) - \Psi(\beta; z, \boldsymbol{p}-\boldsymbol{\kappa}_1-\boldsymbol{\kappa})|^2.\end{aligned} \tag{139}$$

Including the effect of j color excitations by the spectator quark, the backward multiplicity would equal

$$n_B(j,k) \approx \nu\langle n_B\rangle_{pN} = (j+k)\langle n_B\rangle_{pN} \tag{140}$$

and this resummation over j amounts to the resummation over the backward multiplicities

$$n_B > k\langle n_B\rangle_{pN}. \tag{141}$$

In a paradoxical way, such a multiplicity resummation, crude though it is, eliminates the CCG and isolates the topological cross section with k-cut Pomerons, $\not{P}_e + (k-1)\not{P}_r$, complemented by absorption for the exchange by uncut Pomerons $\mathbb{P}$ contained in w_{k-1}. This way one can test experimentally all the properties of $d\sigma_{\rm Qel}^{(k-1)}$ discussed in Sec. VII B 3. We strongly urge this multiplicity resummation technique as an efficient tool to extract the CCG-unbiased single-parton production properties. Evidently, one should not stretch this resummation to multiplicities at the tail of the multiplicity distributions.

VIII. NONLINEAR $k_\perp$-FACTORIZATION FOR TOPOLOGICAL CROSS SECTIONS IN QUARK-GLUON DIJET PRODUCTION

We follow closely the technique of Ref. [29]. The elastic and color-excitation scattering operators for production of quark-gluon dijets in quark-nucleon and quark-nucleus collisions are reported in Appendix B. Here below $\Psi_{qg}(z,\boldsymbol{r})$ will be the wave function of the qg Fock state of the quark. One can think of the Additive Quark Model scenario for the dilute and small projectile interacting with the dense large target. For instance, a heavy quarkonium is well approximated by the $q\bar{q}$ Fock state. The intrinsic transverse momentum of quarks in the quarkonium is small and comoving spectator antiquark cannot give rise to final states with a high-$p_\perp$ quark and high-$p_\perp$ gluon [25]. We resum over all powers of the large parameter in the problem—the nuclear thickness. The comoving antiquark of the projectile will contribute to the excitation of the nucleus, but the effects of its interaction on the dijet spectrum cancel out upon the integration over the antiquark transverse momentum [22,26]. Neither will it affect the energy flow from the qg dijet to a nucleus, which can be treated at the level of the quark-nucleus collisions as the $q \to qg$ excitation. The qg dijet can be in either color-triplet or higher dimension—sextet and 15-plet—representations. We keep these $SU(3)$ labeling of multiplets at arbitrary N_c.

A. Dijets in the color-triplet representation

1. Color-excitation distributions

We start with the universality class of dijets in the same representation as the incident parton, i.e., with the color-triplet channel of the 4-parton interaction. To the leading order in $1/N_c$ perturbation, only the diagonal part of the color-excitation operator (B7) contributes to the color triplet-dijet production and the calculation of $\langle 3\bar{3}|S^{(4)}_{A,\nu}(\boldsymbol{C})|3\bar{3}\rangle$ simplifies to a single-channel problem. The summation over all orderings of the elastic and color-excitation scatterings of the qg dipole i.e., the β integrations in (41) can be performed analytically with the result

$$\langle 3\bar{3}|\mathcal{S}^{(4)}_{A,\nu}(\boldsymbol{C},\boldsymbol{b})|3\bar{3}\rangle = \frac{1}{\nu!}\left[-\frac{1}{2}\Sigma^{\rm ex}_{11}T(\boldsymbol{b})\right]^\nu S[\boldsymbol{b},\Sigma^{\rm el}_{11}(\boldsymbol{C})]. \tag{142}$$

The cross section operators from Eqs. (B5) and (B8) give

$$\begin{aligned}\langle 3\bar{3}|\mathcal{S}^{(4)}_{A,\nu}(\boldsymbol{C},\boldsymbol{b})|3\bar{3}\rangle = \int d^2\boldsymbol{\kappa}\frac{d\sigma^{(\nu)}_{\rm Qel}(\boldsymbol{\kappa})}{\sigma_{\rm Qel}d^2\boldsymbol{\kappa}}\exp[i\boldsymbol{\kappa}(\boldsymbol{s}+\boldsymbol{r}-\boldsymbol{r}')]\\ \times w_\nu(\nu_A(\boldsymbol{b}))S[\boldsymbol{b},\sigma(x,\boldsymbol{r})]\\ \times S[\boldsymbol{b},\sigma(x,\boldsymbol{r}')]\}.\end{aligned} \tag{143}$$

The factor $S[\boldsymbol{b},\sigma_0(x)]$ in $S[\boldsymbol{b},\Sigma^{\rm el}_{11}(\boldsymbol{r},\boldsymbol{r}')] = S[\boldsymbol{b},\sigma_0(x)]S[\boldsymbol{b},\sigma(x,\boldsymbol{r})]S[\boldsymbol{b},\sigma(x,\boldsymbol{r}')]$ was crucial for this identification of $w_\nu(\nu_A(\boldsymbol{b}))$.

The related contributions from the 2-parton and 3-parton states are given by elastic and color-excitation operators from Eqs. (B1)–(B3) ($n = 2, 3$),

$$\langle 3\bar{3}|\mathcal{S}^{(n)}_{A,\nu}(\boldsymbol{C})|3\bar{3}\rangle = \frac{1}{\nu!}\left[-\frac{1}{2}\Sigma^{(n)}_{\rm ex}T(\boldsymbol{b})\right]^\nu S[\boldsymbol{b},\Sigma^{(n)}_{\rm el}(\boldsymbol{C})], \tag{144}$$

with the result

$$\begin{aligned}\langle 3\bar{3}|\mathcal{S}^{(2)}_{A,\nu}(\boldsymbol{b},\boldsymbol{b}')|3\bar{3}\rangle &= \int d^2\boldsymbol{\kappa}\frac{d\sigma^{(\nu)}_{\rm Qel}(\boldsymbol{\kappa})}{\sigma_{\rm Qel}d^2\boldsymbol{\kappa}}\\ &\times\exp[i\boldsymbol{\kappa}(\boldsymbol{s}+(1-z)\boldsymbol{r}-(1-z)\boldsymbol{r}')]\\ &\times w_\nu(\nu_A(\boldsymbol{b})),\\ \langle 3\bar{3}|\mathcal{S}^{(2)}_{A,\nu}(\boldsymbol{B},\boldsymbol{b}')|3\bar{3}\rangle &= \int d^2\boldsymbol{\kappa}\frac{d\sigma^{(\nu)}_{\rm Qel}(\boldsymbol{\kappa})}{\sigma_{\rm Qel}d^2\boldsymbol{\kappa}}\\ &\times\exp[i\boldsymbol{\kappa}(\boldsymbol{s}+\boldsymbol{r}-(1-z)\boldsymbol{r}')]\\ &\times w_\nu(\nu_A(\boldsymbol{b}))S[\boldsymbol{b},\sigma(x,\boldsymbol{r})],\\ \langle 3\bar{3}|\mathcal{S}^{(2)}_{A,\nu}(\boldsymbol{B}',\boldsymbol{b})|3\bar{3}\rangle &= \int d^2\boldsymbol{\kappa}\frac{d\sigma^{(\nu)}_{\rm Qel}(\boldsymbol{\kappa})}{\sigma_{\rm Qel}d^2\boldsymbol{\kappa}}\\ &\times\exp[i\boldsymbol{\kappa}(\boldsymbol{s}+(1-z)\boldsymbol{r}-\boldsymbol{r}')]\\ &\times w_\nu(\nu_A(\boldsymbol{b}))S[\boldsymbol{b},\sigma(x,-\boldsymbol{r}')].\end{aligned} \tag{145}$$

We combine Eqs. (143) and (145), and in a now familiar pattern, reabsorb $S[\boldsymbol{b},\sigma(x,\boldsymbol{r})]$ and $S[\boldsymbol{b},\sigma(x,\boldsymbol{r}')]$ into intranuclear distortion of the qg dipoles. The resulting nonlinear $k_\perp$-factorization for the color triplet-dijet cross section with ν-color-excited nucleons reads

$$\frac{d\sigma_\nu(q\to\{qg\}_3)}{d^2\boldsymbol{b}dzd^2\boldsymbol{\Delta}d^2\boldsymbol{p}}=\frac{1}{(2\pi)^2}w_\nu(\nu_A(\boldsymbol{b}))\times\frac{d\sigma^{(\nu)}_{\rm Qel}(\boldsymbol{\Delta})}{\sigma_{\rm Qel}d^2\boldsymbol{\Delta}}\times|\Psi_{qg}(1;z,\boldsymbol{p})-\Psi_{qg}(z,\boldsymbol{p}-z\boldsymbol{\Delta})|^2. \tag{146}$$

Following the considerations of Sec. V C, this result could have been obtained from the inclusive triplet-dijet cross section of Ref. [29],

$$\frac{d\sigma(q\to\{qg\}_3)}{d^2\boldsymbol{b}dzd^2\boldsymbol{\Delta}d^2\boldsymbol{p}}=\frac{1}{(2\pi)^2}\phi(\boldsymbol{b},x,\boldsymbol{\Delta})|\Psi_{qg}(1;z,\boldsymbol{p})-\Psi_{qg}(z,\boldsymbol{p}-z\boldsymbol{\Delta})|^2, \tag{147}$$

by taking for $\phi(\boldsymbol{b},x,\boldsymbol{\Delta})$ the familiar multiple-scattering expansion. Such a guesswork leaves open a question about multi-Pomeron exchanges in $\Psi_{qg}(1;z,\boldsymbol{p})$, though.

2. Reggeon field theory interpretation

The Reggeon field theory diagrams for the inclusive triplet cross section (147) are shown in Fig. 11. Its large-N_c structure is best seen in the composite quark-antiquark $Q\bar{Q}$ representation for the gluon, $g^\alpha_\beta=\bar{Q}^\alpha Q_\beta$, where Q and $\bar{Q}$ propagate at the same impact parameter. At large-N_c, the triplet state $\{qg\}_3$ has the structure $Q\{\bar{Q}q\}_0$ with the color-singlet $\{\bar{Q}q\}_0$ [29].

The correspondence to the four terms in $|\Psi_{qg}(1;z,\boldsymbol{p})-\Psi_{qg}(z,\boldsymbol{p}-z\boldsymbol{\Delta})|^2$ is as follows: The diagram of Fig. 11(a) corresponds to $|\Psi_{qg}(z,\boldsymbol{p}-z\boldsymbol{\Delta})|^2$. It originates from $S^{(2)}$, i.e., the scattering of the quark is followed by the in-vacuum fragmentation into the dijet behind the nucleus. As such, it is free of intranuclear absorption and distortion of the color dipole. There is an evident shift of the argument of the wave function for the incident quark with the transverse momentum $\boldsymbol{\Delta}$. The diagram of Fig. 11(b) corresponds to $|\Psi_{qg}(1;z,\boldsymbol{p})|^2$ and describes interactions of the qg pair formed before the target and originates from $S^{(4)}$. The open blobs on the two sides of the unitarity cut indicate the operator, Eq. (63), of the intranuclear absorption and distortions of $\Psi_{qg}(1;z,\boldsymbol{p})$—it is the color-singlet $\{\bar{Q}q\}_0$ dipole which is distorted coherently. The diagrams of Figs. 11(c) and 11(d) describe the interference of the two mechanisms and originate from $S^{(3)}$ for the two possible sets of the three-body states.

The contribution from the intermediate state $\{qg\}_3$ to the $q\not{p}_{A,r}q$ vertex $\not{p}(q\to\{qg\}_3;\not{p}_{A,r})$ equals

$$\not{p}(q\to\{qg\}_3;\not{p}_{A,r};\boldsymbol{p},\boldsymbol{\Delta},\boldsymbol{p}_1,\boldsymbol{p}_2,\boldsymbol{\kappa})=\delta(\boldsymbol{\Delta}-\boldsymbol{\kappa})[\Psi^*_{qg}(1;z,\boldsymbol{p}_2)\delta(\boldsymbol{p}-\boldsymbol{p}_2)-\Psi^*_{qg}(z,\boldsymbol{p}_2)\delta(\boldsymbol{p}-z\boldsymbol{\kappa}-\boldsymbol{p}_2)]\times[\Psi_{qg}(1;z,\boldsymbol{p}_1)\delta(\boldsymbol{p}-\boldsymbol{p}_1)-\Psi_{qg}(z,\boldsymbol{p}_1)\delta(\boldsymbol{p}-z\boldsymbol{\kappa}-\boldsymbol{p}_1)]. \tag{148}$$

Its expansion in terms of the in-vacuum cut Pomerons $\not{p}_r$ reads:

$$\begin{aligned}\not{p}(q\to\{qg\}_3;\nu\not{p}_r;\beta;\boldsymbol{p},\boldsymbol{\Delta},\boldsymbol{p}_1,\boldsymbol{p}_2,\{\boldsymbol{\kappa}_i\})=\delta\Big(\boldsymbol{\Delta}-\sum^\nu\boldsymbol{\kappa}_i\Big)S[\boldsymbol{b},\sigma_0]\Big[\Psi^*_{qg}(1;z,\boldsymbol{p}_2)\delta(\boldsymbol{p}-\boldsymbol{p}_2)\\-\Psi^*_{qg}(z,\boldsymbol{p}_2)\delta\Big(\boldsymbol{p}-z\sum^\nu\boldsymbol{\kappa}_i-\boldsymbol{p}_2\Big)\Big]\Big[\Psi_{qg}(1;z,\boldsymbol{p}_1)\delta(\boldsymbol{p}-\boldsymbol{p}_1)\\-\Psi_{qg}(z,\boldsymbol{p}_1)\delta\Big(\boldsymbol{p}-z\sum^\nu\boldsymbol{\kappa}_i-\boldsymbol{p}_1\Big)\Big].\end{aligned} \tag{149}$$

One can expand further in terms of the uncut in-vacuum Pomerons $\mathbb{P}$ in $S[\boldsymbol{b},\sigma_0]$ and $\Psi_{qg}(1;z,\boldsymbol{p})$, we leave this as an exercise.

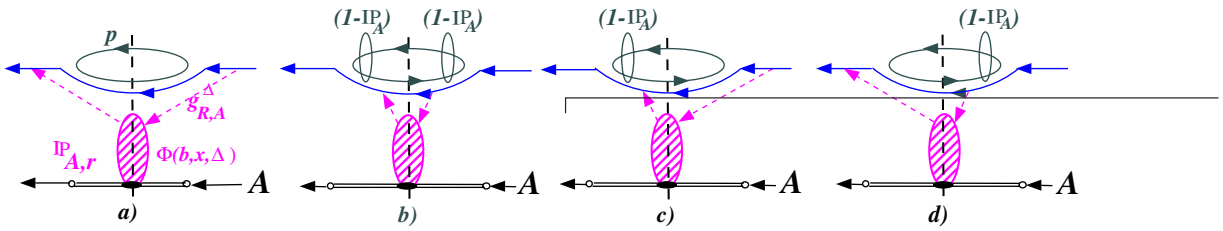

FIG. 11 (color online). The large-N_c Reggeon field theory diagrams for the production of qg dijets on the color-triplet state. The gluon is shown in the composite quark-antiquark representation. The correspondence to the excitation vertex $\propto|\Psi_{qg}(1;z,\boldsymbol{p})-\Psi_{qg}(z,\boldsymbol{p}-z\boldsymbol{\Delta})|^2$ is described in the text: (a) $\Rightarrow|\Psi_{qg}(z,\boldsymbol{p}-z\boldsymbol{\Delta}|^2$, (b) $\Rightarrow|\Psi_{qg}(z,\boldsymbol{p})|^2$, (c) $\Rightarrow\Psi^*_{qg}(1;z,\boldsymbol{p})\Psi_{qg}(z,\boldsymbol{p}-z\boldsymbol{\Delta})$, (d) $\Rightarrow\Psi^*_{qg}(z,\boldsymbol{p}-z\boldsymbol{\Delta})\Psi_{qg}(1;z,\boldsymbol{p})$.

3. Nonperturbative quenching of forward jets in the triplet channel

The quenching of color-triplet quark-gluon jets is entirely controlled by the quark energy loss before a hard fragmentation $q \to qg$, which is parametrized in terms of $z_{\nu-1}$ defined in Sec. VII B 2—compared to the free-nucleon target, here we have $\nu - 1$ extra quasielastic rescatterings. This suggests a hadronization of the quark and gluon jets with the modified quark and gluon fragmentation functions

$$D_{q(g),\nu} = \frac{1}{z_{\nu-1}} D_{q(g)}\left(\frac{x_F}{z_{\nu-1}}\right). \tag{150}$$

4. Integrated topological cross sections in the triplet channel

It is convenient to derive the integrated topological triplet cross sections starting from Eqs. (143)–(145). The integrations over the jet momenta give $\boldsymbol{r}' = \boldsymbol{r}$ and $\boldsymbol{s} = 0$. Taking the relevant elastic and excitation scattering operators from Appendix B, one readily finds

$$\begin{aligned}
\frac{d\sigma_\nu(q \to \{qg\}_3)}{d^2\boldsymbol{b}} &= \int_0^1 dz \int d^2\boldsymbol{r}\Psi^*_{qg}(z,\boldsymbol{r})\Psi_{qg}(z,\boldsymbol{r}) w_\nu(\nu_A(\boldsymbol{b})) \int d^2\boldsymbol{\kappa} \frac{d\sigma^{(\nu)}_{\rm Qel}(\boldsymbol{\kappa})}{\sigma_{\rm Qel} d^2\boldsymbol{\kappa}} \Big\{ \Big(1 - \exp\Big[-\frac{1}{2}\sigma(x,\boldsymbol{r})T(\boldsymbol{b})\Big]\Big)^2 \\
&\quad + 2\exp\Big[-\frac{1}{2}\sigma(x,\boldsymbol{r})T(\boldsymbol{b})\Big](1 - \exp[i(1-z)\boldsymbol{\kappa}\boldsymbol{r}])\Big\} \\
&= \int_0^1 dz \int d^2\boldsymbol{r}\Psi^*_{qg}(z,\boldsymbol{r})\Psi_{qg}(z,\boldsymbol{r}) w_\nu(\nu_A(\boldsymbol{b}))\Big\{\Big(1 - \exp\Big[-\frac{1}{2}\sigma(x,\boldsymbol{r})T(\boldsymbol{b})\Big]\Big)^2 \\
&\quad + 2\exp\Big[-\frac{1}{2}\sigma(x,\boldsymbol{r})T(\boldsymbol{b})\Big]\Big[1 - \Big(1 - \frac{\sigma(x,(1-z)\boldsymbol{r})}{\sigma_0}\Big)^\nu\Big]\Big\} \\
&= \int_0^1 dz \int d^2\boldsymbol{r}\Psi^*_{qg}(z,\boldsymbol{r})\Psi_{qg}(z,\boldsymbol{r})\Big\{w_\nu(\nu_A(\boldsymbol{b}))\Big(1 - \exp\Big[-\frac{1}{2}\sigma(x,\boldsymbol{r})T(\boldsymbol{b})\Big]\Big)^2 \\
&\quad + 2\exp\Big[-\frac{1}{2}\sigma(x,\boldsymbol{r})T(\boldsymbol{b})\Big]\sum_{k=1}^{\nu}\frac{1}{k!}(-1)^{k-1} w_{\nu-k}(\nu_A(\boldsymbol{b}))\Big[\frac{1}{2}\sigma(x,(1-z)\boldsymbol{r})T(\boldsymbol{b})\Big]^k\Big\}.
\end{aligned} \tag{151}$$

For $\nu = 1$ one has an absorption screened impulse approximation. It is proportional to $\sigma(x,(1-z)\boldsymbol{r})$, in agreement to the color multiplet decomposition of the free-nucleon cross section in Eq. (85) of Ref. [29].

B. The universality class of coherent diffraction

The component of (146) with $\nu = 0$ gives the CD excitation of color-triplet dijets:

$$\frac{d\sigma(q \to \{qg\}_3)}{d^2\boldsymbol{b}dzd^2\boldsymbol{\Delta}d^2\boldsymbol{p}}\Big|_{\rm coher} = \frac{1}{(2\pi)^2}\delta(\boldsymbol{\Delta})|\Psi_{qg}(1;z,\boldsymbol{p}) - \Psi_{qg}(z,\boldsymbol{p})|^2 S[\boldsymbol{b},\sigma_0]. \tag{152}$$

This is a known result [29], the above derivation sheds more light on the connection between the diffractive production and the generic color-triplet excitation: Eq. (152) can be obtained putting $\nu = 0$ in (146). Incidentally, the $\nu = 0$ result (151) for the integrated cross section gives the integrated diffraction cross section.

C. The universality class of dijets in higher color multiplets

1. Color-excitation distributions

Excitation of quark-gluon dijets in higher representations, the sextet and 15-plet, is a property of the 4-parton problem, and belongs to the same universality class as an excitation of color-octet dijets in DIS, the only difference is that now the incident quark carries a net color. The leading contribution to the cross section comes from the off-diagonal $\hat{\Sigma}_{\rm ex}$, is of the first order in Ω and $\mathcal{O}(N_c^{-1})$, but this suppression is compensated for by the large number of final states, see Eq. (B10).

Let there be m color-excitation interactions in the initial color-triplet qg, followed by the triplet-to-$\{6+15\}$ transition at the depth $\beta \equiv \beta_{m+1}$, followed by k-color-excitation interactions in the final state. The calculation of the matrix element $\langle 6\bar{6} + 15\overline{15}|S^{(4)}(\boldsymbol{B}',\boldsymbol{B})|3\bar{3}\rangle$ requires the evaluation of

$$\begin{aligned}
&\int_0^1 d\beta_\nu \ldots d\beta \ldots d\beta_1 \theta(1-\beta_\nu)\theta(\beta_\nu - \beta_{\nu-1})\ldots\theta(\beta_1)\sum_{m,k=0}\delta(\nu - 1 - m - k)\exp\Big[-\frac{1}{2}(1-\beta)\Sigma^{\rm el}_{22}T(\boldsymbol{b})\Big] \\
&\times\Big[-\frac{1}{2}\Sigma^{\rm ex}_{22}T(\boldsymbol{b})\Big]^k \frac{1}{2N_c}\Omega T(\boldsymbol{b})\exp\Big[-\frac{1}{2}\beta\Sigma^{\rm el}_{11}T(\boldsymbol{b})\Big]\cdot\Big[-\frac{1}{2}\Sigma^{\rm ex}_{11}T(\boldsymbol{b})\Big]^m.
\end{aligned} \tag{153}$$

The β_i integrations except β give the factors $(1-\beta)^k/k!$ for the final state, and $\beta^m/m!$ for the initial state. The initial-state attenuation $S[\boldsymbol{b},\beta\Sigma_{11}]$ can be decomposed following (145), the familiar identification of the coherent distortion of

dipoles in the slice $[0, \beta]$ and of the probability of m-fold quasielastic scattering of the incident quark follow.

The gluon Casimir C_A enters manifestly the Fourier representation for $\Sigma_{22}^{\rm ex}$ of Eq. (B9) and

$$(-\Sigma_{22}^{\rm ex})^k = \left\{\int d^2\boldsymbol{\kappa} f(x,\boldsymbol{\kappa})\exp(i\boldsymbol{\kappa}\boldsymbol{s}) + \frac{C_A}{C_F}\int d^2\boldsymbol{\kappa} f(x,\boldsymbol{\kappa})\exp[i\boldsymbol{\kappa}(\boldsymbol{s}+\boldsymbol{r}-\boldsymbol{r}')]\right\}^k$$
$$= \sigma_0^k \sum_{j,n=0}\delta(k-j-n)\frac{k!}{j!n!}\int d^2\boldsymbol{\kappa}_1 d^2\boldsymbol{\kappa}_2 \exp[i\boldsymbol{\kappa}_1\boldsymbol{s} + i\boldsymbol{\kappa}_2(\boldsymbol{s}-\boldsymbol{r}+\boldsymbol{r}')]\left(\frac{C_A}{C_F}\right)^n \frac{d\sigma_{\rm Qel}^{(n)}(\boldsymbol{\kappa}_2)}{\sigma_{\rm Qel}d^2\boldsymbol{\kappa}_2}\cdot\frac{d\sigma_{\rm Qel}^{(j)}(\boldsymbol{\kappa}_1)}{\sigma_{\rm Qel}d^2\boldsymbol{\kappa}_1}. \quad (154)$$

The decomposition of the final-state attenuation,

$$S[\boldsymbol{b},(1-\beta)\Sigma_{22}^{\rm el}] = S[\boldsymbol{b},(1-\beta)\sigma_0]S\left[\boldsymbol{b},\frac{C_A}{C_F}(1-\beta)\sigma_0\right], \quad (155)$$

allows an identification of the product $w_n(\frac{C_A}{C_F}(1-\beta)\nu_A(\boldsymbol{b}))w_j((1-\beta)\nu_A(\boldsymbol{b}))$.

Upon the projection onto final states, Eq. (B10), the final nonlinear $k_\perp$-factorization formula for the spectrum of the sextet and 15-plet dijets in final states with color excitation of ν nucleons in the target nucleus reads

$$\frac{d\sigma_\nu(q\to\{qg\}|_{6+15})}{d^2\boldsymbol{b}dzd^2\boldsymbol{\Delta}d^2\boldsymbol{p}} = \frac{1}{(2\pi)^2}T(\boldsymbol{b})\int_0^1 d\beta\int d^2\boldsymbol{\kappa}d^2\boldsymbol{\kappa}_1 d^2\boldsymbol{\kappa}_2 d^2\boldsymbol{\kappa}_3\delta(\boldsymbol{\kappa}+\boldsymbol{\kappa}_1+\boldsymbol{\kappa}_2+\boldsymbol{\kappa}_3-\boldsymbol{\Delta})$$
$$\times|\Psi_{qg}(\beta;z,\boldsymbol{p}-\boldsymbol{\kappa}_1)-\Psi_{qg}(\beta;z,\boldsymbol{p}-\boldsymbol{\kappa}_1-\boldsymbol{\kappa})|^2\sum_{j,k,m,n=0}\delta(\nu-1-m-k)\delta(k-j-n)$$
$$\times w_m(\beta\nu_A(\boldsymbol{b}))w_n\left(\frac{C_A}{C_F}(1-\beta)\nu_A(\boldsymbol{b})\right)w_j((1-\beta)\nu_A(\boldsymbol{b}))\frac{d\sigma_{\rm Qel}(\boldsymbol{\kappa})}{d^2\boldsymbol{\kappa}}\cdot\frac{d\sigma_{\rm Qel}^{(m)}(\boldsymbol{\kappa}_3)}{\sigma_{\rm Qel}d^2\boldsymbol{\kappa}_3}\frac{d\sigma_{\rm Qel}^{(n)}(\boldsymbol{\kappa}_2)}{\sigma_{\rm Qel}d^2\boldsymbol{\kappa}_2}$$
$$\cdot\frac{d\sigma_{\rm Qel}^{(j)}(\boldsymbol{\kappa}_1)}{\sigma_{\rm Qel}d^2\boldsymbol{\kappa}_1}. \quad (156)$$

This result could have been obtained, following the considerations of Sec. V C, from the inclusive cross section of Ref. [29]:

$$\frac{d\sigma(q\to\{qg\}|_{6+15})}{d^2\boldsymbol{b}dzd^2\boldsymbol{\Delta}d^2\boldsymbol{p}} = \frac{1}{(2\pi)^2}T(\boldsymbol{b})\int_0^1 d\beta\int d^2\boldsymbol{\kappa}d^2\boldsymbol{\kappa}_1 d^2\boldsymbol{\kappa}_2 d^2\boldsymbol{\kappa}_3\delta(\boldsymbol{\Delta}-\boldsymbol{\kappa}-\boldsymbol{\kappa}_1-\boldsymbol{\kappa}_2-\boldsymbol{\kappa}_3)$$
$$\times|\Psi_{qg}(\beta;z,\boldsymbol{p}-\boldsymbol{\kappa}_1)-\Psi_{qg}(\beta;z,\boldsymbol{p}-\boldsymbol{\kappa}_1-\boldsymbol{\kappa})|^2 f(x,\boldsymbol{\kappa})\Phi(1-\beta;\boldsymbol{b},x,\boldsymbol{\kappa}_1)$$
$$\times\Phi\left(\frac{C_A}{C_F}(1-\beta);\boldsymbol{b},x,\boldsymbol{\kappa}_2\right)\Phi(\beta;\boldsymbol{b},x,\boldsymbol{\kappa}_3). \quad (157)$$

2. Reggeon field theory interpretation

With hindsight, we realize that the nonlinear $k_\perp$-factorization has a remarkable built-in separation of the uncut, and two kinds of cut, Pomerons. First we recall the large-N_c property $C_A = 2C_F$ and the convolution property

$$(\Phi(\beta_1;\boldsymbol{b})\otimes\Phi(\beta_2;\boldsymbol{b}))(\boldsymbol{\kappa}) = \Phi(\beta_1+\beta_2;\boldsymbol{b},x,\boldsymbol{\kappa}). \quad (158)$$

Anticipating the composite quark-antiquark representation for the large-N_c gluon, we make use of (158) to represent

$$\Phi\left(\frac{C_A}{C_F}(1-\beta);\boldsymbol{b},x,\boldsymbol{\kappa}\right) = \Phi(2(1-\beta);\boldsymbol{b},x,\boldsymbol{\kappa}) = \int d^2\boldsymbol{\kappa}_1 d^2\boldsymbol{\kappa}_2\delta(\boldsymbol{\kappa}-\boldsymbol{\kappa}_1-\boldsymbol{\kappa}_2)\Phi(1-\beta;\boldsymbol{b},x,\boldsymbol{\kappa}_1)\Phi(1-\beta;\boldsymbol{b},x,\boldsymbol{\kappa}_2), \quad (159)$$

where we made use of the large-N_c property $C_A = 2C_F$. Then we cast (157) in the form

$$\frac{d\sigma(q\to\{qg\}|_{6+15})}{d^2\boldsymbol{b}dzd^2\boldsymbol{\Delta}d^2\boldsymbol{p}} = \frac{1}{(2\pi)^2}T(\boldsymbol{b})\int_0^1 d\beta\int d^2\boldsymbol{\kappa}d^2\boldsymbol{\kappa}_1 d^2\boldsymbol{\kappa}_2 d^2\boldsymbol{\kappa}_3 d^2\boldsymbol{\kappa}_4\delta(\boldsymbol{\Delta}-\boldsymbol{\kappa}-\boldsymbol{\kappa}_1-\boldsymbol{\kappa}_2-\boldsymbol{\kappa}_3-\boldsymbol{\kappa}_4)$$
$$\times|\Psi_{qg}(\beta;z,\boldsymbol{p}-\boldsymbol{\kappa}_1)-\Psi_{qg}(\beta;z,\boldsymbol{p}-\boldsymbol{\kappa}_1-\boldsymbol{\kappa})|^2 f(x,\boldsymbol{\kappa})\Phi(1-\beta;\boldsymbol{b},x,\boldsymbol{\kappa}_1)\Phi(1-\beta;\boldsymbol{b},x,\boldsymbol{\kappa}_2)$$
$$\times\Phi(1-\beta;\boldsymbol{b},x,\boldsymbol{\kappa}_3)\Phi(\beta;\boldsymbol{b},x,\boldsymbol{\kappa}_4), \quad (160)$$

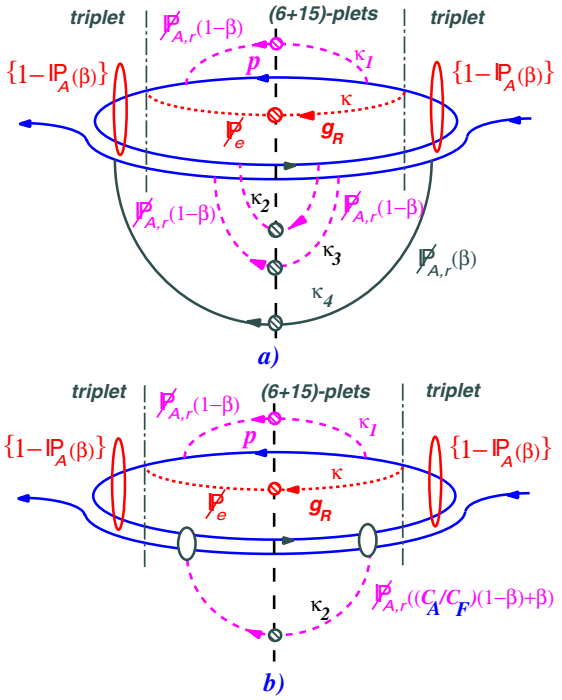

FIG. 12 (color online). The large-N_c structure of cut nuclear Pomeron RFT diagram for production of quark-gluon dijets in higher multiplets (sextet and 15-plet in $SU(3)_c$ and their large-N_c generalizations). The bottom diagram (b) is the RFT representation for the diagram (a) upon the convolution (161). Gluons are shown in the composite quark-antiquark representation. For a more detailed description see the text.

which is custom-tailored for identification of interactions of the composite $Q\bar{Q}$ gluon with different Pomerons.

The corresponding unitarity-cut RFT diagram is shown in Fig. 12(a). In this very busy plot only the gluon—either $g_{R,A}$ or g_R—loops are shown, the dashed cut circles stand for the corresponding gluon densities. We show only one of the four possible couplings of the in-vacuum gluon g_R from the cut Pomeron $I\!P_e$ to the quark loop. Only the Pomeron operator structure of distortions of $\Psi_{qg}(\beta; z, \boldsymbol{p})$ in the slice $[0, \beta]$ is indicated, see Eq. (63), these distortions do not depend on the multiplicity of cut Pomerons. The transitions at the depth β from the initial-state color-triplet qg to the higher representations—sextet and 15-plet—are indicated by a short-dashed vertical line on the right-hand side (r.h.s.) and l.h.s. of the unitarity cut.

In the slice $[0, \beta]$ color rotations only within the triplet state are allowed. Correspondingly, as we learned in Sec. VIII A 2, only the quark Q of the composite gluon would couple to the nuclear glue $g_{R,A}$: the triplet property of this quark is retained after any multiplicity of rescatterings, while the color-singlet $\{\bar{Q}q\}_0$ state is distorted coherently. The higher—sextet and 15-plet—representations are obtained after excitation of the color-singlet $\{\bar{Q}q\}_0$ to the color-octet $\{\bar{Q}q\}_8$, upon which all three partons interact independently.

In the practical calculations it is advisable to make use of the convolution property (158) the other way around,

$$(\Phi(1-\beta;\boldsymbol{b})\otimes\Phi(1-\beta;\boldsymbol{b})\otimes\Phi(\beta;\boldsymbol{b}))(\boldsymbol{\kappa}) = \Phi(\beta^*;\boldsymbol{b},x,\boldsymbol{\kappa}), \tag{161}$$

where

$$\beta^* = \frac{C_A}{C_F}(1-\beta)+\beta, \tag{162}$$

which defines the collective nuclear cut Pomeron $I\!P_{A,r}(\beta^*)$. The corresponding RFT diagram is shown in Fig. 12(b). The above clear-cut origin of different nuclear cut Pomerons is obscured by such a shorthand form of the spectrum, but it brings the spectrum to a close similarity with the spectrum of dijets in inelastic DIS and is convenient for the RFT representation of topological cross sections in terms of multiple exchanges by in-vacuum cut Pomerons $I\!P_r$. For instance, the contribution from intermediate state $\{qg\}_{6+15}$ to the $qI\!P_eI\!P_{A,r}(\beta^*)q$ vertex would equal

$$\begin{aligned}&I\!D(q\to\{qg\}_{6+15};I\!P_{A,r}(1-\beta),I\!P_e,I\!P_{A,r}(\beta^*);\beta;\boldsymbol{p},\boldsymbol{\Delta},\boldsymbol{p}_1,\boldsymbol{p}_2,\boldsymbol{\kappa},\boldsymbol{\kappa}_1,\boldsymbol{\kappa}_2)\\ &=\delta(\boldsymbol{\Delta}-\boldsymbol{\kappa}_1-\boldsymbol{\kappa}_2-\boldsymbol{\kappa})\Psi^*_{qg}(\beta;z,\boldsymbol{p}_2)[\delta(\boldsymbol{p}-\boldsymbol{\kappa}_1-\boldsymbol{p}_2)-\delta(\boldsymbol{p}-\boldsymbol{\kappa}_1-\boldsymbol{\kappa}-\boldsymbol{p}_2)]\\ &\times[\delta(\boldsymbol{p}-\boldsymbol{\kappa}_1-\boldsymbol{p}_1)-\delta(\boldsymbol{p}-\boldsymbol{\kappa}_1-\boldsymbol{\kappa})-\boldsymbol{p}_1)]\Psi_{qg}(\beta;z,\boldsymbol{p}_1),\end{aligned} \tag{163}$$

and its expansion in terms of the in-vacuum cut Pomerons $I\!P_r$ reads

$$\begin{aligned}&I\!D(q\to\{qg\}_{6+15};jI\!P_r,I\!P_e,kI\!P_r;\beta;\boldsymbol{p},\boldsymbol{\Delta},\boldsymbol{p}_1,\boldsymbol{p}_2,\boldsymbol{\kappa},\{\boldsymbol{k}_i\},\{\boldsymbol{q}_m\})\\ &=\delta\Big(\boldsymbol{\Delta}-\sum_{i=1}^{j}\boldsymbol{k}_i-\sum_{m=1}^{k}\boldsymbol{q}_m-\boldsymbol{\kappa}\Big)S[\boldsymbol{b},(1-\beta)\sigma_0(x)]S[\boldsymbol{b},\beta^*\sigma_0(x)](\beta^*)^k(1-\beta)^j\Psi^*_{qg}(\beta;z,\boldsymbol{p}_2)\\ &\times\Big[\delta\Big(\boldsymbol{p}-\sum_{i=1}^{j}\boldsymbol{k}_i-\boldsymbol{p}_2\Big)-\delta\Big(\boldsymbol{p}-\sum_{i=1}^{j}\boldsymbol{k}_i-\boldsymbol{\kappa}-\boldsymbol{p}_2\Big)\Big]\Big[\delta\Big(\boldsymbol{p}-\sum_{i=1}^{j}\boldsymbol{k}_i-\boldsymbol{p}_1\Big)-\delta\Big(\boldsymbol{p}-\sum_{i=1}^{j}\boldsymbol{k}_i-\boldsymbol{\kappa}-\boldsymbol{p}_1\Big)\Big]\Psi_{qg}(\beta;z,\boldsymbol{p}_1).\end{aligned} \tag{164}$$

3. Nonperturbative quenching of leading jets

In comparison to DIS, a new feature is that both the initial and final-state interactions of the qg system contribute to the nonperturbative quenching of jets. One would associate color excitations in the slice $[0, \beta]$ of the nucleus with the m-fold quasielastic scattering of the incident quark. It is followed by hard excitation $q \to qg$ at the depth β. The quark and gluon jet hadronization (fragmentation) functions are different (for the review see [65]) and a correct partition of n-fold color excitations in the slice $[\beta, 1]$ between the quark and gluon quasielastic rescatterings is important. Evidently, $w_k(\frac{C_A}{C_F}(1-\beta)\nu_A(\boldsymbol{b}))$ must be regarded as a probability of the k-fold rescattering of the gluon, while $w_j((1-\beta)\nu_A(\boldsymbol{b}))$ describes the j-fold rescattering of the quark. The nucleon excited into the color-octet state would arguably hadronize independently of the projectile parton. Along the tree of quark interactions we have $(m + j)$ quasielastic scatterings and the average energy of the final-state quark will be scaled down by the factor $z_q = z_{m+j}$ which must be used in the modified fragmentation function (133), while the energy of gluons scales down by the factor $z_g = z_{m+k}$.

4. Integrated topological cross sections

Taking the relevant elastic and excitation scattering operators for $\boldsymbol{s} = 0$ and $\boldsymbol{r} = \boldsymbol{r}'$, we obtain

$$\frac{d\sigma_\nu(q \to \{qg\}_{6+15})}{d^2\boldsymbol{b}} = \int_0^1 dz \int d^2\boldsymbol{r}\Psi^*_{qg}(z,\boldsymbol{r})\Psi_{qg}(z,\boldsymbol{r}) \int_0^1 d\beta \sum_{j,k=0} \delta(\nu - 1 - j - k) w_j(\beta\nu_A(\boldsymbol{b})) w_k\left(\frac{C_{15}}{C_F}(1-\beta)\nu_A(\boldsymbol{b})\right) \times \sigma(x,\boldsymbol{r}) \exp[-\beta\sigma(x,\boldsymbol{r})T(\boldsymbol{b})]. \tag{165}$$

Here the Casimir $C_{15} = C_6$ makes an explicit appearance.

There is a strong distinction between the topological cross section for the triplet and sextet plus 15-plet sectors. It is a clear-cut manifestation of the non-Abelian coupled-channel intranuclear evolution of color dipoles in pQCD.

Regarding the practical applications of (151) and (165) to the proton-nucleus collisions, one can start with the oversimplified Additive Quark Model scenario for multiproduction [58,66]. Here (58) is the Born cross section for the constituent quark-nucleus interaction. This Born cross section must be corrected for pQCD virtual emission as described in Ref. [31]. Then our Eqs. (151) and (165) describe the real emission radiative corrections to the constituent quark-nucleus interaction.

IX. TOPOLOGICAL CROSS SECTIONS FOR GLUON-GLUON DIJET PRODUCTION

A. Color-diagonal and color-excitation interactions

The underlying pQCD subprocess is $gg_t \to gg$, where g is the gluon from the projectile hadron. A full derivation of irreducible color-representations for digluon states, their nomenclature, and the cross section operators $\hat{\Sigma}^{(n)}$ for color-singlet two-gluon, three-gluon, and four-gluon states at arbitrary N_c is found in Ref. [30].

Make notice of the important change of the notations: hereafter the basic quantity is a cross section for the color-singlet octet-octet dipole

$$\sigma_{gg}(x,\boldsymbol{r}) = \frac{C_A}{C_F}\int d^2\boldsymbol{\kappa} f(x,\boldsymbol{\kappa})[1 - \exp(i\boldsymbol{\kappa}\boldsymbol{r})] = \frac{C_A}{C_F}\sigma_{q\bar{q}}(x,\boldsymbol{r}). \tag{166}$$

Similarly, we define the nuclear thickness

$$\nu_{A,gg}(\boldsymbol{b}) = \frac{1}{2}\sigma_{gg,0}(x)T(\boldsymbol{b}) = \frac{1}{2}\cdot\frac{C_A}{C_F}\sigma_{\bar{q}q,0}(x)T(\boldsymbol{b}). \tag{167}$$

The differential cross section of quasielastic gluon-nucleon scattering equals

$$\frac{d\sigma_{g,\mathrm{Qel}}}{d^2\boldsymbol{\kappa}} = \frac{C_A}{C_F}\cdot\frac{1}{2}f(x,\boldsymbol{\kappa}) \tag{168}$$

and

$$\sigma_{g,\mathrm{Qel}} = \int d^2\boldsymbol{\kappa}\frac{d\sigma_{g,\mathrm{Qel}}}{d^2\boldsymbol{\kappa}} = \frac{C_A}{C_F}\cdot\sigma_{q,\mathrm{Qel}}. \tag{169}$$

The octet-octet dipole nuclear S-matrix defines the octet-octet collective nuclear glue

$$\Phi_{gg}(\boldsymbol{b},x,\boldsymbol{\kappa}_1) = \frac{1}{(2\pi)^2}\int d^2\boldsymbol{r}S[\boldsymbol{b},\sigma_{gg}(x,\boldsymbol{r})]\exp[-i\boldsymbol{\kappa}\cdot\boldsymbol{r}] = \sum_{j=0} w_j(\nu_A(\boldsymbol{b}))\frac{d\sigma^{(j)}_{g,\mathrm{Qel}}}{\sigma_{g,\mathrm{Qel}}d^2\boldsymbol{\kappa}}. \tag{170}$$

There is an obvious identity

$$\frac{d\sigma^{(j)}_{g,\mathrm{Qel}}}{\sigma_{g,\mathrm{Qel}}d^2\boldsymbol{\kappa}} = \frac{d\sigma^{(j)}_{\mathrm{Qel}}}{\sigma_{\mathrm{Qel}}d^2\boldsymbol{\kappa}}. \tag{171}$$

Finally, now $\Psi_{gg}(z,\boldsymbol{p})$ would be the wave function of the gg Fock state of the gluon, its relation to the splitting function $P_{gg}(z)$ is found in Ref. [26].

B. Topological cross sections for gluon-gluon dijets

The subsequent derivation of the dijet cross sections would repeat that for the quark-gluon dijets and we sketch it only briefly. The incident parton is the color-octet gluon, and the excitation of color-octet digluons is driven by color

rotations within the octet sector and is $\mathcal{O}(N_c^0)$. Excitation of dijets in higher multiplets—two decuplets, 27, and R_7—is driven by the off-diagonal $\hat{\omega}$ and is also $\mathcal{O}(N_c^0)$: the large number of states in higher multiplets overcomes the suppression of their excitation. Excitation of color-singlet dijets is $\mathcal{O}(N_c^{-2})$. Invoking the considerations of Sec. V E, we can derive the topological dijet cross sections directly from our results for the inclusive cross sections [30], we confine ourselves to the two most important examples. We report the leading terms of the large-N_c perturbation theory.

1. The universality class of color multiplets of the projectile parton: color-octet sector

For dijets in the color-octet final state the inclusive cross section equals

$$\frac{d\sigma(g \to \{g_1 g_2\}_{8_A+8_S})}{d^2\boldsymbol{b}dzd^2\boldsymbol{p}d^2\boldsymbol{\Delta}} = \frac{1}{2(2\pi)^2}\int d^2\boldsymbol{\kappa}_1 \int d^2\boldsymbol{\kappa}_2 \delta^{(2)}(\boldsymbol{\Delta}-\boldsymbol{\kappa}_1-\boldsymbol{\kappa}_2)\{|\Psi_{gg}(1;z,\boldsymbol{p}-\boldsymbol{\kappa}_1)-\Psi_{gg}(z,\boldsymbol{p}-z(\boldsymbol{\kappa}_1+\boldsymbol{\kappa}_2))|^2 + |\Psi_{gg}(1;z,\boldsymbol{p}-\boldsymbol{\kappa}_2)-\Psi_{gg}(z,\boldsymbol{p}-z(\boldsymbol{\kappa}_1+\boldsymbol{\kappa}_2))|^2\}\Phi_g(\boldsymbol{b},x,\boldsymbol{\kappa}_2)\Phi_g(\boldsymbol{b},x,\boldsymbol{\kappa}_1). \tag{172}$$

(Here the symmetrization over $\boldsymbol{\kappa}_{1,2}$ is optional.) Its major subtlety is that the nonlinear $k_\perp$-factorization quadrature is formulated in terms of the collective glue $\Phi_g(\boldsymbol{b},x,\boldsymbol{\kappa}_1)$ for dipoles interacting with one-half of the octet-octet dipole cross section,

$$\Phi_g(\boldsymbol{b},x,\boldsymbol{\kappa}_1) = \frac{1}{(2\pi)^2}\int d^2\boldsymbol{r} S\left[\boldsymbol{b},\frac{1}{2}\sigma_{gg}(x,\boldsymbol{r})\right] = \sum_{j=0} w_j\left(\frac{1}{2}\nu_{A,gg}(\boldsymbol{b})\right)\frac{d\sigma^{(j)}_{g,\mathrm{Qel}}}{\sigma_{g,\mathrm{Qel}}d^2\boldsymbol{\kappa}}. \tag{173}$$

At large N_c we have an equality $\Phi_g(\boldsymbol{b},x,\boldsymbol{\kappa}_1)=\Phi(\boldsymbol{b},x,\boldsymbol{\kappa}_1)$. The topological cross sections derive from the expansion

$$\Phi_g(\boldsymbol{b},x,\boldsymbol{\kappa}_2)\Phi_g(\boldsymbol{b},x,\boldsymbol{\kappa}_1) = \sum_{\nu=0}\sum_{k=0}\sum_{n=0}\delta(\nu-k-n)w_k\left(\frac{1}{2}\nu_{A,gg}(\boldsymbol{b})\right)w_n\left(\frac{1}{2}\nu_{A,gg}(\boldsymbol{b})\right)\frac{d\sigma^{(k)}_{g,\mathrm{Qel}}(\boldsymbol{\kappa}_1)}{\sigma_{g,\mathrm{Qel}}d^2\boldsymbol{\kappa}_1}\cdot\frac{d\sigma^{(n)}_{g,\mathrm{Qel}}(\boldsymbol{\kappa}_2)}{\sigma_{g,\mathrm{Qel}}d^2\boldsymbol{\kappa}_2}. \tag{174}$$

The term with $\nu=0$ gives the CD $g\to gg$.

In view of large-N_c equality $\Phi_g(\boldsymbol{b},x,\boldsymbol{\kappa}_1)=\Phi(\boldsymbol{b},x,\boldsymbol{\kappa}_1)$, the emergence of $\Phi_g(\boldsymbol{b},x,\boldsymbol{\kappa}_1)$ entails a simple RFT representation for (172) in terms of the composite quark-antiquark representation in Fig. 13. Here the central quark loop describes a propagation of the color-singlet quark-antiquark. It is the wave function of this color-singlet dipole which is coherently distorted by intranuclear propagation, as shown by vertical open blobs in diagrams 13(b)–13(d) containing interactions of the preformed gluon-gluon state.

The contribution from the gluon loop with the color-octet intermediate state $g\to\{gg\}_8$ to the $g\not{P}_{A,r}$, $\not{P}_{A,r}g$ vertex is a straightforward generalization of Eq. (148) for color-triplet excitation $q\to\{qg\}_3$:

$$\not{D}(g\to\{gg\}_8;\not{P}_{A,r},\not{P}_{A,r};\boldsymbol{p},\boldsymbol{\Delta},\boldsymbol{p}_1,\boldsymbol{p}_2,\boldsymbol{\kappa}_1,\boldsymbol{\kappa}_2) = \delta(\boldsymbol{\Delta}-\boldsymbol{\kappa}_1-\boldsymbol{\kappa}_1)S[\boldsymbol{b},\sigma_0][\Psi^*_{gg}(1;z,\boldsymbol{p}_2)\delta(\boldsymbol{p}-\boldsymbol{\kappa}_1-\boldsymbol{p}_2) - \Psi^*_{gg}(z,\boldsymbol{p}_2)\delta(\boldsymbol{p}-z(\boldsymbol{\kappa}_1+\boldsymbol{\kappa}_2)-\boldsymbol{p}_2)][\Psi_{gg}(1;z,\boldsymbol{p}_1)\delta(\boldsymbol{p}-\boldsymbol{\kappa}_1-\boldsymbol{p}_1) - \Psi_{gg}(z,\boldsymbol{p}_1)\delta(\boldsymbol{p}-z(\boldsymbol{\kappa}_1+\boldsymbol{\kappa}_2)-\boldsymbol{p}_1)]. \tag{175}$$

The pattern of transformation from (175) to the expansion in terms of the in-vacuum cut Pomerons $\not{P}_r$ is the same as in the

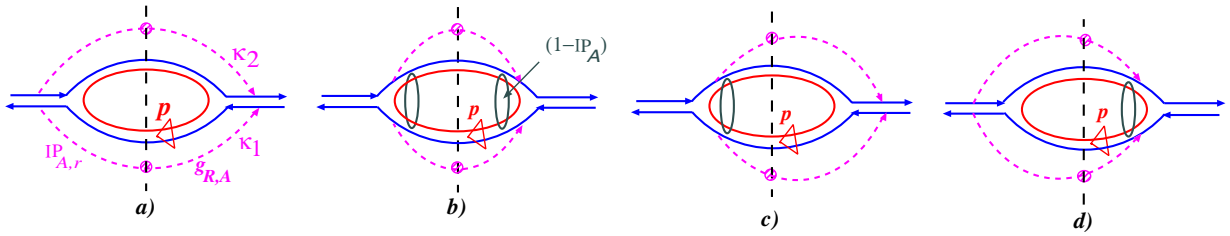

FIG. 13 (color online). The large-N_c structure of cut nuclear Pomeron diagram for production of color-octet gluon-gluon dijets. Gluons are shown in the composite quark-antiquark representation, the shaded circles stand for the collective nuclear gluon densities. The correspondence to the excitation vertex $\propto|\Psi_{gg}(1;z,\boldsymbol{p}-\boldsymbol{\kappa}_1)-\Psi_{gg}(z,\boldsymbol{p}-z(\boldsymbol{\kappa}_1+\boldsymbol{\kappa}_2))|^2$ is as follows: (a) $\Rightarrow|\Psi_{gg}(z,\boldsymbol{p}-z(\boldsymbol{\kappa}_1+\boldsymbol{\kappa}_2))|^2$, (b) $\Rightarrow|\Psi_{gg}(1;z,\boldsymbol{p}-\boldsymbol{\kappa}_1)|^2$, (c) $\Rightarrow\Psi^*_{gg}(1;z,\boldsymbol{p}-\boldsymbol{\kappa}_1)\Psi_{gg}(z,\boldsymbol{p}-z(\boldsymbol{\kappa}_1+\boldsymbol{\kappa}_2))$, (d) $\Rightarrow\Psi^*_{gg}(z,\boldsymbol{p}-z(\boldsymbol{\kappa}_1+\boldsymbol{\kappa}_2))\Psi_{gg}(1;z,\boldsymbol{p}-\boldsymbol{\kappa}_1)$.

transformation from (148) to (149), we leave this as an exercise.

The fully integrated topological cross section can readily be derived:

$$\begin{aligned}\frac{d\sigma_\nu(g\to\{gg\}_8)}{d^2\boldsymbol{b}} &= \int_0^1 dz\int d^2\boldsymbol{r}|\Psi_{gg}(z,\boldsymbol{r})|^2 w_\nu(\nu_A(\boldsymbol{b}))\Big\{\Big(1-\exp\Big[-\frac{1}{2}\sigma_{gg}(x,\boldsymbol{r})T(\boldsymbol{b})\Big]\Big)^2\\ &\quad+2\exp\Big[-\frac{1}{2}\sigma_{gg}(x,\boldsymbol{r})T(\boldsymbol{b})\Big]\Big[1-\Big(1-\frac{\sigma_{gg}(x,(1-z)\boldsymbol{r})+\sigma_{gg}(x,z\boldsymbol{r})}{2\sigma_{gg,0}(x)}\Big)^\nu\Big]\Big\}\\ &= \int_0^1 dz\int d^2\boldsymbol{r}|\Psi_{gg}(z,\boldsymbol{r})|^2\Big\{w_\nu(\nu_A(\boldsymbol{b}))\Big(1-\exp\Big[-\frac{1}{2}\sigma_{gg}(x,\boldsymbol{r})T(\boldsymbol{b})\Big]\Big)^2\\ &\quad+2\exp\Big[-\frac{1}{2}\sigma_{gg}(x,\boldsymbol{r})T(\boldsymbol{b})\Big]\sum_{k=1}^{\nu}\frac{1}{k!}(-1)^{k-1}w_{\nu-k}(\nu_A(\boldsymbol{b}))\Big[\frac{1}{4}[\sigma_{gg}(x,(1-z)\boldsymbol{r})+\sigma_{gg}(x,z\boldsymbol{r})]T(\boldsymbol{b})\Big]^k\Big\}.\end{aligned} \tag{176}$$

In conformity to the concept of universality classes, there is a striking similarity to (151).

2. *The universality class of higher representations:* $\dim(R)=\mathcal{O}(N_c^4)$

We cite the result [30]

$$\begin{aligned}\frac{d\sigma(g\to\{g_1g_2\}_{10+\overline{10}+27+R_7})}{d^2\boldsymbol{b}dzd^2\boldsymbol{p}d^2\boldsymbol{\Delta}} &= \frac{1}{4(2\pi)^2}\int_0^1 d\beta\int d^2\boldsymbol{\kappa}_4 d^2\boldsymbol{\kappa}_3 d^2\boldsymbol{\kappa}_2 d^2\boldsymbol{\kappa}_1 d^2\boldsymbol{\kappa}\,\delta^{(2)}(\boldsymbol{\Delta}-\boldsymbol{\kappa}-\boldsymbol{\kappa}_1-\boldsymbol{\kappa}_2-\boldsymbol{\kappa}_3-\boldsymbol{\kappa}_4)\\ &\quad\times\{|\Psi_{gg}(\beta;z,\boldsymbol{p}-\boldsymbol{\kappa}_2-\boldsymbol{\kappa}_4)-\Psi_{gg}(\beta;z,\boldsymbol{p}-\boldsymbol{\kappa}_2-\boldsymbol{\kappa}_4-\boldsymbol{\kappa})|^2\\ &\quad+|\Psi_{gg}(\beta;z,\boldsymbol{p}-\boldsymbol{\kappa}_1-\boldsymbol{\kappa}_3)-\Psi_{gg}(\beta;z,\boldsymbol{p}-\boldsymbol{\kappa}_1-\boldsymbol{\kappa}_3-\boldsymbol{\kappa})|^2\}\Phi_g(\beta;\boldsymbol{b},x,\boldsymbol{\kappa}_1)\\ &\quad\times\Phi_g(\beta;\boldsymbol{b},x,\boldsymbol{\kappa}_2)\Phi_g\Big(\frac{C_{27}}{C_A}(1-\beta);\boldsymbol{b},x,\boldsymbol{\kappa}_3\Big)\Phi_g\Big(\frac{C_{27}}{C_A}(1-\beta);\boldsymbol{b},x,\boldsymbol{\kappa}_4\Big)\frac{d\sigma_{g,\mathrm{Qel}}(\boldsymbol{\kappa})}{d^2\boldsymbol{\kappa}}.\end{aligned} \tag{177}$$

Here the distorted wave function is evaluated with the nuclear glue Φ_g, i.e., in the shorthand notation, $\Psi_{gg}(\beta;z,\boldsymbol{p})=(1-\mathbb{P}_{A,g}(\beta)\otimes)\Psi_{gg}(z,\boldsymbol{p})$. At large N_c one could have used $C_{27}=2C_A$, we keep the explicit ratio of quadratic Casimirs on purpose to elucidate the color-representation dependence of the initial and final-state interaction effects. Bearing in mind the quark-antiquark description of large-N_c gluons, one can deconvolute

$$\Phi\Big(\frac{C_{27}}{C_A}(1-\beta);\boldsymbol{b},x,\boldsymbol{\kappa}\Big)=\Phi(2(1-\beta);\boldsymbol{b},x,\boldsymbol{\kappa})=\int d^2\boldsymbol{\kappa}_1 d^2\boldsymbol{\kappa}_2\,\delta(\boldsymbol{\kappa}-\boldsymbol{\kappa}_1-\boldsymbol{\kappa}_2)\Phi(1-\beta;\boldsymbol{b},x,\boldsymbol{\kappa}_1)\Phi(1-\beta;\boldsymbol{b},x,\boldsymbol{\kappa}_2). \tag{178}$$

In the integrand of the nonlinear $k_\perp$-factorization quadrature this gives rise to the product

$$\Phi_g(\beta;\boldsymbol{b},x,\boldsymbol{\kappa}_1)\Phi_g(\beta;\boldsymbol{b},x,\boldsymbol{\kappa}_2)\prod_{i=3}^{6}\Phi_g(1-\beta;\boldsymbol{b},x,\boldsymbol{\kappa}_i).$$

In the now familiar reinterpretation, the product $\Phi_g(\beta;\boldsymbol{b},x,\boldsymbol{\kappa}_1)\Phi_g(\beta;\boldsymbol{b},x,\boldsymbol{\kappa}_2)$ describes color rotations of the color-octet $\{gg\}_8$ dipole. These color rotations are accompanied by a coherent distortion of the wave function of the color-singlet quark-antiquark pair. The product

$$\prod_{i=3}^{6}\Phi_g(1-\beta;\boldsymbol{b},x,\boldsymbol{\kappa}_i)$$

describes rotations within the space of higher dimensional representations after the gg dipole has been excited at the depth β from the octet to those higher representations. The corresponding RFT diagram is shown in Fig. 14.

Upon this identification, one can convolute back to the two nuclear cut Pomerons $\not{P}_{A,r}(\beta^*)$, where

$$\beta^*=\frac{C_{27}}{C_A}(1-\beta)+\beta. \tag{179}$$

The $g\not{p}_e\not{p}_{A,r}(\beta^*)\not{p}_{A,r}(\beta^*)g$ vertex would equal

$$\begin{aligned}&\not{D}(g \to \{gg\}_{10+\overline{10}+27+R_7}; \not{p}_{A,r}(\beta^*), \not{p}, \not{p}_{A,r}(\beta^*); \beta; \boldsymbol{p}, \boldsymbol{\Delta}, \boldsymbol{p}_1, \boldsymbol{p}_2, \boldsymbol{\kappa}, \boldsymbol{\kappa}_1, \boldsymbol{\kappa}_2)\\ &= \delta(\boldsymbol{\Delta} - \boldsymbol{\kappa}_1 - \boldsymbol{\kappa}_2 - \boldsymbol{\kappa})\Psi^*_{gg}(\beta; z, \boldsymbol{p}_2)[\delta(\boldsymbol{p} - \boldsymbol{\kappa}_1 - \boldsymbol{p}_2) - \delta(\boldsymbol{p} - \boldsymbol{\kappa}_1 - \boldsymbol{\kappa} - \boldsymbol{p}_2)]\\ &\quad\times[\delta(\boldsymbol{p} - \boldsymbol{\kappa}_1 - \boldsymbol{p}_1) - \delta(\boldsymbol{p} - \boldsymbol{\kappa}_1 - \boldsymbol{\kappa} - \boldsymbol{p}_1)]\Psi_{gg}(\beta; z, \boldsymbol{p}_1),\end{aligned} \tag{180}$$

and its expansion in terms of the in-vacuum cut Pomerons $\not{p}_r$ would read

$$\begin{aligned}&\not{D}(g \to \{gg\}_{10+\overline{10}+27+R_7}); j\not{p}_r, \not{p}_e, k\not{p}_r; \beta; \boldsymbol{p}, \boldsymbol{\Delta}, \boldsymbol{p}_1, \boldsymbol{p}_2, \boldsymbol{\kappa}, \{\boldsymbol{k}_i\}, \{\boldsymbol{q}_m\})\\ &= \delta\Big(\boldsymbol{\Delta} - \sum_{i=1}^{j}\boldsymbol{k}_i - \sum_{m=1}^{k}\boldsymbol{q}_m - \boldsymbol{\kappa}\Big)S[\boldsymbol{b}, \beta^*\sigma_0(x)]S[\boldsymbol{b}, \beta^*\sigma_0(x)](\beta^*)^{k+j}\Psi^*_{gg}(\beta; z, \boldsymbol{p}_2)\\ &\quad\times\Big[\delta\Big(\boldsymbol{p} - \sum_{i=1}^{j}\boldsymbol{k}_i - \boldsymbol{p}_2\Big) - \delta\Big(\boldsymbol{p} - \sum_{i=1}^{j}\boldsymbol{k}_i - \boldsymbol{\kappa} - \boldsymbol{p}_2\Big)\Big]\Big[\delta\Big(\boldsymbol{p} - \sum_{i=1}^{j}\boldsymbol{k}_i - \boldsymbol{p}_1\Big) - \delta\Big(\boldsymbol{p} - \sum_{i=1}^{j}\boldsymbol{k}_i - \boldsymbol{\kappa} - \boldsymbol{p}_1\Big)\Big]\Psi_{gg}(\beta; z, \boldsymbol{p}_1).\end{aligned} \tag{181}$$

Now we cite the integrated topological cross sections for the higher representation sector:

$$\begin{aligned}\frac{d\sigma_\nu(g \to \{gg\}_{10+\overline{10}+27+R_7})}{d^2\boldsymbol{b}} &= T(\boldsymbol{b})\int_0^1 dz\int d^2\boldsymbol{r}|\Psi_{gg}(z, \boldsymbol{r})|^2\int_0^1 d\beta\sum_{j,k=0}\delta(\nu - 1 - k - j)w_k\Big(\frac{C_{27}}{C_A}(1-\beta)\nu_{A,gg}(\boldsymbol{b})\Big)\\ &\quad\times w_j(\beta\nu_{A,gg}(\boldsymbol{b}))\sigma_{gg}(x, \boldsymbol{r})\Big(1 - \frac{\sigma_{gg}(x, \boldsymbol{r})}{\sigma_{gg,0}(x)}\Big)^j\exp\Big[-\frac{1}{2}\sigma_{gg}(x, \boldsymbol{r})T(\boldsymbol{b})\Big].\end{aligned} \tag{182}$$

Taking $\nu = 1$ and neglecting absorption, one would recover the impulse approximation result, cf. Eq. (87) of Ref. [30].

X. TOPOLOGICAL CROSS SECTIONS FOR OPEN-CHARM PRODUCTION IN HADRON-NUCLEUS COLLISIONS

For the sake of completeness we report the results for this last remaining hard pQCD subprocess. It is also of great practical significance since Bremsstrahlung by heavy quarks is weaker than by light quarks [67] and one can utilize nuclear quenching of heavy flavors for the determination of the nonperturbative energy flow to a nucleus. The underlying pQCD process is $gg_t \to c\bar{c}$. Interactions of the 4-parton system, $c\bar{c}c'\bar{c}'$, are described by the same two-channel operator as in DIS [24]. Besides the open heavy flavor (for the sake of definiteness we speak of the open charm), the results are equally applicable to midrapidity hard light quark-antiquark dijets.

The averaging over colors of the initial gluon and summation over the color states of dijets in the final state is of the form

$$\begin{aligned}\frac{1}{\sqrt{\dim[8]}}\sum_f\langle f| &= \sum_R\sqrt{\frac{\dim[R]}{\dim[8]}}\langle R\bar{R}|\\ &= \frac{1}{\sqrt{N_c^2 - 1}}\langle e_1| + \langle e_2|.\end{aligned} \tag{183}$$

In the large-N_c perturbation theory, the reaction is dominated by color rotations within the space of color octet $\{c\bar{c}\}_8$. It differs from the excitation of color-triplet quark-gluon and color-octet gluon-gluon dijets: open charm is excited from the incident parton already in the highest possible representation. In this respect, the open charm is a universality class of its own.

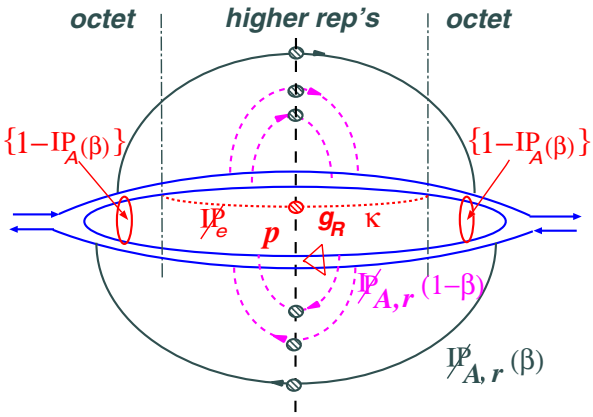

FIG. 14 (color online). The large-N_c structure of the cut nuclear Pomeron diagram for production of gluon-gluon dijets in higher representations. Gluons are shown in the composite quark-antiquark representation. There are three more diagrams with recouplings of the gluon g_R form $\not{p}_e$ within the internal quark loop.

In close similarity to (143) we obtain

$$\langle 88|\mathcal{S}^{(4)}_{A,\nu}(\boldsymbol{C},\boldsymbol{b})|88\rangle = \frac{1}{\nu!}\Big[-\frac{1}{2}\Sigma^{\rm ex}_{22}T(\boldsymbol{b})\Big]^{\nu} S[\boldsymbol{b},\Sigma^{\rm el}_{22}(\boldsymbol{C})]. \tag{184}$$

In the evaluation of two and three-body states we notice that

$$\Sigma^{\rm el}_{22}(\boldsymbol{C}) = \Sigma^{(3)}_{\rm el}(\boldsymbol{B},\boldsymbol{b}') = \Sigma^{(3)}_{\rm el}(\boldsymbol{b},\boldsymbol{B}') = \Sigma^{(2)}_{\rm el}(\boldsymbol{b},\boldsymbol{b}') = \frac{C_A}{C_F}\sigma_0(x) = 2\sigma_0(x). \tag{185}$$

Consequently, in the expansion over color excitations we encounter

$$\begin{aligned}&[-\Sigma^{\rm ex}_{22}(\boldsymbol{C})]^{\nu} + [-\Sigma^{(2)}_{\rm ex}(\boldsymbol{b},\boldsymbol{b}')]^{\nu} - [-\Sigma^{(3)}_{\rm ex}(\boldsymbol{B},\boldsymbol{b}')]^{\nu} - [-\Sigma^{(3)}_{\rm ex}(\boldsymbol{b},\boldsymbol{B}')]^{\nu}\\ &= \sigma_0^{\nu}\sum_{k=0}^{\nu}\frac{\nu!}{k!(\nu-k)!}\int d^2\boldsymbol{\kappa}_1 d^2\boldsymbol{\kappa}_2 \frac{d\sigma^{(k)}_{\rm Qel}(\boldsymbol{\kappa}_1)}{\sigma_{\rm Qel}d^2\boldsymbol{\kappa}_1}\cdot\frac{d\sigma^{(\nu-k)}_{\rm Qel}(\boldsymbol{\kappa}_2)}{\sigma_{\rm Qel}d^2\boldsymbol{\kappa}_2}\exp(i(\boldsymbol{\kappa}_1+\boldsymbol{\kappa}_2)\boldsymbol{s})\\ &\quad\times\{\exp[-i\boldsymbol{\kappa}_2\boldsymbol{r}] - \exp[-i(\boldsymbol{\kappa}_1+\boldsymbol{\kappa}_2)(1-z)\boldsymbol{r}]\}\{\exp[i\boldsymbol{\kappa}_2\boldsymbol{r}'] - \exp[+i(\boldsymbol{\kappa}_1+\boldsymbol{\kappa}_2)(1-z)\boldsymbol{r}']\},\end{aligned} \tag{186}$$

which gives

$$\begin{aligned}\frac{d\sigma_{\nu}(g\to\{c\bar{c}\}_8)}{d^2\boldsymbol{b}dzd^2\boldsymbol{\Delta}d^2\boldsymbol{p}} &= \frac{1}{2(2\pi)^2}\int d^2\boldsymbol{\kappa}_1 d^2\boldsymbol{\kappa}_2\delta^{(2)}(\boldsymbol{\Delta}-\boldsymbol{\kappa}_1-\boldsymbol{\kappa}_2)\{|\Psi_{c\bar{c}}(z,\boldsymbol{p}-\boldsymbol{\kappa}_1)-\Psi_{c\bar{c}}(z,\boldsymbol{p}-z(\boldsymbol{\kappa}_1+\boldsymbol{\kappa}_2))|^2\\ &\quad+|\Psi_{c\bar{c}}(z,\boldsymbol{p}-\boldsymbol{\kappa}_2)-\Psi_{c\bar{c}}(z,\boldsymbol{p}-z(\boldsymbol{\kappa}_1+\boldsymbol{\kappa}_2))|^2\}\sum_{k=0}^{\nu} w_{\nu-k}(\nu_A(\boldsymbol{b}))w_k(\nu_A(\boldsymbol{b}))\frac{d\sigma^{(\nu-k)}_{\rm Qel}(\boldsymbol{\kappa}_2)}{\sigma_{\rm Qel}d^2\boldsymbol{\kappa}_2}\cdot\frac{d\sigma^{(k)}_{\rm Qel}(\boldsymbol{\kappa}_1)}{\sigma_{\rm Qel}d^2\boldsymbol{\kappa}_1}.\end{aligned} \tag{187}$$

Of course, this result could have been derived from the inclusive spectrum [26–28,30]

$$\begin{aligned}\frac{d\sigma_{\nu}(g\to\{c\bar{c}\}_8)}{d^2\boldsymbol{b}dzd^2\boldsymbol{\Delta}d^2\boldsymbol{p}} &= \frac{1}{2(2\pi)^2}\int d^2\boldsymbol{\kappa}_1 d^2\boldsymbol{\kappa}_2\delta^{(2)}(\boldsymbol{\Delta}-\boldsymbol{\kappa}_1-\boldsymbol{\kappa}_2)\{|\Psi_{c\bar{c}}(z,\boldsymbol{p}-\boldsymbol{\kappa}_1)-\Psi_{c\bar{c}}(z,\boldsymbol{p}-z(\boldsymbol{\kappa}_1+\boldsymbol{\kappa}_2))|^2\\ &\quad+|\Psi_{c\bar{c}}(z,\boldsymbol{p}-\boldsymbol{\kappa}_2)-\Psi_{c\bar{c}}(z,\boldsymbol{p}-z(\boldsymbol{\kappa}_1+\boldsymbol{\kappa}_2))|^2\}\Phi(\boldsymbol{b},x,\boldsymbol{\kappa}_1)\Phi(\boldsymbol{b},x,\boldsymbol{\kappa}_2).\end{aligned} \tag{188}$$

The RFT diagrams for (188) are shown in Fig. 15. There is a very close similarity to the case of color-octet digluons, Fig. 13, the absence of the color-singlet quark-antiquark dipole explains the absence of coherent distortions of the dipole wave function. The charm loop contribution to the $g\not{p}_{A,r}\not{p}_{A,r}g$ vertex is readily obtained from Eq. (175) by the substitution $\Psi_{gg}(1;z,\boldsymbol{p})\to\Psi_{c\bar{c}}(z,\boldsymbol{p})$, we skip citing it here.

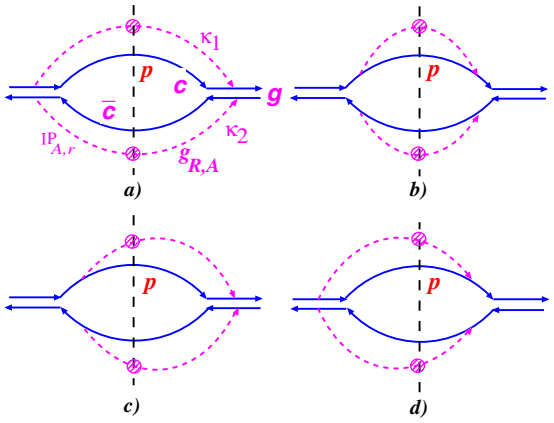

FIG. 15 (color online). The large-N_c structure of the cut nuclear Pomeron diagram for production of open charm. The incident gluon is shown in the composite quark-antiquark representation.

The $\mathcal{O}(N_c^{-2})$ excitation of open charm in the color-singlet representation is entirely similar to the excitation of color-octet dijets in DIS. We leave the derivation of these topological cross sections as an exercise.

XI. TOPOLOGICAL CROSS SECTIONS FOR MIDRAPIDITY GLUONS AND THE t-CHANNEL MULTIPOMERON TRANSITIONS

We briefly comment here on topological cross sections with midrapidity gluons in quark-nucleus and gluon-nucleus collisions which are of special interest from the RFT perspective, more detailed discussion will be reported elsewhere. We consider $z \ll 1$, but $\eta \gtrsim \eta_A$. The basic RFT diagrams for the relevant unitarity cut are the same as shown before. Such a gluon is separated from the projectile parton by a large rapidity gap, and it is tempting to interpret the emerging spectra in terms of the unitarity cuts of diagrams with the t-channel transition of the in-vacuum cut Pomeron $\not{p}_r$ on the beam side to multi-Pomeron states on the nucleus side, as indicated in Fig. 16(c). Here we sketch briefly the nonlinear $k_\perp$-factorization results for the emerging multi-Pomeron vertices.

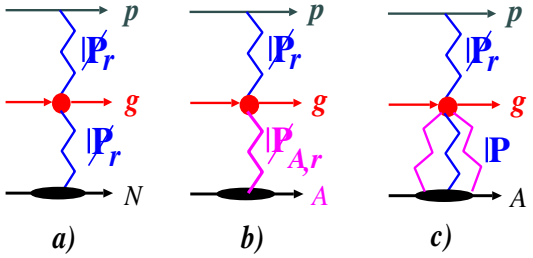

FIG. 16 (color online). The Kancheli-Mueller optical theorem for the midrapidity gluon spectrum: (a) for the free-nucleon target in terms of cut in-vacuum Pomerons, (b) for the nuclear target with a cut nuclear Pomeron on the nucleus side, (c) the anticipated multiple in-vacuum Pomeron exchange on the nucleus side.

A. Single midrapidity gluon spectra: linear $k_\perp$-factorization

Here we start with the seemingly simple RFT properties of single midrapidity gluon spectra. Then, in the spirit of Sec. VI, we recall the pitfalls of the unitarity-cut interpretation of the single-gluon cross sections. Hereafter $\boldsymbol{p} \equiv \boldsymbol{p}_g$ and $z \equiv z_g$, we use the results from Ref. [26] and follow the discussion in Ref. [31].

We need the small-z limit

$$|\Psi_{ga}(z,\boldsymbol{p}) - \Psi_{ga}(z,\boldsymbol{p}-\boldsymbol{\kappa})|^2 = 2\alpha_S P_{ga}(z)\left|\frac{\boldsymbol{p}}{\boldsymbol{p}^2+\mu_g^2} - \frac{\boldsymbol{p}-\boldsymbol{\kappa}}{(\boldsymbol{p}-\boldsymbol{\kappa})^2+\mu_g^2}\right|^2 = 2\alpha_S P_{ga}(z) K(\boldsymbol{p},\boldsymbol{p}-\boldsymbol{\kappa}) = \frac{4\alpha_S C_a}{z} K(\boldsymbol{p},\boldsymbol{p}-\boldsymbol{\kappa}), \tag{189}$$

where μ_g is the (optional) infrared regularization and we used the explicit form of the splitting function $P_{ga}(z)$ for soft gluons. For the transverse momenta above the infrared parameter μ_g we can use

$$K(\boldsymbol{p},\boldsymbol{p}-\boldsymbol{\kappa}) = \frac{\boldsymbol{\kappa}^2}{\boldsymbol{p}^2(\boldsymbol{p}-\boldsymbol{\kappa})^2}. \tag{190}$$

We also recall that

$$\frac{dG_a(z,\boldsymbol{p}-\boldsymbol{\kappa})}{d^2\boldsymbol{p}} = 2\alpha_S z P_{ga}(z)\cdot\frac{1}{(\boldsymbol{p}-\boldsymbol{\kappa})^2} \tag{191}$$

is the unintegrated glue in the incident parton a, at $z \ll 1$ it does not depend on the virtuality of the incident parton a. We define the nuclear counterpart of Eq. (15):

$$\boldsymbol{\kappa}^2\phi_{gg}(\boldsymbol{b},x_A,\boldsymbol{\kappa}) = \frac{4\pi\alpha_s}{N_c}\cdot\frac{dG_{A,gg}(\boldsymbol{b},x_A,\boldsymbol{\kappa})}{d^2\boldsymbol{b}d^2\boldsymbol{\kappa}}. \tag{192}$$

The spectator interaction cancellations are known to entail the linear $k_\perp$-factorization form of the quadrature for the single midrapidity gluon spectrum [26,68]. Making use of (190)–(192), one can cast it in the beam-target symmetric form:

$$\frac{(2\pi)^2 d\sigma_A}{d\eta_g d^2\boldsymbol{p}d^2\boldsymbol{b}}\bigg|_{a\to ag} = z\int d^2\boldsymbol{\kappa}\phi_{gg}(\boldsymbol{b},x_A,\boldsymbol{\kappa}) \times |\Psi_{ga}(z,\boldsymbol{p}) - \Psi_{ga}(z,\boldsymbol{p}-\boldsymbol{\kappa})|^2 = \frac{4\pi\alpha_s}{N_c}\int d^2\boldsymbol{\kappa}d^2\boldsymbol{p}_a V_{\mathrm{BFKL}}(\boldsymbol{p};\boldsymbol{\kappa},\boldsymbol{p}_a) \times \frac{dG_a(z,\boldsymbol{p}_a)}{d^2\boldsymbol{p}_a}\cdot\frac{dG_{A,gg}(\boldsymbol{b},x_A,\boldsymbol{\kappa})}{d^2\boldsymbol{b}d^2\boldsymbol{\kappa}}. \tag{193}$$

The remaining factor

$$V_{\mathrm{BFKL}}(\boldsymbol{p};\boldsymbol{\kappa},\boldsymbol{p}_a) = \frac{1}{\boldsymbol{p}^2}\delta(\boldsymbol{p}-\boldsymbol{p}_a-\boldsymbol{\kappa}) \tag{194}$$

is familiar from the square of the BFKL vertex of radiation of the gluon by a Reggeized t-channel gluon, or a fusion $g_R(\boldsymbol{p}_a) + g_R(\boldsymbol{\kappa}) \to g(\boldsymbol{p})$ [50]. The absence of any nuclear renormalization of this vertex is noteworthy. Notice a correspondence

$$V_{\mathrm{BFKL}}(\boldsymbol{p};\boldsymbol{\kappa},\boldsymbol{p}_a) = \frac{1}{2\alpha_S P_{ga}(z)}\cdot\frac{(\boldsymbol{p}-\boldsymbol{\kappa})^2}{\boldsymbol{\kappa}^2} \times |\Psi_{ga}(z,\boldsymbol{p}) - \Psi_{ga}(z,\boldsymbol{p}-\boldsymbol{\kappa})|^2 \times \delta(\boldsymbol{p}-\boldsymbol{p}_a-\boldsymbol{\kappa}), \tag{195}$$

which can be used in all other cases for the identifications (191) and (192).

When viewed from the Kancheli-Mueller optical theorem perspective, Eq. (193) invites the cut-Pomeron expansion for $\phi_{gg}(\boldsymbol{b},x_A,\boldsymbol{\kappa})$ and the cut-Pomeron structure shown in Fig. 16. One should not be mislead, though: Sec. VI was a good warning of pitfalls of the unitarity-cut reinterpretation of $\phi_{gg}(\boldsymbol{b},x_A,\boldsymbol{\kappa})$ in Eq. (193). Such an operational expansion in the multi-Pomeron exchanges is possible,[1] but it would lack a direct connection to color excitations of the nucleus. Now we move to the cut-Pomeron structure which follows from the nonlinear $k_\perp$-factorization results reported in previous sections.

B. Single midrapidity gluon spectra: cut-Pomeron structure

1. Spectator interactions and Cheshire Cat grin

We consider first the universality class of dijets in the same color representation as the incident quark. For the incident quarks Eq. (147) gives

[1]Such an expansion for the recoil multiplicity distribution appeared, for instance, in Ref. [69], which was posted after this manuscript was finalized.

$$\frac{d\sigma_\nu(q\to\{qg\}_3)}{d^2\boldsymbol{b}d\eta_g d^2\boldsymbol{p}}=\frac{1}{(2\pi)^2}w_\nu(\nu_A(\boldsymbol{b}))\int d^2\boldsymbol{\kappa}\frac{d\sigma^{(\nu)}_{\rm Qel}(\boldsymbol{\kappa})}{\sigma_{\rm Qel}d^2\boldsymbol{\kappa}}\times z|\Psi_{qg}(1;z,\boldsymbol{p}-\boldsymbol{\kappa})-\Psi_{qg}(z,\boldsymbol{p})|^2. \tag{196}$$

Here we changed from the quark to gluon momentum and took a limit $z\equiv z_g\to 0$, which simplifies $\Psi_{qg}(z,\boldsymbol{p}-z\boldsymbol{\kappa})\to\Psi_{qg}(z,\boldsymbol{p})$. The similar result for incident gluons is (for the sake of a comparison with Eq. (196) we make use of the large-N_c property $\nu_{A,gg}(\boldsymbol{b})=2\nu_A(\boldsymbol{b})$)

$$\frac{d\sigma(g\to\{gg\}_{8_A+8_S})}{d^2\boldsymbol{b}d\eta_g d^2\boldsymbol{p}}==\frac{1}{(2\pi)^2}\sum_{\nu=0}\sum_{j,k=0}\delta(\nu-j-k)w_k(\nu_A(\boldsymbol{b}))w_j(\nu_A(\boldsymbol{b}))\times\int d^2\boldsymbol{\kappa}_2\frac{d\sigma^{(j)}_{g,\rm Qel}(\boldsymbol{\kappa}_1)}{\sigma_{g,\rm Qel}d^2\boldsymbol{\kappa}_1}\cdot\frac{d\sigma^{(k)}_{g,\rm Qel}(\boldsymbol{\kappa}_2)}{\sigma_{g,\rm Qel}d^2\boldsymbol{\kappa}_2}z|\Psi_{gg}(1;z,\boldsymbol{p}-\boldsymbol{\kappa}_1)-\Psi_{gg}(z,\boldsymbol{p})|^2. \tag{197}$$

Upon the integration over $\boldsymbol{\kappa}_2$ the momentum structure of (197) will be exactly the same as in (196), the difference is in the CCG—the contribution k to the total multiplicity of cut Pomerons. The difference between the two cases is evident from a close comparison of Figs. 11 and 13. In Fig. 11 the nuclear cut Pomeron $\not{P}_{A,r}$ couples only to the quark of the gluon in the quark-antiquark representation, the spectator quark interacts only with uncut Pomerons and does not contribute to the nucleus excitation. In contrast to that, in Fig. 11 the spectator gluon too couples to $\not{P}_{A,r}$ and contributes exactly the above k to the nucleus excitation. Neither of the two topological cross sections to the mid-rapidity gluon spectrum can be cast in the linear $k_\perp$-factorizable form suggested by Eq. (193). Even for the incident quark, when spectator interactions do not contribute to the nucleus excitation, the uncut-Pomeron exchanges in $\Psi_{qg}(1;z,\boldsymbol{p}-\boldsymbol{\kappa})$ make Eq. (196) dissimilar to (193). As we learned in Sec. VI, in the general case it is impossible to guess out the correct unitarity structure brought into the problem by the CCG of the integrated out spectator interactions.

Now comes the universality class of dijets in higher color representations. Here taking $z\to 0$ does not bring in any principal simplifications, but working with the maximally convoluted form of the nuclear glue does help. For the incident quarks we find

$$\frac{d\sigma_\nu(q\to\{qg\}|_{6+15})}{d^2\boldsymbol{b}d\eta_g d^2\boldsymbol{p}}=\frac{1}{(2\pi)^2}T(\boldsymbol{b})\int_0^1 d\beta\sum_{j,k\geq 0}\delta(\nu-1-j-k)w_k((1-\beta)\nu_A(\boldsymbol{b}))w_j\left(\left[\frac{C_A}{C_F}(1-\beta)+\beta\right]\nu_A(\boldsymbol{b})\right)\times\int d^2\boldsymbol{\kappa}d^2\boldsymbol{\kappa}_1d^2\boldsymbol{\kappa}_2\frac{d\sigma_{\rm Qel}(\boldsymbol{\kappa})}{d^2\boldsymbol{\kappa}}\frac{d\sigma^{(k)}_{\rm Qel}(\boldsymbol{\kappa}_2)}{\sigma_{\rm Qel}d^2\boldsymbol{\kappa}_2}\cdot\frac{d\sigma^{(j)}_{\rm Qel}(\boldsymbol{\kappa}_1)}{\sigma_{\rm Qel}d^2\boldsymbol{\kappa}_1}.|\Psi_{qg}(\beta;z,\boldsymbol{p}-\boldsymbol{\kappa}_1)-\Psi_{qg}(\beta;z,\boldsymbol{p}-\boldsymbol{\kappa}_1-\boldsymbol{\kappa})|^2. \tag{198}$$

The dependence on the momentum $\boldsymbol{\kappa}_2$ of the spectator quark integrates out entirely, see Eq. (97), but CCG—the contribution k to the multiplicity ν of excited nucleons—stays on, which is made obvious by Fig. 12.

In conformance to the universality class concept, the story repeats itself for gluons. Working again with the maximally convoluted form of the collective nuclear glue, we have

$$\frac{d\sigma_\nu(g\to\{gg\}|_{10+\overline{10}+27+R_7})}{d^2\boldsymbol{b}d\eta_g d^2\boldsymbol{p}}=\frac{1}{(2\pi)^2}T(\boldsymbol{b})\int_0^1 d\beta\sum_{j,k\geq 0}\delta(\nu-1-j-k)w_k\left(\left[\frac{C_{27}}{C_A}(1-\beta)+\beta\right]\nu_A(\boldsymbol{b})\right)\times w_j\left(\left[\frac{C_{27}}{C_A}(1-\beta)+\beta\right]\nu_A(\boldsymbol{b})\right)\int d^2\boldsymbol{\kappa}d^2\boldsymbol{\kappa}_1d^2\boldsymbol{\kappa}_2\frac{d\sigma_{\rm Qel}(\boldsymbol{\kappa})}{d^2\boldsymbol{\kappa}}\frac{d\sigma^{(k)}_{\rm Qel}(\boldsymbol{\kappa}_2)}{\sigma_{\rm Qel}d^2\boldsymbol{\kappa}_2}\cdot\frac{d\sigma^{(j)}_{\rm Qel}(\boldsymbol{\kappa}_1)}{\sigma_{\rm Qel}d^2\boldsymbol{\kappa}_1}\cdot\times|\Psi_{gg}(\beta;z,\boldsymbol{p}-\boldsymbol{\kappa}_1)-\Psi_{gg}(\beta;z,\boldsymbol{p}-\boldsymbol{\kappa}_1-\boldsymbol{\kappa})|^2. \tag{199}$$

Again the dependence on $\boldsymbol{\kappa}_2$ integrates out. The change of the projectile parton from the quark to a gluon changes substantially the β dependence of the CCG—$w_k(\beta^*\nu_A(\boldsymbol{b}))$ for incident gluons vs $w_k((1-\beta)\nu_A(\boldsymbol{b}))$ for incident quarks. We reiterate the same comment that neither (198) nor (199) can be made reminiscent of Eq. (193).

C. What are the multi-Pomeron vertices?

The point that spectator partons contribute to the excitation of the nucleus cannot be contested—within QCD as a gauge theory one cannot delimitate interactions of colored spectator partons. Then it is not surprising that this CCG depends on the process. It is not surprising that the pattern of coherent distortions by uncut-Pomeron exchanges depends on the color structure of final states. In conjunction with the discussion in Sec. VI, this casts a shadow on the possibility of the formulation of a Kancheli-Mueller optical theorem, Fig. 16(c), in terms of universal multi-Pomeron couplings.

Still sort of a universality is recovered at the expense of losing a direct contact with the event-by-event observables and going to the multiplicity resummed cross sections. Following the discussion in Sec. VII C, we define the multiplicity resummed topological cross section of processes with at least j-cut Pomerons,

$$d\sigma^{(j)} = \sum_{\nu>j} d\sigma_\nu. \tag{200}$$

Here j is the midrapidity gluon contribution to the nucleus excitation, unlike ν it cannot be determined experimentally on an event-by-event basis. Following Sec. VII C one would argue, that such a resummation eliminates CCG not only from the spectator quark of the hard dijet, but also from the comoving partons of the parent hadron the incident parton, q or g, belongs to. As we shall see in a minute, such a multiplicity resummed $d\sigma^{(j)}$ has very interesting properties and we urge the multiplicity resummation analysis of the experimental data.

First, we notice that at $z \ll 1$

$$|\Psi_{gg}(1; z, \boldsymbol{p} - \boldsymbol{\kappa}_1) - \Psi_{gg}(z, \boldsymbol{p})|^2 = \frac{C_A}{C_F}|\Psi_{qg}(1; z, \boldsymbol{p} - \boldsymbol{\kappa}_1) - \Psi_{qg}(z, \boldsymbol{p})|^2. \tag{201}$$

Then, apart from this ratio of Casimirs, upon such a multiplicity resummation the integrand of Eq. (197) would become identical to that of (196) and

$$d\sigma^{(j)}(g \to \{gg\}_8) = \frac{C_A}{C_F} d\sigma^{(j)}(q \to \{qg\}_3). \tag{202}$$

Here C_A/C_F is a ratio of couplings of the in-vacuum Pomeron to the beam gluon and quark—a part of the generic Regge factorization. Then, according to Fig. 11, and (196), the Kancheli-Mueller diagram for the universality class of dijets in the color representation of the incident parton will contain the following set of Pomeron transitions in the t-channel:

$$\begin{aligned}&\Psi^*_{ga}(z, \boldsymbol{p})\{\not{P}_r \to \not{P}_{A,r}\}\Psi_{ga}(z, \boldsymbol{p}) + \Psi^*_{ga}(z, \boldsymbol{p} - \boldsymbol{\kappa}_1)(1 - \otimes\mathbb{P}_A)\{\not{P}_r \to \not{P}_{A,r}\}(1 - \mathbb{P}_A\otimes)\Psi_{ga}(z, \boldsymbol{p} - \boldsymbol{\kappa}_1)\\ &- \Psi^*_{ga}(z, \boldsymbol{p} - \boldsymbol{\kappa}_1)(1 - \otimes\mathbb{P}_A)\{\not{P}_r \to \not{P}_{A,r}\}\Psi_{ga}(z, \boldsymbol{p}) - \Psi^*_{ga}(z, \boldsymbol{p})\{\not{P}_r \to \not{P}_{A,r}\}(1 - \mathbb{P}_A\otimes)\Psi_{ga}(z, \boldsymbol{p} - \boldsymbol{\kappa}_1).\end{aligned} \tag{203}$$

Here the position of $\otimes$ indicates the action of the distortion operator on either $\Psi_{ga}(z, \boldsymbol{p})$ or $\Psi^*_{ga}(z, \boldsymbol{p})$. The representation of these vertices in terms of the in-vacuum and coherent nuclear gluons can easily be read from the above cited $\not{D}$'s, we leave this as an exercise. We only notice, that in the expansion of $\not{P}_{A,r}$ in $j\not{P}_r$ the term with $j = 1$ is the absorbed impulse approximation, see Eq. (149). Next comes the triple-Pomeron transition $\not{P}_r \to \not{P}_r\not{P}_r$. All such transitions $\not{P}_r \to j\not{P}_r$ are furnished by uncut-Pomeron exchanges in the absorption factor and in the wave function distortions as indicated in (203).

The expansion of (203) in $\not{P}_r$'s contains also the term with $j = 0$, i.e., the diffractive cut. This diffractive cut defines the t-channel transition $\not{P}_r \to \mathbb{P}_A\mathbb{P}_A$, and the corresponding transitions $\not{P}_r \to (k\mathbb{P})(m\mathbb{P})$ with k and m uncut in-vacuum Pomerons on the two sides of the unitarity cut, respectively.

The similar resummation of topological cross sections in the universality class of higher color representations leads to the counterpart of the Regge factorization (202):

$$d\sigma^{(j)}(g \to \{gg\}_{(10+\overline{10}+27+R_7)}) = \frac{C_A}{C_F} d\sigma^{(j)}(q \to \{qg\}_{6+15}). \tag{204}$$

Here the crucial point is the large-N_c equality

$$\frac{C_A}{C_F} = \frac{C_{27}}{C_A}, \tag{205}$$

by which β^* as a function of β is the same for both channels. All the wave functions are coherently distorted in the same slice of the nucleus and, suppressing the wave functions, we have the following structure of t-channel transitions:

$$\not{P}_r \to (1 - \otimes\mathbb{P}_A(\beta))\not{P}_{A,r}(\beta^*)\not{P}_e(1 - \mathbb{P}_A(\beta)\otimes). \tag{206}$$

The distinction between the two major universality classes persists even after the multiplicity resummations.

The absorbed impulse approximation starts with the transition $\not{P}_r \to \not{P}_e$. Next comes the triple-Pomeron transition $\not{P}_r \to \not{P}_r\not{P}_e$ which is evidently different from $\not{P}_r \to \not{P}_r\not{P}_r$ in the previous universality class, and from the diffractive transition cut $\not{P}_r \to \mathbb{P}\mathbb{P}$. One can readily verify that from the afore cited $\not{D}$'s. Such a variety of triple-Pomeron vertices is a new observation not found in the previous literature. One can readily read from the same results for $\not{D}$'s the triple-Pomeron vertices $\not{P}_r \to \not{P}_r\mathbb{P}$ and $\not{P}_r \to \not{P}_e\mathbb{P}$. The experimentally observed $d\sigma^{(j)}$ will be a

sum of topological cross sections for the two universality classes.

The pseudodiffractive channels, when dijets in the color representation of the beam parton are produced via the intermediate state in higher multiplets, defines the triple-Pomeron vertex $I\!P_r \to I\!P_e I\!P_e$. Such a vertex is $\mathcal{O}(N_c^{-2})$, though.

Our results for $I\!D$ in the open-charm production can readily be reformulated in terms of the quark loop contribution to the triple-Pomeron vertex $I\!P_r \to I\!P_{A,r} I\!P_{A,r}$ and its derivatives in terms of multiple in-vacuum $I\!P_r$'s. Finally, we notice that the multi-Pomeron vertices $I\!P_r \to jI\!P_r + kI\!P_e + m\mathbb{P}$ must be regarded *as local ones in the rapidity, rather than a branching tree (fan) of triple-Pomeron vertices.* A detailed discussion and comparison of all those vertices, including the one which appeared in the nonlinear evolution for the collective nuclear glue [31], will be reported elsewhere.

XII. CONCLUSIONS

Starting from the first principles of pQCD, we derived nonlinear $k_\perp$-factorization quadratures for hard scattering off nuclei with a fixed multiplicity of color-excited nucleons. Within pQCD each color-excited nucleon is associated with a cut Pomeron, and our results must be regarded as a pQCD version of the AGK unitarity rules. On the technical side, our S-matrix formalism allows a consistent separation of color-diagonal and color-excitation rescatterings in the course of the non-Abelian intranuclear evolution of color dipoles. An indispensable feature of the coupled-channel non-Abelian evolution of dipoles are the two distinct classes of cut Pomerons—excitation $I\!P_e$ and color-rotation $I\!P_r$. This distinction of $I\!P_r$ and $I\!P_e$ permeates the topological cross sections for all projectiles and is a new finding not contained in the early literature on the AGK rules.

We reported the Reggeon field theory interpretation of topological cross sections for different reaction universality classes. Here the concept of the collective nuclear glue as a coherent state of the in-vacuum (Reggeized) gluons proves to be extremely useful. After the role of the uncut, $\mathbb{P}$, and the two cut, $I\!P_r$ and $I\!P_e$, Pomerons has been identified, one would readily deduce the topological cross sections from the known nonlinear $k_\perp$-factorization results for the inclusive dijet spectra [24–30]. This is a unique example when going from the total to topological cross sections does work. We demonstrate that, in contrast to the common wisdom, in the general case it is not possible to guess the topological cross sections from the Glauber formulas for the total cross section. This is the case, for instance, with the topological cross sections in DIS off nuclei for which our results differ from the earlier discussed Glauber model guesses.

In DIS the topological cross sections are tagged by the multiplicity of hadrons in the backward (nucleus) hemisphere and all our results can be subjected to the direct experimental test. On the phenomenological side, there is a long shopping list of possible numerical predictions for long-range rapidity correlations between leading quark-antiquark dijets in the photon hemisphere and multiproduction in the backward hemisphere. One notable example is a nonperturbative contribution to the quenching of leading jets. In the single-jet problem, both in DIS and hadron induced processes, the effects of spectator, and comover, interactions can be eliminated by the multiplicity resummation technique of Sec. VII C, which might become an important tool in the analysis of the experimental data.

In this communication we confined ourselves to tree diagrams of the RFT, an extension to Pomeron loops requires further scrutiny. Even at the tree level we found very interesting properties of the topological cross sections. We focused on topological cross sections for lowest order pQCD hard final states. Based on our experience with small-x radiative corrections [31], we maintain that principal features of the derived topological cross sections must be stable against small-x evolution. Our finding that the multi-Pomeron vertices are local ones in rapidity rather than a branching tree (fan) of in-vacuum triple-Pomeron vertices must persist to higher orders of the $LL(1/x)$ evolution. The numerical applications of the reported formalism will be reported elsewhere.

ACKNOWLEDGMENTS

We are grateful to B. G. Zakharov for helpful discussions.

APPENDIX A: COLOR-DIAGONAL AND COLOR-EXCITATION INTERACTIONS IN DIS AND OPEN-CHARM PRODUCTION

1. Color-singlet projectile: DIS

The assignment of partons is $a = \gamma^*$, $b = q$, and $c = \bar{q}$. The results for the multiparton cross section operators for all relevant partonic pQCD subprocesses are found in [21,24,29–31], here we only need to describe $\hat{\Sigma}_{\rm el}(\boldsymbol{C})$.

First we notice that Eq. (33) entails a property

$$\hat{\Sigma}_{\rm el}(\boldsymbol{C}) = \hat{\Sigma}_{R,{\rm el}}(\boldsymbol{B}) + \hat{\Sigma}_{R',{\rm el}}(\boldsymbol{B}'). \tag{A1}$$

The simplest case is of a single parton b,

$$\sigma_{b,{\rm el}} = \frac{C_b}{2C_F}\,\sigma_0(x), \tag{A2}$$

while for the two-parton system bc in the color representation R one has

$$\sigma_{R,{\rm el}}(x) = \frac{C_b + C_c - C_R}{2C_F}\,\sigma(x,\boldsymbol{r}) + \frac{C_R}{2C_F}\,\sigma_0(x). \tag{A3}$$

In DIS the incoming parton is an Abelian photon which does not couple to a gluon. For the 2-body, $\gamma^{*'}\gamma^*$, and 3-body, $\gamma^{*'} q\bar{q}$ and $\gamma^* q'\bar{q}'$, states this entails

$$\mathcal{S}^{(2)}_{A,\nu}(\boldsymbol{b}',\boldsymbol{b}) = \delta_{\nu 0}\mathbb{1},$$
$$\mathcal{S}^{(3)}_{A,\nu}(\boldsymbol{B}',\boldsymbol{b}) = \delta_{\nu 0}S[\boldsymbol{b},\sigma(x,\boldsymbol{r}')], \tag{A4}$$
$$\mathcal{S}^{(3)}_{A,\nu}(\boldsymbol{b}',\boldsymbol{B}) = \delta_{\nu 0}S[\boldsymbol{b},\sigma(x,\boldsymbol{r})].$$

The non-Abelian evolution of color-singlet 4-parton systems $q\bar{q}q'\bar{q}'$ is a coupled two-channel problem in the basis of states $|e_1\rangle = |1\bar{1}\rangle$ and $|e_2\rangle = |8\bar{8}\rangle$. The summation over the final-state dijets is of the form

$$\sum_f \langle f| = \sum_R \sqrt{\dim[R]}\langle R\bar{R}| = \langle e_1| + \sqrt{N_c^2-1}\langle e_2|. \tag{A5}$$

The corresponding $\hat{\Sigma}^{(4)}(\boldsymbol{C})$ for DIS was derived in [24]. Making use of Eqs. (A1)–(A3), we decompose it into the color-diagonal and color-excitation components:

$$\hat{\Sigma}^{(4)}_{\rm el}(\boldsymbol{C}) = \Sigma^{\rm el}_{11}|e_1\rangle\langle e_1| + \Sigma^{\rm el}_{22}|e_2\rangle\langle e_2|,$$
$$\Sigma^{\rm el}_{11} = \sigma(x,\boldsymbol{r}) + \sigma(x,\boldsymbol{r}'),$$
$$\Sigma^{\rm el}_{22} = \frac{C_A}{C_F}\sigma_0(x) - \frac{1}{N_c^2-1}[\sigma(x,\boldsymbol{r}) + \sigma(x,\boldsymbol{r}')], \tag{A6}$$

and

$$\hat{\Sigma}^{(4)}_{\rm ex}(\boldsymbol{C}) = \Sigma^{\rm ex}_{12}[|e_1\rangle\langle e_2| + |e_2\rangle\langle e_1|] + \Sigma^{\rm ex}_{22}|e_2\rangle\langle e_2|$$
$$= \Sigma^{\rm ex}_{12}{\rm P}_{\rm ex} + \Sigma^{\rm ex}_{22}{\rm P}_2,$$
$$\Sigma^{\rm ex}_{22} = \frac{C_A}{2C_F}[\sigma(x,\boldsymbol{s}) + \sigma(x,\boldsymbol{s}-\boldsymbol{r}+\boldsymbol{r}') - 2\sigma_0] + \frac{2}{N_c^2-1}\Omega, \tag{A7}$$
$$\Sigma^{\rm ex}_{21} = -\frac{1}{\sqrt{N_c^2-1}}\Omega.$$

The operator

$$\Omega = \sigma(x,\boldsymbol{s}-\boldsymbol{r}) + \sigma(x,\boldsymbol{s}+\boldsymbol{r}') - \sigma(x,\boldsymbol{s}) - \sigma(x,\boldsymbol{s}-\boldsymbol{r}+\boldsymbol{r}') \tag{A8}$$

will be encountered in all the transitions of color dipoles between color representations of different dimension [29,30]. There is a clear-cut $1/N_c$ hierarchy: singlet-to-octet transitions are N_c suppressed, while the octet-to-octet rotations are not. In the $k_\perp$-factorization form

$$\Omega = \int d^2\boldsymbol{\kappa} f(x,\boldsymbol{\kappa})[1-\exp(-i\boldsymbol{\kappa}\boldsymbol{r})][1-\exp(i\boldsymbol{\kappa}\boldsymbol{r}')] \times \exp(i\boldsymbol{\kappa}\boldsymbol{s})$$
$$= \sigma_0(x)\int d^2\boldsymbol{\kappa}\frac{1}{\sigma_{\rm Qel}}\frac{d\sigma_{\rm Qel}(\boldsymbol{\kappa})}{d^2\boldsymbol{\kappa}}[1-\exp(-i\boldsymbol{\kappa}\boldsymbol{r})] \times [1-\exp(i\boldsymbol{\kappa}\boldsymbol{r}')]\exp(i\boldsymbol{\kappa}\boldsymbol{s}). \tag{A9}$$

At large N_c, the color rotations within the color-octet states are described by

$$-\Sigma^{\rm ex}_{22} = 2\sigma_0(x) - \sigma(x,\boldsymbol{s}) - \sigma(x,\boldsymbol{s}-\boldsymbol{r}+\boldsymbol{r}')$$
$$= \int d^2\boldsymbol{\kappa} f(x,\boldsymbol{\kappa})\{\exp[i\boldsymbol{\kappa}\boldsymbol{s}] + \exp[i\boldsymbol{\kappa}(\boldsymbol{s}-\boldsymbol{r}+\boldsymbol{r}')]\}. \tag{A10}$$

The identification (56) leads to

$$(-\Sigma^{\rm ex}_{22})^\nu = \sigma_0^\nu(x)\sum_{k=0}^{\nu}\frac{\nu!}{k!(\nu-k)!}\int d^2\boldsymbol{\kappa}_1 d^2\boldsymbol{\kappa}_2 \times \exp[i\boldsymbol{\kappa}_1\boldsymbol{s} + i\boldsymbol{\kappa}_2(\boldsymbol{s}-\boldsymbol{r}+\boldsymbol{r}')]\frac{d\sigma^{(k)}_{\rm Qel}(\boldsymbol{\kappa}_1)}{\sigma_{\rm Qel}d^2\boldsymbol{\kappa}_1} \cdot \frac{d\sigma^{(\nu-k)}_{\rm Qel}(\boldsymbol{\kappa}_2)}{\sigma_{\rm Qel}d^2\boldsymbol{\kappa}_2}. \tag{A11}$$

2. Color-octet projectile: open-charm production

The assignment of partons is $a = g$, $b = q$, and $c = \bar{q}$. The results hold for any flavor, for the sake of definiteness we speak of the open-charm excitation $g \to c\bar{c}$, the early discussion is found in [26–28]. Here $\hat{\Sigma}^{(4)}(\boldsymbol{C})$ is exactly the same as in DIS. Here the incident parton has a net color, which changes the 2-body, gg, and 3-body, $gc'\bar{c}'$ and $g'c\bar{c}$, interactions which are all single-channel problems. We only list the results which did not appear before:

$$\Sigma^{(2)}(\boldsymbol{b},\boldsymbol{b}') = \frac{C_A}{C_F}\sigma(x,\boldsymbol{s}-(1-z)\boldsymbol{r}+(1-z)\boldsymbol{r}'),$$
$$\Sigma^{(2)}_{\rm el}(\boldsymbol{b},\boldsymbol{b}') = \frac{C_A}{C_F}\sigma_0(x),$$
$$\Sigma^{(2)}_{\rm ex}(\boldsymbol{b},\boldsymbol{b}') = \frac{C_A}{C_F}[\sigma(x,\boldsymbol{s}-(1-z)\boldsymbol{r}+(1-z)\boldsymbol{r}') - \sigma_0(x)],$$
$$\Sigma^{(3)}(\boldsymbol{B},\boldsymbol{b}') = \frac{C_A}{2C_F}[\sigma(x,\boldsymbol{s}+(1-z)\boldsymbol{r}') + \sigma(x,\boldsymbol{s}-\boldsymbol{r}+(1-z)\boldsymbol{r}') - \sigma(x,\boldsymbol{r})] + \sigma(x,\boldsymbol{r}),$$
$$\Sigma^{(3)}_{\rm el}(\boldsymbol{B},\boldsymbol{b}') = \frac{C_A}{C_F}\sigma_0(x) + \frac{2C_F-C_A}{2C_F}\sigma(\boldsymbol{r}),$$
$$\Sigma^{(3)}_{\rm ex}(\boldsymbol{B},\boldsymbol{b}') = \frac{C_A}{2C_F}[\sigma(x,\boldsymbol{s}+(1-z)\boldsymbol{r}') + \sigma(x,\boldsymbol{s}-\boldsymbol{r}+(1-z)\boldsymbol{r}') - 2\sigma_0(x)],$$
$$\Sigma^{(3)}(\boldsymbol{b},\boldsymbol{B}') = \frac{C_A}{2C_F}[\sigma(x,\boldsymbol{s}-(1-z)\boldsymbol{r}) + \sigma(x,\boldsymbol{s}+\boldsymbol{r}'-(1-z)\boldsymbol{r}) - \sigma(x,\boldsymbol{r}')] + \sigma(x,\boldsymbol{r}'),$$
$$\Sigma^{(3)}_{\rm el}(\boldsymbol{b},\boldsymbol{B}') = \frac{C_A}{C_F}\sigma_0(x) + \frac{2C_F-C_A}{2C_F}\sigma(\boldsymbol{r}'),$$
$$\Sigma^{(3)}_{\rm ex}(\boldsymbol{b},\boldsymbol{B}') = \frac{C_A}{2C_F}[\sigma(x,\boldsymbol{s}-(1-z)\boldsymbol{r}) + \sigma(x,\boldsymbol{s}+\boldsymbol{r}'-(1-z)\boldsymbol{r}) - 2\sigma_0(x)]. \tag{A12}$$

The corresponding $\mathcal{S}^{(4)}_{A,\nu}$ are given by Eqs. (A6)–(A8).

APPENDIX B: COLOR-DIAGONAL AND COLOR-EXCITATION INTERACTIONS FOR EXCITATION OF THE QUARK-GLUON DIJETS

2-parton ($q\bar{q}$) and 3-parton ($qg\bar{q}$) states

The assignment of partons is $a = q$, $b = q$, and $c = g$. The overall color-singlet quark-antiquark and quark-gluon-antiquark states have a unique color structure and their intranuclear propagation is a single-channel problem. In contrast to the photon in DIS, the incident quark has a net color charge and both pure elastic and color-excitation interactions are possible in all three channels.

In the color-singlet system $\bar{q}qg$ the qg dipole is in the color-triplet state. We simply borrow the results for the 2-parton and 3-parton cross sections from Ref. [29]

$$\begin{aligned}
\Sigma^{(2)}(\boldsymbol{b},\boldsymbol{b}') &= \sigma(x,\boldsymbol{s}+(1-z)\boldsymbol{r}-(1-z)\boldsymbol{r}'),\\
\Sigma^{(3)}(\boldsymbol{B},\boldsymbol{b}') &= \frac{C_A}{2C_F}[\sigma(x,\boldsymbol{r})+\sigma(x,\boldsymbol{s}+\boldsymbol{r}-(1-z)\boldsymbol{r}')\\
&\quad-\sigma(x,\boldsymbol{s}-(1-z)\boldsymbol{r}')]+\sigma(x,\boldsymbol{s}-(1-z)\boldsymbol{r}'),\\
\Sigma^{(3)}(\boldsymbol{b},\boldsymbol{B}') &= \frac{C_A}{2C_F}[\sigma(x,-\boldsymbol{r}')+\sigma(x,\boldsymbol{s}-\boldsymbol{r}'+(1-z)\boldsymbol{r})\\
&\quad-\sigma(x,\boldsymbol{s}+(1-z)\boldsymbol{r})]+\sigma(x,\boldsymbol{s}+(1-z)\boldsymbol{r}).
\end{aligned} \tag{B1}$$

The elastic cross sections are given by Eqs. (A1)–(A3),

$$\begin{aligned}
\Sigma^{(2)}_{\rm el}(\boldsymbol{b},\boldsymbol{b}') &= \sigma_0(x),\\
\Sigma^{(3)}_{\rm el}(\boldsymbol{B},\boldsymbol{b}') &= \sigma_0(x)+\frac{C_A}{2C_F}\sigma(x,\boldsymbol{r}),\\
\Sigma^{(3)}_{\rm el}(\boldsymbol{b},\boldsymbol{B}') &= \sigma_0(x)+\frac{C_A}{2C_F}\sigma(x,-\boldsymbol{r}'),
\end{aligned} \tag{B2}$$

and the excitation cross sections equal

$$\begin{aligned}
\Sigma^{(2)}_{\rm ex}(\boldsymbol{b},\boldsymbol{b}') &= \sigma(x,\boldsymbol{s}+(1-z)\boldsymbol{r}-(1-z)\boldsymbol{r}')-\sigma_0(x),\\
\Sigma^{(3)}_{\rm ex}(\boldsymbol{B},\boldsymbol{b}') &= \sigma(x,\boldsymbol{s}+\boldsymbol{r}-(1-z)\boldsymbol{r}')-\sigma_0(x)\\
&\quad+\left(\frac{C_A}{2C_F}-1\right)[\sigma(x,\boldsymbol{s}+\boldsymbol{r}-(1-z)\boldsymbol{r}')\\
&\quad-\sigma(x,\boldsymbol{s}-(1-z)\boldsymbol{r}')],\\
\Sigma^{(3)}_{\rm ex}(\boldsymbol{B}',\boldsymbol{b}) &= \sigma(x,\boldsymbol{s}-\boldsymbol{r}'+(1-z)\boldsymbol{r})-\sigma_0(x)\\
&\quad+\left(\frac{C_A}{2C_F}-1\right)[\sigma(x,\boldsymbol{s}-\boldsymbol{r}'+(1-z)\boldsymbol{r})\\
&\quad-\sigma(x,\boldsymbol{s}+(1-z)\boldsymbol{r}')].
\end{aligned} \tag{B3}$$

The results for the leading order in $1/N_c$ expansion are obtained putting $C_A = 2C_F$.

4-parton ($q\bar{q}gg'$) states

We use the triplet, sextet, and 15-plet qg states and four-body states $|E_1\rangle = |3\bar{3}\rangle$, $|E_2\rangle = |6\bar{6}\rangle$, $|E_3\rangle = |15\overline{15}\rangle$. The diagonal matrix $\hat{\Sigma}_{R,\rm el}$ is defined by Eq. (A1), for $\Sigma_{3,\rm el}(\boldsymbol{r})$ see Eq. (B2), for higher representations

$$\begin{aligned}
\Sigma_{6,\rm el}(\boldsymbol{r}) &= \frac{1}{2}\left[\frac{C_6}{C_F}\sigma_0(x)+\frac{N_c}{N_c^2-1}\sigma(x,\boldsymbol{r})\right],\\
C_6 &= \frac{3N_c+1}{N_c+1}C_F,\\
\Sigma_{15,\rm el}(\boldsymbol{r}) &= \frac{1}{2}\left[\frac{C_{15}}{C_F}\sigma_0(x)-\frac{N_c}{N_c^2-1}\sigma(x,-\boldsymbol{r})\right],\\
C_{15} &= \frac{3N_c-1}{N_c-1}C_F.
\end{aligned} \tag{B4}$$

In the large-N_c approximation $C_6 = C_{15} = C_A + C_F$ and we find

$$\begin{aligned}
\Sigma^{\rm el}_{11}(\boldsymbol{r},\boldsymbol{r}') &= \sigma_0(x)+\sigma(x,\boldsymbol{r})+\sigma(x,-\boldsymbol{r}'),\\
\Sigma^{\rm el}_{22}(\boldsymbol{r},\boldsymbol{r}') &= \frac{C_6}{C_F}\sigma_0(x) = \left[1+\frac{C_A}{C_F}\right]\sigma_0(x) = 3\sigma_0(x),\\
\Sigma^{\rm el}_{33}(\boldsymbol{r},\boldsymbol{r}') &= \frac{C_{15}}{C_F}\sigma_0(x) = \left[1+\frac{C_A}{C_F}\right]\sigma_0(x)\\
&= 3\sigma_0(x) = \Sigma^{\rm el}_{22}(\boldsymbol{r},\boldsymbol{r}').
\end{aligned} \tag{B5}$$

A transformation to the basis

$$\begin{aligned}
|e_1\rangle = |E_1\rangle, \qquad |e_2\rangle &= \frac{1}{\sqrt{2}}(|E_2\rangle+|E_3\rangle),\\
|e_3\rangle &= \frac{1}{\sqrt{2}}(|E_2\rangle-|E_3\rangle),
\end{aligned} \tag{B6}$$

leads to the following 4-body operator $\hat{\Sigma}^{(4)}$ [29]:

$$\begin{aligned}
\hat{\Sigma}^{(4)}_{\rm el} &= {\rm diag}(\Sigma^{\rm el}_{11},\Sigma^{\rm el}_{22},\Sigma^{\rm el}_{22}),\\
\hat{\Sigma}^{(4)}_{\rm ex} &= {\rm diag}\{\Sigma^{\rm ex}_{11},\Sigma^{\rm ex}_{22},\Sigma^{\rm ex}_{33}\}-\frac{1}{N_c}\Omega[|e_1\rangle\langle e_2|+|e_2\rangle\langle e_1|].
\end{aligned} \tag{B7}$$

Here Ω is the familiar transition operator of Eq. (A8), and the diagonal elements equal

$$\begin{aligned}
\Sigma^{\rm ex}_{11} &= \sigma(x,\boldsymbol{s}+\boldsymbol{r}-\boldsymbol{r}')-\sigma_0(x)\\
&= -\sigma_0(x)\int d^2\boldsymbol{\kappa} f(x,\boldsymbol{\kappa})\exp[i\boldsymbol{\kappa}(\boldsymbol{s}+\boldsymbol{r}-\boldsymbol{r}')],\\
\Sigma^{\rm ex}_{22} &= \frac{C_A}{C_F}\sigma(x,\boldsymbol{s}+\boldsymbol{r}-\boldsymbol{r}')+\sigma(x,\boldsymbol{s})-\left[\frac{C_A}{C_F}+1\right]\sigma_0(x)\\
&= -\sigma_0(x)\left\{\int d^2\boldsymbol{\kappa} f(x,\boldsymbol{\kappa})\exp(i\boldsymbol{\kappa}\boldsymbol{s})\right.\\
&\quad\left.+\frac{C_A}{C_F}\int d^2\boldsymbol{\kappa} f(x,\boldsymbol{\kappa})\exp[i\boldsymbol{\kappa}(\boldsymbol{s}+\boldsymbol{r}-\boldsymbol{r}')]\right\},\\
\Sigma^{\rm ex}_{33} &= \lambda_2+\Omega.
\end{aligned} \tag{B8}$$

The large-N_c hierarchy in $\hat{\Sigma}^{(4)}_{\rm ex}$ is the same as in DIS: the

diagonal elements $\Sigma^{\rm ex}_{ii}$ which describe color rotations of dipoles within the same color representation, are $\mathcal{O}(1)$, whereas color-excitation transitions between representations of different size are $\mathcal{O}(N_c^{-1})$. To the considered order in $1/N_c$, the state $|e_3\rangle$ decouples from the intranuclear evolution [29].

The projection onto the final states,

$$\sum_f \langle f| = \sum_R \sqrt{\dim(R)}\langle R\bar{R}| = \sqrt{N_c}\langle 3\bar{3}| + \sqrt{\tfrac{1}{2}N_c(N_c+1)(N_c-2)}\langle 6\bar{6}| + \sqrt{\tfrac{1}{2}N_c(N_c-1)(N_c+2)}\langle 15\overline{15}|, \tag{B9}$$

at large N_c reads as

$$\sum_f \langle f| = \sum_R \sqrt{\dim(R)}\langle R\bar{R}| = \sqrt{N_c}\langle e_1| + (\sqrt{N_c})^3\langle e_2|. \tag{B10}$$

APPENDIX C: COLOR-DIAGONAL AND COLOR-EXCITATION INTERACTIONS FOR EXCITATION OF THE GLUON-GLUON DIJETS

Interactions of the two and three-gluon systems are single-channel problems:

$$\begin{aligned}
\Sigma^{(2)}_{\rm el}(\boldsymbol{b},\boldsymbol{b}') &= \sigma_{gg,0}(x),\\
\Sigma^{(2)}_{\rm ex}(\boldsymbol{b},\boldsymbol{b}') &= \sigma_{gg}(x,\boldsymbol{s}+z\boldsymbol{r}-z\boldsymbol{r}') - \sigma_{gg,0}(x),\\
\Sigma^{(3)}_{\rm el}(\boldsymbol{B},\boldsymbol{b}') &= \sigma_{gg,0}(x) + \tfrac{1}{2}\sigma_{gg}(x,\boldsymbol{r}),\\
\Sigma^{(3)}_{\rm ex}(\boldsymbol{B},\boldsymbol{b}') &= \tfrac{1}{2}[\sigma_{gg}(x,\boldsymbol{s}+\boldsymbol{r}-z\boldsymbol{r}') - \sigma_{gg,0}(x)] + \tfrac{1}{2}[\sigma_{gg}(x,\boldsymbol{s}-z\boldsymbol{r}') - \sigma_{gg,0}(x)],\\
\Sigma^{(3)}_{\rm el}(\boldsymbol{b},\boldsymbol{B}') &= \sigma_{gg,0}(x) + \tfrac{1}{2}\sigma_{gg}(x,-\boldsymbol{r}'),\\
\Sigma^{(3)}_{\rm ex}(\boldsymbol{b},\boldsymbol{B}') &= \tfrac{1}{2}[\sigma_{gg}(x,\boldsymbol{s}-\boldsymbol{r}'+z\boldsymbol{r}) - \sigma_{gg,0}(x)] + \tfrac{1}{2}[\sigma_{gg}(x,\boldsymbol{s}+z\boldsymbol{r}) - \sigma_{gg,0}(x)].
\end{aligned} \tag{C1}$$

For the 4-gluon states we use the results of Ref. [30]. The Clebsch-Gordan series for the product of two-gluon (adjoint) states reads

$$\begin{aligned}
(N_c^2-1)\times(N_c^2-1) &= \\
&= 1 + (N_c^2-1)_A + (N_c^2-1)_S + \frac{(N_c^2-4)(N_c^2-1)}{4}\\
&\quad + \left[\frac{(N_c^2-4)(N_c^2-1)}{4}\right]^* + \frac{N_c^2(N_c+3)(N_c-1)}{4}\\
&\quad + \frac{N_c^2(N_c-3)(N_c+1)}{4}\\
&= 1 + 8_A + 8_S + 10 + \overline{10} + 27 + R_7,
\end{aligned} \tag{C2, C3}$$

where we named the representations by their $SU(3)$ dimensions, except for one of the symmetric representations that vanishes for $N_c = 3$, and will be referred to as R_7. These representations naturally group according to their dimension: the singlet state $|1\rangle$ with $\dim[1] = 1$, two octets with $\dim[8_{A,S}] = \mathcal{O}(N_c^2)$, and four higher representations $|R\rangle = |10\rangle, |\overline{10}\rangle, |27\rangle, |R_7\rangle$ with the dimension $\dim[R] = \mathcal{O}(N_c^4)$. The non-Abelian evolution of tetra-gluons is a forbidding multichannel problem: a full menagerie of possible color-singlet tetra-gluons includes 9 states, of which 3 states, $|(8_S8_A)^{(\pm)}\rangle$ and $(|10\overline{10}\rangle - |\overline{10}10\rangle)/\sqrt{2}$, decouple from our problem exactly. Excitation of one more state, $(|2727\rangle - |R_7R_7\rangle)/\sqrt{2}$ is $\mathcal{O}(N_c^{-2})$ and it decouples in the considered leading order of large-N_c perturbation theory.

In the basis of remaining 5 states,

$$\begin{aligned}
|e_1\rangle &= |11\rangle,\\
|e_2\rangle &= \frac{1}{\sqrt{2}}(|8_A8_A\rangle + |8_S8_S\rangle),\\
|e_3\rangle &= \frac{1}{\sqrt{2}}(|8_A8_A\rangle - |8_S8_S\rangle),\\
|e_4\rangle &= \frac{1}{2}(|10\overline{10}\rangle + |\overline{10}10\rangle + |2727\rangle + |R_7R_7\rangle),\\
|e_5\rangle &= \frac{1}{2}(|10\overline{10}\rangle + |\overline{10}10\rangle - |2727\rangle - |R_7R_7\rangle),
\end{aligned} \tag{C4}$$

the color-diagonal and color-excitation operators take the form

$$\begin{aligned}
\hat{\Sigma}^{(4)}_{\rm el} &= {\rm diag}(\Sigma^{\rm el}_{11}, \Sigma^{\rm el}_{22}, \Sigma^{\rm el}_{33}, \Sigma^{\rm el}_{44}, \Sigma^{\rm el}_{55}),\\
\Sigma^{\rm el}_{11} &= \sigma_{gg}(x,\boldsymbol{r}) + \sigma_{gg}(x,-\boldsymbol{r}'),\\
\Sigma^{\rm el}_{22} &= \sigma_{gg,0}(x) + \frac{1}{2}[\sigma_{gg}(x,\boldsymbol{r}) + \sigma_{gg}(x,-\boldsymbol{r}')],\\
\Sigma^{\rm el}_{33} &= \sigma_{gg,0}(x) + \frac{1}{2}[\sigma_{gg}(x,\boldsymbol{r}) + \sigma_{gg}(x,-\boldsymbol{r}')],\\
\Sigma^{\rm el}_{44} &= \frac{C_{27}}{C_A}\sigma_{gg,0}(x),\\
\Sigma^{\rm el}_{55} &= \frac{C_{27}}{C_A}\sigma_{gg,0}(x).
\end{aligned} \tag{C5}$$

In the considered large-N_c approximation, quadratic Casimirs for all higher multiplets are equal to each other:

$$C_{27} = C_{R_7} = C_{10} = 2C_A. \tag{C6}$$

We expand the color-excitation operator into the diagonal and off-diagonal components:

$$
\begin{aligned}
\hat{\Sigma}^{(4)}_{\rm ex} &= {\rm diag}\{\Sigma^{\rm ex}_{11}, \Sigma^{\rm ex}_{22}, \Sigma^{\rm ex}_{33}, \Sigma^{\rm ex}_{44}, \Sigma^{\rm ex}_{55}\} + \hat{\omega},\\
\Sigma^{\rm ex}_{11} &= 0,\\
\Sigma^{\rm ex}_{22} &= \frac{1}{2}[\sigma_{gg}(x,\boldsymbol{s}) - \sigma_{gg,0}(x)]\\
&\quad + \frac{1}{2}[\sigma_{gg}(x,\boldsymbol{s}+\boldsymbol{r}-\boldsymbol{r}') - \sigma_{gg,0}(x)],\\
\Sigma^{\rm ex}_{33} &= \frac{1}{2}[\sigma_{gg}(x,\boldsymbol{s}+\boldsymbol{r}) - \sigma_{gg,0}(x)]\\
&\quad + \frac{1}{2}[\sigma_{gg}(x,\boldsymbol{s}-\boldsymbol{r}') - \sigma_{gg,0}(x)],\\
\Sigma^{\rm ex}_{44} &= \frac{1}{2}[\sigma_{gg}(x,\boldsymbol{s}) + \sigma_{gg}(x,\boldsymbol{s}+\boldsymbol{r}-\boldsymbol{r}')] - \frac{C_{27}}{C_A}\sigma_{gg,0}(x),\\
\Sigma^{\rm ex}_{55} &= \frac{1}{2}[\sigma_{gg}(x,\boldsymbol{s}+\boldsymbol{r}) + \sigma_{gg}(x,\boldsymbol{s}-\boldsymbol{r}')] - \frac{C_{27}}{C_A}\sigma_{gg,0}(x),\\
\hat{\omega} &= -\frac{1}{\sqrt{2}N_c}\Omega\{|e_1\rangle\langle e_2| + |e_1\rangle\langle e_3| + |e_4\rangle\langle e_2|\\
&\quad - |e_5\rangle\langle e_3| + {\rm H.c}\}.
\end{aligned}
\tag{C7}
$$

The final-state summation goes as

$$
\begin{aligned}
\sum_f \langle f| &= \sum_R \sqrt{\dim[R]}\langle R\bar{R}|\\
&= \underbrace{\langle e_1|}_{1} + \underbrace{N_c\sqrt{2}\langle e_2|}_{8_A+8_S} + \underbrace{N_c^2\langle e_4|}_{10+\overline{10}+27+R_7}
\end{aligned}
\tag{C8}
$$

and the averaging over incoming colors shall introduce a factor $1/N_c$,

$$
|{\rm in}\rangle = \frac{1}{\sqrt{\dim[8]}}|8_A 8_A\rangle = \frac{1}{\sqrt{2}N_c}(|e_2\rangle + |e_3\rangle). \tag{C9}
$$

[1] B. B. Back *et al.* (PHOBOS Collaboration), Phys. Rev. C **74**, 011901 (2006).
[2] P. Jacobs and X. N. Wang, Prog. Part. Nucl. Phys. **54**, 443 (2005); J. Jalilian-Marian and Y. V. Kovchegov, Prog. Part. Nucl. Phys. **56**, 104 (2006).
[3] L. Simic *et al.*, Phys. Rev. C **37**, 2064 (1988); A. Olszewski *et al.* (PHOBOS Collaboration), Acta Phys. Pol. B **33**, 1449 (2002), and references therein.
[4] R. S. Hollis *et al.* (PHOBOS Collaboration), J. Phys.: Conf. Ser. **5**, 46 (2005).
[5] V. N. Gribov, Zh. Eksp. Teor. Fiz. **53**, 654 (1967) [Sov. Phys. JETP **26**, 414 (1968)].
[6] V. A. Abramovsky, V. N. Gribov, and O. V. Kancheli, Yad. Fiz. **18**, 595 (1973) [Sov. J. Nucl. Phys. **18**, 308 (1974)].
[7] A. Capella and A. Kaidalov, Nucl. Phys. **B111**, 477 (1976).
[8] L. Bertocchi and D. Treleani, J. Phys. G **3**, 147 (1977).
[9] A. B. Kaidalov and K. A. Ter-Martirosian, Phys. Lett. B **117**, 247 (1982).
[10] D. Treleani, Int. J. Mod. Phys. A **11**, 613 (1996).
[11] A. Capella, A. Kaidalov, and J. Tran Thanh Van, Acta. Phys. Hung. N.S **9**, 169 (1999).
[12] Y. V. Kovchegov, Phys. Rev. D **72**, 094009 (2005).
[13] K. G. Boreskov, A. B. Kaidalov, V. A. Khoze, A. D. Martin, and M. G. Ryskin, Eur. Phys. J. C **44**, 523 (2005).
[14] J. Bartels, M. Salvadore, and G. P. Vacca, Eur. Phys. J. C **42**, 53 (2005).
[15] M. A. Braun, Eur. Phys. J. C **42**, 169 (2005).
[16] M. A. Braun, hep-ph/0603060.
[17] J. R. Andersen *et al.* (Small x Collaboration), DESY Report No. DESY-06-052.
[18] B. G. Zakharov, Yad. Fiz. **46**, 148 (1987) [Sov. J. Nucl. Phys. **46**, 92 (1987)].
[19] N. N. Nikolaev and B. G. Zakharov, Z. Phys. C **49**, 607 (1991); **53**, 331 (1992).
[20] N. N. Nikolaev, B. G. Zakharov, and V. R. Zoller, Pis'ma Zh. Eksp. Teor. Fiz. **59**, 8 (1994) [JETP Lett. **59**, 6 (1994)].
[21] N. N. Nikolaev and B. G. Zakharov, Zh. Eksp. Teor. Fiz. **105**, 1117 (1994) [J. Exp. Theor. Phys. **78**, 598 (1994)]; Z. Phys. C **64**, 631 (1994).
[22] N. N. Nikolaev, G. Piller, and B. G. Zakharov, Zh. Eksp. Teor. Fiz. **108**, 1554 (1995) [J. Exp. Theor. Phys. **81**, 851 (1995)]; Z. Phys. A **354**, 99 (1996).
[23] N. N. Nikolaev, W. Schäfer, and G. Schwiete, Phys. Rev. D **63**, 014020 (2000); Pis'ma Zh. Eksp. Teor. Fiz. **72**, 583 (2000) [JETP Lett. **72**, 405 (2000)].
[24] N. N. Nikolaev, W. Schäfer, B. G. Zakharov, and V. R. Zoller, Zh. Eksp. Teor. Fiz. **124**, 491 (2003) [J. Exp. Theor. Phys. **97**, 441 (2003)].
[25] N. N. Nikolaev, W. Schäfer, B. G. Zakharov, and V. R. Zoller, Yad. Fiz. **68**, 692 (2005) [Phys. At. Nucl. **68**, 661 (2005)].
[26] N. N. Nikolaev and W. Schäfer, Phys. Rev. D **71**, 014023 (2005).
[27] N. N. Nikolaev, W. Schäfer, and B. G. Zakharov, Phys. Rev. Lett. **95**, 221803 (2005).
[28] N. N. Nikolaev, W. Schäfer, B. G. Zakharov, and V. R. Zoller, Pis'ma Zh. Eksp. Teor. Fiz. **82**, 364 (2005) [JETP Lett. **82**, 325 (2005)].
[29] N. N. Nikolaev, W. Schäfer, B. G. Zakharov, and V. R. Zoller, Phys. Rev. D **72**, 034033 (2005).
[30] N. N. Nikolaev, W. Schäfer, and B. G. Zakharov, Phys. Rev. D **72**, 114018 (2005).

[31] N. N. Nikolaev and W. Schäfer, Phys. Rev. D **74**, 014023 (2006).
[32] L. N. Lipatov, Nucl. Phys. **B452**, 369 (1995); E. N. Antonov, L. N. Lipatov, E. A. Kuraev, and I. O. Cherednikov, Nucl. Phys. **B721**, 111 (2005).
[33] A. Kovner, Acta Phys. Pol. B **36**, 3551 (2005); D. N. Triantafyllopoulos, Acta Phys. Pol. B **36**, 3593 (2005).
[34] A. Bialas, M. Bleszynski, and W. Czyz, Nucl. Phys. **B111**, 461 (1976).
[35] A. Bialas and W. Czyz, Acta Phys. Pol. B **36**, 905 (2005).
[36] J. Adams *et al.* (STAR Collaboration), Phys. Rev. C **70**, 044901 (2004), and references therein.
[37] W. Busza and R. Ledoux, Annu. Rev. Nucl. Part. Sci. **38**, 119 (1988).
[38] X. N. Wang and M. Gyulassy, Phys. Rev. D **44**, 3501 (1991).
[39] B. Müller and J. L. Nagle, nucl-th/0602029.
[40] O. V. Kancheli, Pis'ma Zh. Eksp. Teor. Fiz. **18**, 465 (1973) [JETP Lett. **18**, 312 (1973)].
[41] N. N. Nikolaev and V. I. Zakharov, Yad. Fiz. **21**, 434 (1975) [Sov. J. Nucl. Phys. **21**, 227 (1975)]; Phys. Lett. B **55**, 397 (1975).
[42] N. N. Nikolaev, Yad. Fiz. **24**, 772 (1976) [Sov. J. Nucl. Phys. **24**, 402 (1976)]; G. V. Davidenko and N. N. Nikolaev, Nucl. Phys. **B135**, 333 (1978).
[43] L. Cunqueiro, E. G. Ferreiro, F. del Moral, and C. Pajares, Phys. Rev. C **72**, 024907 (2005).
[44] A. Adil, M. Gyulassy, W. A. Horowitz, and S. Wicks, nucl-th/0606010.
[45] W. Busza, Acta Phys. Pol. B **35**, 2873 (2004).
[46] B. B. Back *et al.* (PHOBOS Collaboration), Phys. Rev. C **72**, 031901 (2005).
[47] I. Arsene *et al.* (BRAHMS Collaboration), Phys. Rev. Lett. **94**, 032301 (2005).
[48] L. C. Bland *et al.*, Eur. Phys. J. C **43**, 427 (2005); P. Steinberg *et al.*, nucl-ex/0503002.
[49] N. N. Nikolaev and B. G. Zakharov, Phys. Lett. B **332**, 184 (1994).
[50] E. A. Kuraev, L. N. Lipatov, and V. S. Fadin, Zh. Eksp. Teor. Fiz.. **71**, 840 (1976) [Sov. Phys. JETP **44**, 443 (1976)]; Zh. Eksp. Teor. Fiz. **72**, 377 (1977) [Sov. Phys. JETP **45**, 199 (1977)]; I. I. Balitsky and L. N. Lipatov, Yad. Fiz. **28**, 1597 (1978) [Sov. J. Nucl. Phys. **28**, 822 (1978)].
[51] R. J. Glauber, in *Lectures in Theoretical Physics,* edited by W. E. Brittin *et al.* (Interscience, New York, 1959), Vol. 1, p. 315; R. J. Glauber and G. Matthiae, Nucl. Phys. **B21**, 135 (1970).
[52] V. N. Gribov, Zh. Eksp. Teor. Fiz. **56**, 892 (1969) [Sov. Phys. JETP **29**, 483 (1969)].
[53] R. J. Glauber, Phys. Rev. **131**, 2766 (1963).
[54] S. Mandelstam, Nuovo Cimento **30**, 1127 (1963); **30**, 1148 (1963).
[55] N. N. Nikolaev, W. Schäfer, B. G. Zakharov, and V. R. Zoller, Pis'ma Zh. Eksp. Teor. Fiz. **83**, 233 (2006) [JETP Lett. **83**, 192 (2006)].
[56] N. N. Nikolaev, W. Schäfer, B. G. Zakharov, and V. R. Zoller, Pis'ma Zh. Eksp. Teor. Fiz. **76**, 231 (2002) [JETP Lett. **76**, 195 (2002)].
[57] N. N. Nikolaev, B. G. Zakharov, and V. R. Zoller, Z. Phys. A **351**, 435 (1995).
[58] N. N. Nikolaev, Usp. Fiz. Nauk **134**, 369 (1981) [Sov. Phys. Usp. **24**, 531 (1981)].
[59] B. G. Zakharov, Pis'ma Zh. Eksp. Teor. Fiz. **63**, 906 (1996) [JETP Lett. **63**, 952 (1996)]; Pis'ma Zh. Eksp. Teor. Fiz. **65**, 585 (1967) [JETP Lett.**65**, 615 (1997)]; Yad. Fiz. **61**, 924 (1998) [Phys. At. Nucl. **61**, 838 (1998)].
[60] R. Baier, D. Schiff, and B. G. Zakharov, Annu. Rev. Nucl. Part. Sci. **50**, 37 (2000).
[61] K. Werner, F. M. Liu, S. Ostapchenko, and T. Pierog, Acta. Phys. Hung. N.S **21**, 279 (2004), and references therein.
[62] B. Z. Kopeliovich, N. N. Nikolaev, and I. K. Potashnikova, Phys. Rev. D **39**, 769 (1989).
[63] A. Bialas and M. Gyulassy, Nucl. Phys. **B291**, 793 (1987).
[64] B. Andersson, G. Gustafson, G. Ingelman, and T. Sjostrand, Phys. Rep. **97**, 31 (1983); T. Sjostrand, Comput. Phys. Commun. **82**, 74 (1994).
[65] I. M. Dremin and J. W. Gary, Phys. Rep. **349**, 301 (2001).
[66] V. V. Anisovich, Y. M. Shabelski, and V. M. Shekhter, Nucl. Phys. **B133**, 477 (1978); V. V. Anisovich, M. N. Kobrinsky, J. Nyiri, and Yu. M. Shabelski, *Quark Model and High Energy Collisions* (World Scientific, Singapore, 2004), 2nd ed.
[67] M. Djordjevic and M. Gyulassy, Phys. Lett. B **560**, 37 (2003); Nucl. Phys. **A733**, 265 (2004); M. Djordjevic, M. Gyulassy, and S. Wicks, Phys. Rev. Lett. **94**, 112301 (2005).
[68] Y. V. Kovchegov and A. H. Mueller, Nucl. Phys. **B529**, 451 (1998); Y. V. Kovchegov and K. Tuchin, Phys. Rev. D **65**, 074026 (2002).
[69] N. Borghini and F. Gelis, Phys. Rev. D **74**, 054025 (2006).